bioRxiv preprint doi: https://doi.org/10.1101/2020.06.10.143941; this version posted June 12, 2020. The copyright holder for this preprint (which was not certified by peer review) is the author/funder, who has granted bioRxiv a license to display the preprint in perpetuity. It is made available under aCC-BY 4.0 International license.

CD38 dependent NAD^+ depletion contributes to oligodendrocyte loss and inhibition of myelin regeneration

Authors

Monica R. Langley[1], Chan-Il Choi[1], Thais R. Peclat[3], Whitney Simon[1], Hyesook Yoon[1,2], Laurel Kleppe[1], Claudia C.S. Chini[3,4], Eduardo N. Chini[3,4], and Isobel A. Scarisbrick[1,2,*]

Affiliations

[1] Department of Physical Medicine & Rehabilitation, Rehabilitation Medicine Research Center, Mayo Clinic, Rochester, MN 55905, USA

[2] Department of Physiology and Biomedical Engineering, Mayo Clinic, Rochester, MN 55905, USA

[3] Robert & Arlene Kogod Center on Aging, Mayo Clinic, Rochester, MN 55905, USA

[4] Department of Anesthesiology, Mayo Clinic, Rochester, MN 55905, USA

[*] Corresponding author. Tel: 507-774-0124; E-mail:scarisbrick.isobel@mayo.edu

bioRxiv preprint doi: https://doi.org/10.1101/2020.06.10.143941; this version posted June 12, 2020. The copyright holder for this preprint (which was not certified by peer review) is the author/funder, who has granted bioRxiv a license to display the preprint in perpetuity. It is made available under aCC-BY 4.0 International license.

Abstract

Western-style diets cause disruptions in myelinating cells and astrocytes within the CNS. We identified increased CD38 expression in the mouse spinal cord following chronic high fat consumption or focal demyelinating injury. CD38-catalytically inactive mice are significantly protected from high fat-induced NAD^+ depletion, oligodendrocyte loss, oxidative damage, and astrogliosis. 78c, a CD38 inhibitor, increased NAD^+ and attenuated neuroinflammatory changes in astrocytes induced by saturated fat. Conditioned media from saturated fat-treated astrocytes impaired oligodendrocyte differentiation pointing to indirect mechanisms of oligodendrogliopathy. Combined saturated fat and lysolecithin demyelination in cerebellar slices resulted in additional deficits in myelin proteins that were mitigated by concomitant 78c treatment. Importantly, oral 78c increased counts of oligodendrocytes and remyelinated axons after focal demyelination. Our findings suggest that high fat diet impairs oligodendrocyte survival and differentiation through astrocyte-linked mechanisms mediated by the NAD^+ase CD38, and highlight the use of CD38 inhibitors as potential therapeutic candidates to improve myelin regeneration.

Keywords

CD38, Glia, high fat diet, NAD^+, remyelination

bioRxiv preprint doi: https://doi.org/10.1101/2020.06.10.143941; this version posted June 12, 2020. The copyright holder for this preprint (which was not certified by peer review) is the author/funder, who has granted bioRxiv a license to display the preprint in perpetuity. It is made available under aCC-BY 4.0 International license.

Introduction

Obesity is a key risk factor for developing multiple sclerosis (MS) (Gianfrancesco, Acuna et al., 2014), which further increases risk when interacting with other known genetic, lifestyle, and environmental risk factors (Olsson, Barcellos et al., 2017). Moreover, recent studies suggest that obesity and related metabolic comorbidities also influence disease progression and disability burden in MS patients (Manouchehrinia, Hedstrom et al., 2018, Marrie, Rudick et al., 2010, Tettey, Simpson et al., 2014). Although current investigations point to obesity-induced white matter abnormalities and loss of oligodendrocytes within the central nervous system (CNS) following chronic consumption of high fat diets (HFD) in rodent models, how this may influence MS pathophysiology is largely unknown (Graham, Grabowska et al., 2019, Langley, Yoon et al., 2019, Yoon, Kleven et al., 2016).

Astrocyte activation occurs following chronic HFD feeding in the CNS and exerts oligotoxic effects (Buckman, Thompson et al., 2015, Buckman, Thompson et al., 2013, Clarke, Liddelow et al., 2018, Liddelow, Guttenplan et al., 2017, Wanrooy, Kumar et al., 2018). On the other hand, building and maintenance of myelin membranes requires oligodendrocyte fatty acid synthesis. In addition, oligodendrocytes can utilize lipids from the diet or synthesized by astrocytes, at least under normal conditions (Camargo, Goudriaan et al., 2017, Dimas, Montani et al., 2019). The potential to target astrocytes to improve outcomes in MS is already suggested since some currently prescribed MS disease modifying therapies do impact astrocytes (Ponath, Park et al., 2018). Prior studies regarding the role of HFDs in MS animal models have utilized immune-mediated models such as experimental autoimmune encephalomyelitis (EAE) and demonstrate exacerbation of peripheral immune responses or neuroinflammation with HFD consumption (Hasan, Seo et al., 2017, Herrmann, Barth et al., 2016, Ji, Wu et al., 2019,

bioRxiv preprint doi: https://doi.org/10.1101/2020.06.10.143941; this version posted June 12, 2020. The copyright holder for this preprint (which was not certified by peer review) is the author/funder, who has granted bioRxiv a license to display the preprint in perpetuity. It is made available under aCC-BY 4.0 International license.

Timmermans, Bogie et al., 2014). Also, recent findings suggest that insulin sensitizing agents such as metformin and pioglitazone provide benefit to MS patients with metabolic syndrome (Negrotto, Farez et al., 2016). There are few if any studies regarding the effects of HFD on the capacity for remyelination. Since oligodendrocyte function is intimately linked to neighboring glial cells and neuronal activity, in addition to microenvironmental factors, the most promising interventions will likely involve a combinatorial approach (Alizadeh, Dyck et al., 2015, Alizadeh & Karimi-Abdolrezaee, 2016, Ohtomo, Iwata et al., 2018).

CD38 is an NAD^+-degrading enzyme expressed by astrocytes and was recently shown to be upregulated in MS animal models (Herrmann et al., 2016, Roboon, Hattori et al., 2019, Zhang, Chen et al., 2014, Zhang, Sloan et al., 2016). CD38 is the main NAD^+ase in many mammalian tissues and regulates tissue and cellular NAD^+ homeostasis as well as NAD^+ dependent enzymes such as PARPs and Sirtuins (Aksoy, Escande et al., 2006, Aksoy, White et al., 2006). Global CD38 knockout confers protection against demyelination, T cell responses, and EAE disease severity as well as HFD-induced metabolic dysfunction in rodent models (Barbosa, Soares et al., 2007, Chiang, Harrington et al., 2015, Herrmann et al., 2016, Roboon et al., 2019). Here we test the hypotheses that HFD consumption promotes oligodendrocyte loss in a CD38-dependent manner and that CD38 inhibition will enhance myelin regeneration. First we established increased CD38 expression following HFD consumption. Next, we demonstrated that CD38 catalytically inactive mice fed either a regular or HFD were protected from HFD-mediated loss of oligodendrocytes with concomitant increases in NAD^+ levels and reduced neuroinflammation and oxidative damage. *In vitro* approaches identified oligodendrocyte direct and astrocyte-linked indirect mechanisms by which excessive fatty acid impairs myelinating cell function. Finally, the value of a small molecule inhibitor of CD38, 78c, was then identified as a

bioRxiv preprint doi: https://doi.org/10.1101/2020.06.10.143941; this version posted June 12, 2020. The copyright holder for this preprint (which was not certified by peer review) is the author/funder, who has granted bioRxiv a license to display the preprint in perpetuity. It is made available under aCC-BY 4.0 International license.

novel protective strategy to enhance myelin regeneration in a model of focal demyelinating injury. Together these findings highlight a novel indirect pathway of myelin injury involving pathogenic changes in astrocytes. Moreover, these changes can be attenuated by inhibition of CD38 in the context of chronic HFD consumption and targeted to improve myelin regeneration in the CNS.

bioRxiv preprint doi: https://doi.org/10.1101/2020.06.10.143941; this version posted June 12, 2020. The copyright holder for this preprint (which was not certified by peer review) is the author/funder, who has granted bioRxiv a license to display the preprint in perpetuity. It is made available under aCC-BY 4.0 International license.

Results

Astrocytes increase CD38 in the spinal cord following chronic HFD or demyelination

Our recent studies revealed spinal cord changes involving ER stress, mitochondrial dysfunction, and oxidative stress in the spinal cords of mice chronically consuming a HFD and the direct potential of saturated fat palmitate (PA) to inhibit differentiation of primary murine oligodendrocytes from their progenitors or neural stem cells (Langley et al., 2019, Yoon et al., 2016). Although saturated fat inhibited markers of differentiation *in vitro*, it was not oligotoxic, suggesting a more complex mechanism at play *in vivo* (Langley et al., 2019). Considering the emerging role of astrocytes in the pathology of various neurological disorders (Liddelow et al., 2017, Ponath et al., 2018, Yoon, Choi et al., 2020) and in the CNS following chronic HFD (Buckman et al., 2015, Ogrodnik, Zhu et al., 2019, Wanrooy et al., 2018), along with their known essential metabolic and functional links with oligodendrocytes (Domingues, Portugal et al., 2016, Kiray, Lindsay et al., 2016), we decided to address the possibility of indirect effects of HFD mediated by astrocytes (Fig 1A).

NAD^+ is a key mediator of cellular energy status and is involved in mitochondrial function and quality control processes primarily through the activity of sirtuins that require NAD^+ as a cofactor (Camacho-Pereira, Tarrago et al., 2016, Canto, Menzies et al., 2015, Long, Klimova et al., 2017)(Foolad, Khodagholi et al., 2019). Exercise is known to increase NAD^+ levels in various tissues and protected against “Western-style diet”-induced deficits in myelin and myelinating cells in two recent studies (Chiang et al., 2015, Graham et al., 2019, Yoon et al., 2016). Our recent untargeted metabolomics profiling of spinal cord tissue identified NAD^+ metabolism as one of the top pathways impacted by HFD consumption (Langley et al., 2019), which prompted us to quantify spinal cord NAD^+ levels using a cycling assay. Spinal cord NAD^+

bioRxiv preprint doi: https://doi.org/10.1101/2020.06.10.143941; this version posted June 12, 2020. The copyright holder for this preprint (which was not certified by peer review) is the author/funder, who has granted bioRxiv a license to display the preprint in perpetuity. It is made available under aCC-BY 4.0 International license.

119 levels from HFD-fed mice were less than half that of RD-fed mice (Fig 1B). A heatmap with
120 HFD-induced gene expression changes in NAD^+-related enzymes was also derived from this
121 papers sequencing results (Figure 1- figure supplement 1a)(Langley et al., 2019).
122 Since CD38 is the main NAD^+-glycohydrolase in many mammalian tissues (Camacho-
123 Pereira et al., 2016, Chini, Chini et al., 2018), we next quantified CD38 expression in spinal cord
124 astrocytes to establish a potential link. Quantification by qPCR indicated higher RNA expression
125 of CD38 in HFD-fed mice compared to regular diet-fed controls (Fig 1C). Consistent with
126 findings demonstrating CD38 is primarily localized to astrocytes within the CNS (Hattori, Kaji et
127 al., 2017, Kou, Banerjee et al., 2009, Roboon et al., 2019, Zhang et al., 2014, Zhang et al., 2016),
128 increases in CD38 immunoreactivity (Fig 1D-G) were observed in GFAP+ astrocytes following
129 either HFD (Fig 1D,F) or lysolecithin-induced demyelination (Fig 1E,G). Using multiplex *in*
130 *situ* hybridization, CD38 RNA levels were also higher in ALDH1L1+ astrocytes of HFD-fed
131 mice (Figure 1- supplement 1b). Similar to the HFD spinal cords, primary murine astrocytes
132 cultured with PA (100 μM, 24 h) showed increased GFAP (Fig 1H) and CD38 (Fig 1I) RNA
133 expression and depleted NAD^+ levels (Fig 1J). Collectively, these data suggest that HFD can
134 induce astrocytosis in the spinal cord or primary cultures, which increases expression of CD38
135 and subsequently depletes NAD^+ levels.

136 **CD38 catalytically inactive (CD38ci) mice are resistant to HFD-induced oligodendrocyte**
137 **loss**

138 To determine the potential therapeutic significance of CD38 upregulation to HFD-
139 induced oligodendrocyte loss, we collected spinal cords from wildtype (WT) and CD38-
140 catalytically inactive (CD38ci) mice fed a regular diet (RD) or HFD for 30 wk beginning at 50
141 wk of age for histological analysis (Fig 2A). CD38ci mice have the CD38 gene knocked out and

bioRxiv preprint doi: https://doi.org/10.1101/2020.06.10.143941; this version posted June 12, 2020. The copyright holder for this preprint (which was not certified by peer review) is the author/funder, who has granted bioRxiv a license to display the preprint in perpetuity. It is made available under aCC-BY 4.0 International license.

reinserted with a mutation at E230 of the CD38 gene, rendering the CD38-NAD^+ase catalytic site inactive while preserving overall expression levels of CD38 (Tarrago, Chini et al., 2018). As seen in our previous studies (Langley et al., 2019, Yoon et al., 2016), there was a significant reduction in the number of Olig2+ oligodendrocyte progenitors (Fig 2B) as well as GST3+ mature oligodendrocytes (Fig 2C) in the HFD-fed wildtype mice compared to regular diet-fed mice. However, CD38ci mice fed HFD did not have reductions in oligodendrocyte lineage cell counts compared to their regular diet genotype controls. Across spinal cord regions, no significant changes in MBP due to genotype or diet group were found (Fig 2D). Overall, these data suggest that oligodendrocyte lineage cell survival is preserved in CD38ci mice following chronic HFD consumption.

Diminished neuroinflammatory responses and oxidative damage in CD38ci mice following chronic HFD

Neuroinflammation, including complex interplay between microglia and astrocytes, is now appreciated to contribute to oligotoxicity and MS pathophysiology (Domingues et al., 2016, Liddelow et al., 2017). To explore the potential impact of blocking CD38 catalytic activity on CNS neuroinflammation following chronic HFD consumption, we next performed immunohistochemical analysis on the spinal cords from wildtype and CD38ci mice fed regular or HFD for markers of microglia and astrocytes. Quantification of the thresholded area considered positive for ionized calcium-binding adapter molecule 1 (IBA1) demonstrated decreased microglia (Fig 3A) in the ventral grey matter of spinal cords from CD38ci mice compared to wildtype mice overall. In addition, HFD-fed CD38ci mice showed significantly reduced IBA1 immunoreactivity in the ventral grey and white matter of the spinal cord compared to wildtype mice fed a HFD. Considering that astrocytes have endogenous expression of CD38

bioRxiv preprint doi: https://doi.org/10.1101/2020.06.10.143941; this version posted June 12, 2020. The copyright holder for this preprint (which was not certified by peer review) is the author/funder, who has granted bioRxiv a license to display the preprint in perpetuity. It is made available under aCC-BY 4.0 International license.

as well as elevated CD38 expression following HFD or demyelination (Roboon et al., 2019, Zhang et al., 2014, Zhang et al., 2016) (Fig 1), we also investigated astrocyte reactivity in these mice. In the ventral spinal cord, quantification of astrocyte marker glial fibrillary acidic protein (GFAP, Fig 3B) demonstrated significantly reduced positive area in the white matter of CD38ci mice compared to wildtype mice. Wildtype HFD-fed mice showed significantly more astrocyte reactivity compared to either regular diet or HFD-fed CD38ci mice.

Given our previous data suggesting increased oxidative damage markers in the CNS following chronic consumption of HFDs (Langley et al., 2019, Yoon et al., 2016) and the relevance of oxidative stress in glia of MS lesions (Haider, Fischer et al., 2011, Lassmann & van Horssen, 2016, Miller, Dziedzic et al., 2019), we next sought to compare the extent of oxidative damage in the spinal cords of wildtype and CD38ci mice fed regular or HFD. More abundant lipid peroxidation marker 4-hydroxynonenal (4HNE) was present in the HFD-fed wildtype mice than regular diet-fed wildtype mice in the spinal cord dorsal column. Importantly, a significant reduction in 4HNE was found in the HFD-CD38ci mice compared to HFD-wildtype mice in the dorsal column and ventral spinal cord (grey and white matter). To confirm that preservation of NAD^+ levels was achieved in the CD38ci mice, we next measured NAD^+ levels on spinal cord tissue from the same cohort of mice. As expected based on our data in Fig 1, NAD^+ levels were significantly reduced following chronic HFD consumption in wildtype mice (Fig 3D). Moreover, in CD38ci mice, which had diminished CD38 activity (Fig 3E), NAD^+ levels were significantly higher overall and in the CD38ci-HFD mice compared to the wildtype-HFD mice. Next, our histological findings were further substantiated by observed gene expression differences in SOD2 (Fig 3F) and pro-repair astrocyte markers genes BDNF and S100a10, as determined by qRT-PCR (Fig 3G-H). Overall, the observed reductions in neuroinflammation and oxidative

bioRxiv preprint doi: https://doi.org/10.1101/2020.06.10.143941; this version posted June 12, 2020. The copyright holder for this preprint (which was not certified by peer review) is the author/funder, who has granted bioRxiv a license to display the preprint in perpetuity. It is made available under aCC-BY 4.0 International license.

stress makers and increased NAD^+ levels in the CD38ci mice likely provide a more suitable microenvironment for oligodendrocyte survival, differentiation, and repair following chronic HFD consumption.

Astrocytes cultured in high saturated fat conditions increase CD38 and pro-inflammatory cytokine expression and inhibit oligodendrocyte differentiation

Astrocytes release various growth factors, cytokines, chemokines, extracellular matrix proteins, glutamate, and reactive oxygen species that heavily influence oligodendrocyte proliferation and differentiation (Alizadeh & Karimi-Abdolrezaee, 2016, Domingues et al., 2016, Kiray et al., 2016, Lassmann & van Horssen, 2016). Therefore, we next investigated the effects of culturing oligodendrocytes in conditioned media obtained from PA-treated astrocytes with or without 78c co-treatment, as depicted in Fig 4A. 78c is a thiazoloquin(az)olin(on)e CD38 inhibitor that increases NAD^+ levels in various tissues and cell types and is orally bioavailable (Boslett, Helal et al., 2018, Haffner, Becherer et al., 2015, Tarrago et al., 2018). As expected, astrocyte-conditioned medium (ACM) from PA-treated astrocytes significantly reduced oligodendrocyte PLP and MBP expression. However, this negative impact on myelin protein production was partially rescued by co-treatment with the small molecule CD38 inhibitor 78c (3 µM) (Haffner et al., 2015, Tarrago et al., 2018). Likewise, addition of exogenous NAD^+ (50 µM) to the PA-treated astrocyte cultures (Fig 4B) significantly increased PLP expression, while ACM-treated oligodendrocyte numbers remained unchanged across treatment groups. Along with other research that indicates the role of NAD^+ in reducing astrocyte proinflammatory and oxidative stress responses (Harlan, Pehar et al., 2016, Roboon et al., 2019, Wilhelm & Hirrlinger, 2012), these data indicate the importance of maintaining proper astrocyte NAD^+ levels in order to promote oligodendrocyte differentiation.

bioRxiv preprint doi: https://doi.org/10.1101/2020.06.10.143941; this version posted June 12, 2020. The copyright holder for this preprint (which was not certified by peer review) is the author/funder, who has granted bioRxiv a license to display the preprint in perpetuity. It is made available under aCC-BY 4.0 International license.

To address whether the possible NAD^+-driven astrocytic changes indirectly mediate the observed effects on oligodendrocyte, we next used primary murine astrocyte cultures to assess NAD^+ levels and transcriptional changes. Addition of 78c (3μM) was effective to restore NAD^+ levels in PA-treated astrocytes when quantified using an NAD^+ cycling assay (Fig 4C). However, astrocytes derived from CD38 knockout mice did not have depleted NAD^+ levels in response to PA. Next, we determined whether CD38 regulates astrocyte pro-inflammatory responses. After treating astrocyte cultures with PA and/or 78c, we used qRT-PCR and a multiplex bioassay for determining cytokine RNA transcripts and release into culture supernatant, respectively. We observed significant increases in IL-1β and IL-6 expression (Fig 4D) in astrocytes stimulated with PA and 78c significantly attenuated PA-induced RNA expression of IL-1β, IL-6, TNFα, and reactive astrocyte marker H2D1. Additionally, the mitochondrial antioxidant SOD2 was significantly increased in astrocytes treated with 78c or both PA and 78c. Significant increases in secretion of cytokines triggered by PA were observed using a Bioplex assay including CXCL1 (KC), MIP1α, RANTES, IL-6, MIP1β, and MCP1 (Fig 4E). Notably, co-treatment with 78c successfully mitigated PA-stimulated secretion of CXCL1, MIP1α, RANTES, IL-6, MIP1β, and MCP1. Thus, inflammatory and oxidative stress-related changes in cultures astrocytes may help to explain reduced differentiation potential of the oligodendrocyte progenitors in the presence of PA-treated astrocyte conditioned medium.

NAD^+ and NMN restore oligodendrocyte differentiation in PA-treated cultures

Our recent findings demonstrated that PA can directly impair oligodendrocyte differentiation from neural stem cells or oligodendrocyte progenitors (Langley et al., 2019), and others have indicated that depletions in cellular NAD^+ can prevent differentiation of stem cells to mature oligodendrocytes (Stein & Imai, 2014). To examine the effects of replenishing NAD^+ levels on

bioRxiv preprint doi: https://doi.org/10.1101/2020.06.10.143941; this version posted June 12, 2020. The copyright holder for this preprint (which was not certified by peer review) is the author/funder, who has granted bioRxiv a license to display the preprint in perpetuity. It is made available under aCC-BY 4.0 International license.

oligodendrocytes, we next supplemented cultures with exogenous NAD^+ (50 μM) and monitored PLP expression (Fig 5A). Co-treatment with PA and NAD^+ significantly enhanced PLP expression (Fig 5 B) compared to exclusive PA treatment. However, treatment of oligodendrocytes with CD38 inhibitor 78c did not attenuate this effect (Figure 2- figure supplement 1).

Interestingly, CD38+ cells can deplete NAD^+ and metabolites available for low-CD38 expressing cells (Chini, Hogan et al., 2019, Tarrago et al., 2018), such as oligodendrocytes (Hattori et al., 2017, Roboon et al., 2019, Zhang et al., 2014, Zhang et al., 2016). We found that direct effects of saturated fat treatment on oligodendrocytes include mitochondria function and morphology changes (Langley et al., 2019) while other mechanisms, potentially including NAD^+-depleting mechanisms (Penberthy & Tsunoda, 2009, Penke, Schuster et al., 2017, Stein & Imai, 2014), could also play a part. We hypothesized that the pro-myelinating effects of increasing NAD^+ are SIRT1-dependent, so we determined if the beneficial effects of NAD^+ in the presence of PA could be blocked with a SIRT1 inhibitor Ex-527. Similar to adding exogenous NAD^+, treatment with the NAD^+ precursor NMN (100 μM) also restored markers of oligodendrocyte differentiation in PA-treated cultures (Fig 5C). However, in the presence of Ex-527 (5 μM), the increases in PLP and MBP protein in response to NMN were suppressed. At the doses used, PA, NMN, and Ex-527 did not significantly alter the number of oligodendrocytes. Hence, the impaired ability of oligodendrocytes cultured with excess saturated fat to differentiate is at least partially regulated by NAD^+-dependent sirtuin activity.

78c prevents lysolecithin- and PA-mediated myelin protein and oligodendrocyte loss

Since we observed protective effects of genetic CD38 inhibition on oligodendrocyte survival following HFD (Fig 2), as well as increased CD38 expression in a demyelination model

bioRxiv preprint doi: https://doi.org/10.1101/2020.06.10.143941; this version posted June 12, 2020. The copyright holder for this preprint (which was not certified by peer review) is the author/funder, who has granted bioRxiv a license to display the preprint in perpetuity. It is made available under aCC-BY 4.0 International license.

(Fig 1), we next sought to explore benefits conferred by pharmacologic inhibition using 78c in a model of lysolecithin-induced *ex vivo* demyelination. Murine cerebellar slices from postnatal day 7-9 day pups were demyelinated using lysolecithin (LL, 0.5 mg/ml, 18 h), followed by a period of one week to allow for repair (Fig 6A). Confocal imaging of immunofluorescence staining demonstrated reductions in MBP after LL that was significantly attenuated by 78c co-treatment (Fig 6 B).

Finally, to evaluate the therapeutic potential of 78c in a model of high fat exposure combined with demyelination, organotypic cerebellar slices were demyelinated as described above and cultured for 7 d in the presence or absence of PA and/or 78c. All cerebellar slices showed fewer Olig2+ cells and less MBP immunoreactivity following LL insult (Fig 6 C). After 7 d of recovery, MBP levels were successfully restored, although Olig2+ cells remained significantly depleted in the 7 d LL group. Inclusion of PA in the media further diminished Olig2+ cells in the LL slices. Importantly, 78c and PA co-treatment significantly increased the percentage of Olig2+ cells and MBP expression in the demyelinated cerebellar slices. However, neither palmitate nor 78c alone, without lysolecithin, for two weeks significantly altered MBP expression (Figure 6- figure supplement 1). These findings demonstrate the capability of 78c to restore myelin protein expression even in a combined saturated fat- and demyelinating agent-induced condition.

CD38 inhibition with 78c improves myelin repair following lysolecithin-induced focal demyelination of the ventral spinal cord

To determine whether pharmacologic inhibition of CD38 NAD^+ase activity affects the potential for remyelination *in vivo,* we administered 78c to mice in each diet group (regular or high fat) and used histological approaches to investigate numbers of oligodendrocyte lineage

bioRxiv preprint doi: https://doi.org/10.1101/2020.06.10.143941; this version posted June 12, 2020. The copyright holder for this preprint (which was not certified by peer review) is the author/funder, who has granted bioRxiv a license to display the preprint in perpetuity. It is made available under aCC-BY 4.0 International license.

cells and remyelinated axons in the lysolecithin model of demyelination. Six-week old male wildtype mice were given either a regular or HFD for 5 weeks, then split into additional groups: receiving the same diet with or without 78c (600ppm) (Fig 7A). All mice were subjected to a focal demyelinating injury to the ventral spinal cord by microinjection of 1% lysolecithin. At the study endpoint, HFD mice had gained significantly more weight than their RD counterparts, irrespective of genotype, while 78c treatment slightly decreased yet did not have a significant effect on body weights (Figure 7-figure supplement 1a). Relative to wild type mice, the 78c-treated mice in the regular and high-fat groups consumed significantly less chow (Figure 7-figure supplement 1b). Based on the average food intake and 78c concentration (600ppm) in the diets, it can be approximated that mice consumed 16-19.5 mg 78c daily through oral consumption. Hematoxylin and eosin (H&E) staining indicates that lesion area (Figure 7-figure supplement 1C) and neurofilament (a marker of axon integrity, Figure 7- figure supplement 1D) remain unchanged by drug or diet.

After two weeks of recovery, lesions were collected from perfused mice and used for subsequent counting of remyelinated axons and myelinating cells. Overall, lysolecithin mice fed 78c along with either a RD or HFD showed significantly greater numbers of remyelinated axons compared to the lysolecithin mice fed a RD or HFD without 78c (Fig 7B). In particular, more than double the number of remyelinated axons was present in the 78c-regular diet mice over regular diet alone. Further supporting a role in myelin repair, MBP immunoreactivity in the total lesion or the lesion rim was higher in the 78c-treated mice irrespective of diet (Fig 7C). Importantly, numbers of Olig2+ (Fig 7D) and GST3+ (Fig 7E) cells were significantly higher in the combined 78c group (which includes LL-RD-78c and LL-HFD-78c mice) versus the combined group without 78c treatment (which includes LL-RD and LL-HFD). Moreover, the

bioRxiv preprint doi: https://doi.org/10.1101/2020.06.10.143941; this version posted June 12, 2020. The copyright holder for this preprint (which was not certified by peer review) is the author/funder, who has granted bioRxiv a license to display the preprint in perpetuity. It is made available under aCC-BY 4.0 International license.

303 number of Olig2+ cells in the lesion rim and GST3+ cells in the rim or total lesion were
304 significantly higher in the LL-RD-78c versus the LL-RD group. In addition to the demyelinated
305 lesion site, 78c also attenuated HFD-induced oligodendrocyte loss on the uninjected side of the
306 ventral spinal cord (Figure 7-figure supplement 2). These findings suggest that, *in vivo*, 78c helps
307 to preserve or replenish myelinating cells and their progenitors, leading to increased markers of
308 myelin repair. Furthermore, these results provide a strong rationale for targeting CD38 and
309 overall NAD^+ metabolism as a new strategy to attenuate oligodendrocyte loss and aid in myelin
310 regeneration.

311 **78c promotes pro-repair astrocytes after lysolecithin-induced demyelination**

312 Next, we chose to explore the role of 78c on neuroinflammation markers in the spinal cord
313 following demyelination. Histological quantification of threshold-positive staining for microglia
314 marker IBA1 (Fig 8A) indicated a significant interaction between diet and drug treatment on the
315 lesion rim, yet no significant effect of diet or drug alone. Although there is a trend of decrease
316 for both IBA1 and GFAP in the 78c treated group, no statistically significant attenuation of
317 astrocyte marker GFAP was observed (Fig 8B). In both the RD- and HFD-fed mice, there was,
318 however, a significant increase in S100a10 immunoreactivity with 78c treatment (Fig 8C),
319 considered a marker for pro-repair astrocytes. There was also a slight decrease in C3d staining, a
320 marker of reactive astrocytes, although this did not reach statistical significance (Fig 8D).
321 Overall, these data suggest that 78c modulates astrocyte responses elicited by demyelinating
322 injury, skewing them towards a phenotype that enhances oligodendrocyte survival and
323 differentiation and myelin repair (Fig 9).

324

325

bioRxiv preprint doi: https://doi.org/10.1101/2020.06.10.143941; this version posted June 12, 2020. The copyright holder for this preprint (which was not certified by peer review) is the author/funder, who has granted bioRxiv a license to display the preprint in perpetuity. It is made available under aCC-BY 4.0 International license.

Discussion

Diet-induced obesity increases the risk for developing MS, especially when combined with other known risk factors (Gianfrancesco et al., 2014, Mokry, Ross et al., 2016, Olsson et al., 2017). The results of the current study suggest that metabolic disturbances, triggered by consumption of a diet high in fat, promote oligodendrogliopathy and impair myelin regeneration through astrocyte-linked indirect NAD^+-dependent mechanisms. We demonstrate that restoring NAD^+ levels via genetic inactivation of CD38 can overcome these effects. Moreover, we show that therapeutic inactivation of CD38 can enhance myelin regeneration. Together these findings point to a new metabolic targeting strategy positioned to improve disease course in MS and other conditions in which the integrity of myelin is a key concern.

Neuroinflammation and astrogliosis are predominant pathological mediators of neurodegenerative conditions, including MS, and astrogliosis is linked to HFD-induced CNS pathology in rodent models (Buckman et al., 2015, Buckman et al., 2013, Liddelow et al., 2017, Mizunoya, Ohnuki et al., 2013, Ogrodnik et al., 2019, Ponath, Ramanan et al., 2017, Thaler, Yi et al., 2012, Wanrooy et al., 2018). In spinal cord astrocytes of HFD mice, we observed increases in CD38 expression and an overall depletion of NAD^+. This suggests that CD38, the major constitutively active NAD^+-degrading enzyme, is induced in astrocytes with chronic exposure to a HFD. These findings are consistent with outcomes in studies of neuroinflammation that indicate increased expression of CD38 in the brain of individuals with MS or human immunodeficiency virus encephalitis and in rodent experimental models of Alzheimer's disease (AD), sepsis associated brain injury, and toxin-induced brain convulsions (Blacher, Dadali et al., 2015, Ginwala, McTish et al., 2016, Kou et al., 2009, Machado-Santos, Saji et al., 2018, Mamik, Banerjee et al., 2011, Peng, Wang et al., 2018, Zou, He et al., 2017). In the current study, we

bioRxiv preprint doi: https://doi.org/10.1101/2020.06.10.143941; this version posted June 12, 2020. The copyright holder for this preprint (which was not certified by peer review) is the author/funder, who has granted bioRxiv a license to display the preprint in perpetuity. It is made available under aCC-BY 4.0 International license.

found that HFD or focal lysolecithin-mediated demyelinating injury each drove increased CD38 expression in astrocytes, while genetic or pharmacological CD38 inhibition after HFD or demyelination, respectively, attenuated astrocyte activation.

Upstream activators of CD38 expression include cytokines, lipopolysaccharide (LPS), 25-hydroxycholesterol (25-HC), glutamate, and factors secreted by senescent cells (Bruzzone, Verderio et al., 2004, Chini, Hogan et al., 2019, Chini et al., 2018, Mamik et al., 2011). Separately, astrocytosis and CD38 are reported to increase with normal aging, and growing evidence supports a role for HFD-induced neuroinflammation in promoting premature "inflammaging" (Camacho-Pereira et al., 2016, Chini et al., 2019, Clarke et al., 2018, Denver, Gault et al., 2018, Escande, Nin et al., 2013, Freeman, Haley-Zitlin et al., 2014). Likely related to the older age of mice in the current study (~80 wks), HFD did not increase IBA1 or GFAP levels. In palmitate-stimulated astrocytes, downstream inflammatory indicators of TLR4 activation, including IL-6 and TNFα were increased. Pointing to a therapeutic strategy, this response was blunted when NAD^+ levels were restored by co-treatment with 78c. Also, studies reporting the role of CD38 in neuroinflammation indicate CD38 inhibition or knockout decreases cytokine secretion in LPS-stimulated microglia, macrophages, and monocytes (Amici, Young et al., 2018, Iqbal & Zaidi, 2007, Matalonga, Glaria et al., 2017, Roboon et al., 2019, Wang, Liu et al., 2017). Therefore, improving NAD^+ levels by targeting CD38 shows therapeutic promise across multiple neurological and non-neurological disease types, and here we establish its significance to oligodendrocyte heath and regeneration with strong linkage to its effects on astrocyte metabolism.

Astrocytes and microglia secrete a variety of chemokines, cytokines and growth factors that regulate myelin injury and regeneration (Alizadeh & Karimi-Abdolrezaee, 2016, Domingues

bioRxiv preprint doi: https://doi.org/10.1101/2020.06.10.143941; this version posted June 12, 2020. The copyright holder for this preprint (which was not certified by peer review) is the author/funder, who has granted bioRxiv a license to display the preprint in perpetuity. It is made available under aCC-BY 4.0 International license.

et al., 2016, Kiray et al., 2016). Of cytokines increased in astrocytes after palmitate-exposure, CCL3/MIP1α, MIP1β, and RANTES also increase in active demyelinating MS lesions and fluids (Boven, Montagne et al., 2000, Janssen, Rickert et al., 2016, Mori, Nistico et al., 2016). These factors are thought to enhance disease progression by recruiting peripheral immune cells and by activating resident glia (Boven et al., 2000, Mori et al., 2016, Tejera-Alhambra, Casrouge et al., 2015). Opposing effects are seen for CXCL1/KC on myelination and glia activation (Clarner, Janssen et al., 2015, Karim, Kim et al., 2018), while combined CCL2/MCP1 and CCL3/MIP1α absence attenuates demyelination, oligodendrocyte loss, and astrogliosis in the cuprizone model (Janssen et al., 2016). Recently, knockout of CD38 or supplementation with NAD^+ was shown to suppress activation of astrocytes in culture (Roboon et al., 2019). Here we showed that saturated fat- induced reductions in NAD^+ result in proinflammatory responses in astrocytes which trigger impaired differentiation and survival in oligodendrocyte lineage cells. Moreover, we demonstrate that 78c mitigates the dysmyelinating effects of astrocyte secreted factors.

In addition to cytokines such as IL-1β and TNFα, reactive oxygen species can inhibit oligodendrocyte survival (Liddelow et al., 2017, Valentin-Torres, Savarin et al., 2016). Oxidative damage can also activate inflammasome signaling in peripheral immune cells and glia, including astrocytes (Lassmann & van Horssen, 2016, Liao, Lai et al., 2018, Moyon, Dubessy et al., 2015, Sarkar, Malovic et al., 2017). Complementing this, we provide new RNA evidence for more SOD2 and less IL1β in high fat-78c co-treated astrocyte cultures compared to treatment with high fat alone. We also found more SOD2, BDNF and S100a10 in the CD38ci mouse spinal cord pointing to a shift towards pro-repair astrocyte properties (Liddelow et al., 2017). Blocking downstream CD38 signaling also reduced markers of oxidative damage in a rodent toxin-induced convulsion model (Zou et al., 2017). Our findings suggest that the beneficial effects of CD38

bioRxiv preprint doi: https://doi.org/10.1101/2020.06.10.143941; this version posted June 12, 2020. The copyright holder for this preprint (which was not certified by peer review) is the author/funder, who has granted bioRxiv a license to display the preprint in perpetuity. It is made available under aCC-BY 4.0 International license.

395 inhibition include protection against astrocyte pro-inflammatory factors and reactive oxygen
396 species known to negatively impact oligodendrocyte renewal and maturation.

397 The effects of CD38 activity and NAD^+ levels may depend heavily on cell type and
398 disease context, with findings here supporting a critical protective role of lowering astrocyte
399 CD38 activity for protection of myelinating cells and for myelin regeneration in the adult CNS.
400 In addition, CD38+ cells regulate NAD^+ levels in neighboring CD38- cells by influencing NAD^+
401 precursor availability (Chini et al., 2019, Tarrago et al., 2018), and this may also be the case for
402 astrocytes and oligodendrocytes in our cell culture studies of high fat and experimental
403 demyelination. Consistent with this model, 78c had no direct effect on oligodendrocyte
404 differentiation in the context of palmitate *in vitro*. In a recent study, palmitate inhibited NAMPT
405 activity, depleted cellular NAD^+ levels, and resulted in apoptosis in neurons at a higher dose than
406 studied here (Penke, Schuster et al., 2017). Another report indicates NAMPT inhibition prevents
407 differentiation of stem cells to oligodendrocyte lineage cells (Stein & Imai, 2014). These studies
408 align well with the direct inhibitory effect of palmitate on oligodendrocyte differentiation
409 observed here. PARP deficiency has been shown to either increase severity of disease or
410 attenuate clinical signs in animal models of MS (Selvaraj et al, 2009). Thus, complex alterations
411 in NAD^+ biosynthesis, salvage, and degradation pathways may contribute to the effects of
412 palmitate on oligodendrocytes that we document can be rescued by NAD^+ replenishment.

413 Several recent studies have explored supplementing NAD^+ precursors or flavonoids
414 known to inhibit NAD^+ase activity to improve myelin repair, neuroprotection, and to decrease
415 immune cellular responses. For example, an NAD^+/BDNF/TrkB pathway is proposed to be
416 involved in nicotinamide-mediated protection, including improved remyelination in a stroke
417 model and precursor supplementation increased BDNF in a Huntington's disease model

bioRxiv preprint doi: https://doi.org/10.1101/2020.06.10.143941; this version posted June 12, 2020. The copyright holder for this preprint (which was not certified by peer review) is the author/funder, who has granted bioRxiv a license to display the preprint in perpetuity. It is made available under aCC-BY 4.0 International license.

(Hathorn, Snyder-Keller et al., 2011, Wang, Zhang et al., 2017). Supporting a possible NAD^+-BDNF pathway for remyelination, we observed increased BDNF expression in the spinal cord of CD38ci mice and improved remyelination with oral 78c administration. Although direct effects on myelinating cells were not examined, mice with CD38-knockout, given the CD38 inhibitor apigenin, or supplemented with NAD^+ each showed reduced EAE disease severity (Ginwala et al., 2016, Herrmann et al., 2016, Wang, Zhao et al., 2016). NAD^+ levels can impact oligodendrocyte lineage cell proliferation and survival via cyclins and E2f1, while differentiation is reported to be regulated redundantly by SIRT1 and SIRT2 (Jablonska, Gierdalski et al., 2016, Ji, Doucette et al., 2011, Penberthy & Tsunoda, 2009, Stein & Imai, 2014). Results here demonstrate that the ability of NAD^+ supplementation to promote oligodendrocyte differentiation *in vitro* is indeed at least partially reliant on SIRT1 function. Restoring NAD^+ levels was also beneficial in the context of palmitate or high fat-induced inflammation and oxidative stress via SIRT1 in liver, heart, and muscle (Escande, Chini et al., 2010, Li, Dou et al., 2015, Prola, Pires Da Silva et al., 2017, Sadeghi, Seyyed Ebrahimi et al., 2017). Improvements in expression of myelin proteins in the spinal cord of mice consuming a high fat high sucrose diet in conjunction with coordinate wheel running, were also linked to increases in SIRT1 expression (Yoon et al., 2016). Collectively, these findings are particularly encouraging since effective modulation of disease progression will likely include a combination of therapeutic strategies encompassing anti-inflammatory, myelin regeneration, and neuroprotective interventions.

HFD consumption did not further impair markers of myelin integrity in our *in vivo* model of myelin injury and repair as it did in *ex vivo* remyelinating cerebellar slice cultures. Although treatment with 78c did improve myelin regeneration in mice consuming a regular diet, little impact was seen in mice consuming a HFD, suggesting the need to explore additional factors in

bioRxiv preprint doi: https://doi.org/10.1101/2020.06.10.143941; this version posted June 12, 2020. The copyright holder for this preprint (which was not certified by peer review) is the author/funder, who has granted bioRxiv a license to display the preprint in perpetuity. It is made available under aCC-BY 4.0 International license.

the context of HFD-demyelination that contribute impaired remyelination. Alternately, a higher dose or even a combination of drugs (to target various aspects of astrocyte responses) may be required to improve remyelination in the context of HFD. Although a preference for pro-repair versus pro-inflammatory phenotype was indicated following 78c treatment in the lysolecithin model of focal demyelination studied, a complete astrocyte-specific transcriptomic profile in the HFD mice with demyelination will be needed to elucidate specific pathogenic astrocyte populations. This approach would additionally identify novel genes in the astrocyte transcriptome that could be targeted to mitigate the indirect oligotoxic effects we observe.

Genetic CD38 inhibition attenuated HFD-induced oligodendrocyte loss and dietary supplementation with 78c increased counts of oligodendrocytes and remyelinated axons following focal demyelinating injury. These findings suggest that increases in astrocyte CD38, and the associated depletion of NAD^+ levels, may contribute indirectly to impairments in oligodendrocyte health and myelin regeneration via inflammation and oxidative stress. Tarrago et al. (2018) recently established 78c as a specific, reversible, and non-competitive inhibitor of CD38 NAD^+ase activity improves age-related metabolic function (Hattori et al., 2017). Altogether, these findings suggest that genetic or pharmacologic CD38 inhibition provides therapeutic benefits in HFD-induced metabolic dysfunction and downstream signaling events in the CNS, in addition to the already described peripheral benefits on age-related metabolic dysfunction. Importantly, inhibition of CD38 with 78c can improve myelin regeneration in the adult CNS including reducing the pro-inflammatory profile while increasing the pro-repair profile of astrocytes. Together these findings point to the potential translational value of targeting CD38 to improve outcomes in MS and other demyelinating conditions.

bioRxiv preprint doi: https://doi.org/10.1101/2020.06.10.143941; this version posted June 12, 2020. The copyright holder for this preprint (which was not certified by peer review) is the author/funder, who has granted bioRxiv a license to display the preprint in perpetuity. It is made available under aCC-BY 4.0 International license.

463 A few current MS disease modifying therapies (i.e. glatiramer acetate, fingolimod,
464 dimethyl fumarate) affect CD38+ cell counts or inhibit astrocyte activation, but these roles have
465 not been directly linked to therapeutic benefits (Bruck, Popescu et al., 2012, Choi, Gardell et al.,
466 2011, Herrmann et al., 2016, Pavelek, Vysata et al., 2018, Ponath et al., 2018, van de Donk,
467 Richardson et al., 2018, Wilms, Sievers et al., 2010). For instance, fingolimod treatment
468 decreased CD38 expression in a rat EAE model (Herrmann et al., 2016), and was shown to
469 promote beneficial astrocyte responses in culture (Hoffmann, Hofereiter et al., 2015).
470 Monoclonal antibodies targeting CD38 have already met with success in clinical trials for
471 conditions outside the CNS (Chini et al., 2018, Deckert, Wetzel et al., 2014, Lokhorst, Plesner et
472 al., 2015, Martin, Baz et al., 2017), including Daratumumab which is FDA approved for use in
473 multiple myeloma. Accordingly, the research findings we present should inspire further research
474 into ways to mitigate the negative consequences of HFD on oligodendrocytes alone and in the
475 context of white matter injury which may include dietary intake of NAD^+ precursors,
476 administration of CD38 inhibitors, or exercise-related rehabilitation strategies.
477

bioRxiv preprint doi: https://doi.org/10.1101/2020.06.10.143941; this version posted June 12, 2020. The copyright holder for this preprint (which was not certified by peer review) is the author/funder, who has granted bioRxiv a license to display the preprint in perpetuity. It is made available under aCC-BY 4.0 International license.

Materials and Methods

Key Resources Table

Reagent or Resource	Source	Additional information
Antibodies		
Mouse anti-CD38	Novus	1g7f4 (1:500)
Rabbit anti-GFAP	Dako	Z0334 (1:5000)
mouse anti-Olig2	Millipore	MABN50(1:200)
rabbit anti-Olig2	Millipore	Ab9610; AB_10141047 (1:500)
Rabbit anti-GST3	Abcam	Ab153949 (1:1000)
rat anti-Myelin basic protein (MBP)	Millipore	MAB386; AB_94975 (1:750)
Rabbit anti-PLP	Abcam	A28486 (1:750)
Rabbit anti-IBA1	Wako	019-19741(1:3000)
rabbit anti-4-hydroxynonenol	Abcam	ab46545 (1:500)
chicken anti-GFAP	Abcam	ab4647 (1:2000)
rabbit anti-Neurofilament	Sigma Aldrich	N4142; AB_477272 (1:1300)
Goat anti-C3d	R&D Systems	AF2655 (1:500)
Rabbit anti-S100a10	Proteintech	11250-1-AP (1:7500)
biotinylated goat anti-rat secondary	Jackson	112-066-072 (1:100)
biotinylated donkey anti-rabbit secondary	Jackson	711-065-152 (1:100)
biotinylated donkey anti-mouse secondary	Jackson	715-066-151 (1:100)
goat-anti-rabbit AF488 secondary	Jackson	111-545-047 (1:100)
goat anti-rat Cy3 secondary	Jackson	112-166-072 (1:100)
goat anti-chicken AF647 secondary	Jackson	703-606-155 (1:100)
goat anti-rabbit AF488 secondary	Jackson	111-545-041 (1:100)
donkey anti-rabbit Cy3 secondary	Jackson	711-166-152 (1:100)
goat anti-rabbit AF647 secondary	Jackson	111-606-144 (1:100)
goat anti-rat AF647 secondary	Jackson	112-606-143 (1:100)
Oligonucleotides		

bioRxiv preprint doi: https://doi.org/10.1101/2020.06.10.143941; this version posted June 12, 2020. The copyright holder for this preprint (which was not certified by peer review) is the author/funder, who has granted bioRxiv a license to display the preprint in perpetuity. It is made available under aCC-BY 4.0 International license.

(primers/probes)		
BDNF	Applied Biosystems	Mm04230607_s1
SOD2	Applied Biosystems	Mm01313000_m1; NM_013671.3;
S100a10	Integrated DNA Technologies	Mm.PT.58.6571055
CD38	Applied Biosystems	Mm01220906_m1
OLIG2	Applied Biosystems	NM_016967; Mm.PT.58.42319010
MBP	Integrated DNA Technologies	NM_001025251; CCAGTAGTCCATTTCTTCAAGAACAT/GCCG ATTTATAGTCGGAAGCTC
PLP	Integrated DNA Technologies	NM_011123.2; TCTTTGGCGACTACAAGACCAC/CACAAACT TGTCGGGATGTCCTA
GFAP	Integrated DNA Technologies	NM_010277.2; GCAGATGAAGCCACCCTGG/ GAGGTCTGGCTTGGCCAC
IL1β	Integrated DNA Technologies	Mm.PT.51.17212823
IL6	Applied Biosystems	NM_031168.1; Mm00446190_m1
H2D1	Integrated DNA Technologies	Mm.PT.58.42136026.g
TNFα	Applied Biosystems	Mm00443258_m1
Rn18s	Applied Biosystems	NR_003278.3; Mm03928990_g1
GAPDH	Applied biosystems	Mm99999915_g1
RNAscope Probe - Mm-Aldh1l1-C2	Advanced Cell Diagnostics	405891-C2
RNAscope Probe - Mm-CD38	Advanced Cell Diagnostics	513061
Chemicals		
78c CD38 inhibitor	Millipore	Cat#538763
Nicotinamide adenine dinucleotide	Sigma Aldrich	Cat#10127965001
Nicotinamide 1,N6-	Sigma Aldrich	Cat#41628

bioRxiv preprint doi: https://doi.org/10.1101/2020.06.10.143941; this version posted June 12, 2020. The copyright holder for this preprint (which was not certified by peer review) is the author/funder, who has granted bioRxiv a license to display the preprint in perpetuity. It is made available under aCC-BY 4.0 International license.

ethenoadenine dinucleotide		
flavin mononucleotide	Sigma Aldrich	Cat#F8399
Alcohol dehydrogenase	Sigma Aldrich	Cat#A3263
Diaphorase	Sigma Aldrich	Cat#D5540
resazurin	Sigma Aldrich	Cat#119303
palmitate	Sigma Aldrich	Cat#P0500
DAPI	ThermoFisher	Cat#D1306; AB_2629482
lysolecithin	Sigma Aldrich	Cat#L-4129
Methyl green	Sigma Aldrich	67060
Commercial kits		
RNA scope Duplex Manual kit	Advanced Cell Diagnostics	Cat#322430
Bio-Plex Mouse Cytokine 23-plex Assay	Bio-Rad	Cat#m60009rdpd
Software		
GraphPad Prism 7	GraphPad Software	https://www.graphpad.com/scientificsoftware/prism
CellSens	Olympus	https://www.olympus-lifescience.com/en/software/cellsens/
Zen	Zeiss	https://www.zeiss.com/microscopy/us/products/microscope-software/zen.html
Fuji ImageJ	NIH	https://imagej.net/Fiji

Animal husbandry and diets

All experimental diets and procedures were approved by The Mayo Clinic Institutional Animal Care and Use Committee (IACUC) and performed in accordance with institutional and regulatory guidelines. Mice were provided *ad libitum* access to diets along with tap water. For initial characterization of CD38 expression and NAD^+ levels following a high-fat diet, male C57BL6/J mice were obtained from Jackson Labs (Bar Harbor, ME) and were randomly assigned to feeding on either a regular diet (RD, 10 % kcal fat, D12450K, Research Diets, New Brunswick, NJ) or a high-fat diet (HFD, 60% kcal fat, D12492, Research Diets, New Brunswick, NJ) beginning at 10 wk of age, as previously described (Langley et al., 2019).

bioRxiv preprint doi: https://doi.org/10.1101/2020.06.10.143941; this version posted June 12, 2020. The copyright holder for this preprint (which was not certified by peer review) is the author/funder, who has granted bioRxiv a license to display the preprint in perpetuity. It is made available under aCC-BY 4.0 International license.

For studies comparing wildtype and CD38ci mice fed RD and HFDs, mice were bred onsite after initial generation at TransViragen (Chapel Hill, NC) via recombineering technology, as previously described (Partida-Sanchez, Cockayne et al., 2001, Tarrago et al., 2018). Male mice received a regular (10.4% kcal fat, Teklad TD000357) or HFD (42% kcal fat, Teklad TD88137) beginning at 50 wk of age for 30 wk. Diets used for lysolecithin demyelination studies were these same diets, with or without 600 ppm 78c added, and were started one week prior to the spinal cord microinjection procedure. Food intake and body weights were monitored weekly.

Lysolecithin microinjection into spinal cord

For focal demyelination of the ventral white matter (laminectomy at thoracic 10th vertebra; mediolateral 0.3, dorsoventral -1.4 mm relative to the dorsal surface) of the murine spinal cord, 8 wk old male mice were injected with 2 µl of a saline solution containing 1% lysophosphatidyl choline with 0.01% Evan's Blue (Sigma L4129) at 0.2 µl/min using a 30-40 µm glass micropitppette and stereotaxic microinjection device (Stoelting, Inc., Wood Dale, IL).

For anesthesia, 100 mg/kg ketamine and 10 mg/kg xylazine were administered intraperitoneally prior to surgery, while postoperative care consisted of an antibiotic (Baytril 50 mg/kg/day, i.p.), an analgesic (buprinex 0.05 mg/kg, twice daily, subcutaneous) and saline (0.2ml/d, intraperitoneal) for three days. After a two-week recovery period, mice were deeply anesthetized (ketamine 150mg/kg and xylazine 15 mg/kg, i.p.) and transcardially perfused with 4% paraformaldehyde (Fisher T353-500) for collection of spinal cord tissue. Spinal cord segments were microdissected, with the rostral 2 mm segment processed for paraffin-embedded blocks and the caudal segment osmicated (1% osmium tetroxide, 0223B, Polysciences) and embedded in Araldite. To identify myelin sheaths, Araldite blocks were cut to 1 µm sections, stained with p-phenylendiamine (Sigma P6001), imaged with 60x objective (Olympus BX51

bioRxiv preprint doi: https://doi.org/10.1101/2020.06.10.143941; this version posted June 12, 2020. The copyright holder for this preprint (which was not certified by peer review) is the author/funder, who has granted bioRxiv a license to display the preprint in perpetuity. It is made available under aCC-BY 4.0 International license.

513 microscope), and stitched together (Adobe Photoshop) to comprise the entire lesion. Number of
514 remyelinated axons per square millimeter of lesion was reported after blinded counting in ImageJ
515 (Yoon et al., 2020). Immunohistochemical analysis of focal demyelinated lesions utilized overall
516 neuropathological changes (hematoxylin and eosin) along with myelin loss to determine the
517 lesion core, while the lesion rim was defined as also encompassing neuroinflammatory markers
518 (GFAP, IBA1). Lesion areas between 50,000 - 180,000 µm2 were included in the analysis.

519 **Immunohistochemistry**

520 Spinal cords were fixed in 4% paraformaldehyde, processed, paraffin-embedded, and cut
521 to 6 µm for all immunoperoxidase and immunofluorescence procedures, as described previously
522 (Langley et al., 2019, Yoon et al., 2020). When necessary, heat-induced antigen retrieval was
523 achieved through incubation with sodium citrate (10 mM, pH 6.0) in a steamer basket. Sections
524 were blocked (20 % normal goat serum), then incubated in primary antibodies described in the
525 key resources table.

526 The following day, incubation with appropriate secondary antibodies (biotinylated or
527 fluorochrome-conjugated, Jackson, 1:200) for immunoperoxidase or immunofluorescence
528 staining was performed. After incubating in an avidin peroxidase solution (Vectastain Elite ABC
529 kit, PK-6100, Vector Laboratories), color development was achieved by incubation with 3,3-
530 diaminobenzidine (DAB, Sigma D5637) and counterstaining with methyl green (Sigma, 67060).
531 Slides were dehydrated, coverslipped with DPX (Sigma), and images acquired using and
532 Olympus BX51 microscope with DP72 camera. Immunofluroescence slides were counterstained
533 with 4',6'-diamindino-2-phenylindole (DAPI), mounted with fluoromount, and imaged with an
534 Olympus BX51 microscope and captured with Olympus XM10 camera. Cell and axon counting,
535 as well as thresholding of images, was performed in ImageJ (NIH) without knowledge of

bioRxiv preprint doi: https://doi.org/10.1101/2020.06.10.143941; this version posted June 12, 2020. The copyright holder for this preprint (which was not certified by peer review) is the author/funder, who has granted bioRxiv a license to display the preprint in perpetuity. It is made available under aCC-BY 4.0 International license.

536 treatment groups using cropped regions of interest (Adobe Photoshop) and averaged from two
537 sections per animal. Rolled or damaged tissue sections were excluded from histological
538 quantification.

539 ***in situ* hybridization using multiplex RNAscope:**

540 For visualizing RNA expression of CD38 in tissue sections, slides containing RD- or
541 HFD-fed mouse corpus callosum were processed for RNAscope *in situ* as previously described
542 (Choi, Yoon et al., 2018, Wang, Flanagan et al., 2012). In short, slides were deparaffinized, and
543 incubated with hydrogen peroxide for 10 min at room temperature (RT), target retrieval solution
544 at 100 °C for 30 min, and protease plus solution at 40°C for 30 min. Next, probes (Mm-CD38-
545 C1, 513061 and Mm-Aldh1l1-C2, 405891, ACD) were incubated at 40 °C for 2 h and sections
546 were stored in 5x saline sodium citrate (SSC) buffer overnight. The following day, probes were
547 hybridized and chromogenic development steps were performed in freshly prepared solutions
548 following manufacturer instructions as previously described (322430, ACD, Newark, CA)1.
549 Briefly, six amplification steps and washes were performed prior to AP-based Fast Red color
550 development for 10 min at RT. Then, four additional amplification steps and HRP-based Green
551 chromogen development was achieved by incubating for 10 min at RT. Stained slides were
552 counterstained with dilute hematoxylin and allowed to dry for 20 min at 60 °C prior to being
553 cooled and mounted with Vectamount (H5000, Vector Labs, Burlingame, CA). All probes and
554 RNAscope 2.5 HD Multiplex reagents were purchased from Advanced Cell Diagnostics
555 (322430, ACD, Newark, CA).

556 **RNA isolation and qRT-PCR**

557 To determine gene expression from spinal cord or primary murine cells, total RNA was
558 extracted using RNA Stat60 (Tel-Test; Friendswood, TX) per manufacturer's instructions and

bioRxiv preprint doi: https://doi.org/10.1101/2020.06.10.143941; this version posted June 12, 2020. The copyright holder for this preprint (which was not certified by peer review) is the author/funder, who has granted bioRxiv a license to display the preprint in perpetuity. It is made available under aCC-BY 4.0 International license.

used for qRT-PCR using BioRad iTaq Universal Probes or primers and SYBR Green One-step kits. Starting quantity for quantification of each gene's expression was normalized to Rn18s or GAPDH. Detailed primer and probe information are annotated in the key resources table.

Mixed glial preparations and primary cell cultures

Primary mixed glial cultures were prepared from P0-3 mice, as previously described (Langley et al., 2019, Yoon et al., 2020). In brief, dissected cerebral cortices were dissociated and grown in DMEM (Fisher 11960-044) with 1 mM sodium pyruvate (Corning 11360070), 20 mM HEPES (Gibco 15630-080), 100 U/ml PenStrep (Life Technologies 15140122), 10% fetal bovine serum (FBS, Atlanta 337 Biologicals S11150), and 5 µg/ml insulin. Following 10-12 days in culture, sequential immunopanning was performed to separate astrocyte, microglia, and oligodendrocyte progenitor cells by agitating at 225 rpm on an orbital shaker (Innova 2000). After removing microglia via differential adhesion, purified oligodendrocyte progenitors were plated onto PLL-coated glass coverslips and cultured in differentiation medium (Neurobasal A media (Life Technologies, 10888022) with N2 (17502048), B27 (17504044), PenStrep, sodium pyruvate, 2 mM glutamax (35050-061), 40 ng/ml T3, and 5% BSA (Sigma A4503)) for two days. Treatments with palmitate (PA, 100 µM) NAD^+ (50 µM), NMN (100 µM), EX527 (5 µM) and/or 78c (3 µM) were added and cultures were allowed to differentiate for 72 hr. Positive staining for myelin proteins was compared to control levels by immunofluorescence staining and threshold quantification in ImageJ.

In experiments characterizing astrocyte responses and effects of astrocyte-conditioned media on oligodendrocytes, astrocytes were plated at a density of 450,000 cells/well on PLL-coated 6-well plates and grown for 2-3 days in serum-free Neurobasal A media containing 1% N2, 2% B27, P/S, 1mM sodium pyruvate, 0.45% glucose, 5% BSA, and 50µM β-

bioRxiv preprint doi: https://doi.org/10.1101/2020.06.10.143941; this version posted June 12, 2020. The copyright holder for this preprint (which was not certified by peer review) is the author/funder, who has granted bioRxiv a license to display the preprint in perpetuity. It is made available under aCC-BY 4.0 International license.

582 mercaptoethanol before treating with or without palmitate (PA, 100 µM) and 78c (3 µM).
583 Astrocytes were collected for an NAD^+ cycling assay or RNA isolation. Supernatants from
584 treated astrocytes were collected 24 h post-treatment and concentrated using Vivaspin sample
585 concentrators (10 and 100 kDa molecular weight cutoffs, Sigma) and stored frozen as 10x
586 protein concentrate until use for treating OLCs (Liddelow et al., 2017, Yoon et al., 2020).
587 Conditioned medium from astrocytes (ACM) was brought back to 1x concentration in
588 oligodendrocyte differentiation medium and placed on oligodendrocytes to differentiate as
589 described above.

590 **NAD^+ cycling and CD38 activity assays**

591 To determine intracellular NAD^+ levels, one well of a 6-well plate of astrocytes, or
592 approximately 20 mg of spinal cord tissue, was homogenized in 300 µl of 10% trichloroacetic
593 acid. Samples were extracted using an organic solvent mixture (1,1,2-Trichloro-1,2,2-
594 trifluoroethane and triocylamine), diluted, and measured along with a standard curve, as
595 previously described (Tarrago et al., 2018). Briefly, a cycling reagent (0.76% ethanol, 4 µM
596 FMN, 27.2 U/ml alcohol dehydrogenase, 0.44 U/ml diaphorase, and 8 µM resazurin) was
597 prepared in phosphate buffer (100 mM NaH_2PO_4/Na_2HPO_4, pH 8.0) and added to an equal
598 volume of pre-diluted cell or tissue extract. Plates were measured every 30 seconds for 1 h at
599 544nm using a SpectraMax plate reader. Raw values were normalized to protein quantification
600 (Bradford reagent, Biorad) and expressed as nmols/mg protein. For measuring CD38 NAD^+ase
601 activity, spinal cord tissue was homogenized in NETN buffer (100 mM NaCl, 1 mM EDTA, 20
602 mM Tris-HCl, and 0.5% Nonidet P-40) supplemented with 5 mM NaF and protease and
603 phosphatase inhibitors (Tarrago et al., 2018). After centrifugation (12000 rpm, 10 min),
604 supernatant volumes were adjusted to protein concentrations and reaction mix containing 50 µM

bioRxiv preprint doi: https://doi.org/10.1101/2020.06.10.143941; this version posted June 12, 2020. The copyright holder for this preprint (which was not certified by peer review) is the author/funder, who has granted bioRxiv a license to display the preprint in perpetuity. It is made available under aCC-BY 4.0 International license.

1,N6-Etheno NAD^+ in 0.25 M sucrose buffer was added at an equal volume just prior to reading the plate at 300 excitation and 410 emission every minute for 1 hr on a Spark Magellan plate reader.

Bioplex assay for cytokines

Astrocyte supernatants from cell treatments described above were used for determination of secreted cytokine levels using a Bio-Plex Mouse cytokine 23-plex assay (BioRad m60009rdpd) per manufacturer instructions, as previously described (Langley, Ghosh et al., 2017). Briefly, post-treatment medium was collected and incubated with primary antibody-conjugated magnetic beads for 30 min. Wells were washed thrice and then incubated for 30 min with detection antibodies. After washing, samples were incubated for 10 min with a streptavidin-phycoerythrin solution, and then washed again prior to resuspension and reading with a BioPlex 200 (BioRad) reader and Bio-Plex Manager software.

Organotypic cerebellar slice culture and demyelination

Organotypic cerebellar slice cultures were cultured and demyelinated using previously described methods (Birgbauer, Rao et al., 2004, Hill, Medved et al., 2014, Zhang, Jarjour et al., 2011). Cerebella were dissected from postnatal day 7-9 pups, embedded in low-melting point agar (Invitrogen 16520050), and 350 µm slices collected into artificial CSF solution using a McIlwain tissue chopper (Mickle Laboratory Engineering Co; Guildford, UK). Four slices were transferred and grown per each Millicell insert (Sigma PIHP03050) in 50% MEM, 22.5% HBSS, 24% HI Horse Serum, 1.5% Glucose, 1% GlutaMax, 1% P/S medium.

Demyelination was induced after 7 d in culture by treating with 0.5 mg/ml lysophosphatidycholine (LL, Sigma) for 18 h. Organotypic slices were placed back in LL-free medium and collected for immunohistochemistry and confocal imaging after 24 h

bioRxiv preprint doi: https://doi.org/10.1101/2020.06.10.143941; this version posted June 12, 2020. The copyright holder for this preprint (which was not certified by peer review) is the author/funder, who has granted bioRxiv a license to display the preprint in perpetuity. It is made available under aCC-BY 4.0 International license.

(demyelination) or 7 d (myelin regeneration) with or without addition of PA (100 µM) and/or 78c (3 µM) added to the growth media. Confocal images were acquired at 20x magnification from 5 regions randomly selected per slice using a Zeiss LSM 780 and Zen Software in the Mayo Clinic Microscopy and Cell Analysis Core. Images were thresholded for each stain, and immunoreactivity or counts were quantified in ImageJ.

Statistical analysis

Data were graphed with bars representing mean ± SEM with sample size for each experiment indicated in the figure legends. To determine sample size, power analysis using the fpower macro in SAS was used to determine animal numbers for each endpoint based on 80% power, α=0.05, and 4 treatment groups. Differences and SD used to determine δ were used from analysis of previous similarly-designed studies in our laboratory. No power analysis or other statistical method was used to compute sample size for cell culture experiments. Cell culture studies were repeated twice and each biological replicate per group was isolated from different pups. Assays were run in technical duplicate or triplicate.

No statistical outliers were removed, but the ROUT test in GraphPad Prism was used to check for outliers. Comparisons between two groups were analyzed by Student's t-test, whereas one-way or two-way ANOVAs with Bonferroni post-test were applied for multiple-comparisons. Analysis was performed in GraphPad Prism 7.0 software with p-values ≤ 0.05 considered significant.

Acknowledgements

78c-containing chow for these experiments was generously provided by Calico Life Sciences LLC. The diagrams within figures were created using elements from the Biomedical-PPT-Toolkit-Suite (Motifolio).

bioRxiv preprint doi: https://doi.org/10.1101/2020.06.10.143941; this version posted June 12, 2020. The copyright holder for this preprint (which was not certified by peer review) is the author/funder, who has granted bioRxiv a license to display the preprint in perpetuity. It is made available under aCC-BY 4.0 International license.

Author Contributions

IAS and MRL conceived and designed the study. MRL, CC, and TRPM conducted *in vivo* experiments and necropsies. Embedding and histological staining was performed by MRL and LK. Image acquisition and quantifications were performed by MRL under guidance from CC. MRL completed *in vitro* assays and qRT-PCR. WS and HY assisted with glial preparations and organotypic slice cultures. TRP, CCSC, and ENC provided expertise in NAD^+ quantification and experimental design as well as CD38 mice. MRL and IAS wrote the manuscript and all authors reviewed and edited the manuscript.

Conflict of Interest

ENC holds a patent on the use of CD38 inhibitors for metabolic diseases. The other authors have no conflicts of interest to disclose.

bioRxiv preprint doi: https://doi.org/10.1101/2020.06.10.143941; this version posted June 12, 2020. The copyright holder for this preprint (which was not certified by peer review) is the author/funder, who has granted bioRxiv a license to display the preprint in perpetuity. It is made available under aCC-BY 4.0 International license.

References

Aksoy P, Escande C, White TA, Thompson M, Soares S, Benech JC, Chini EN (2006) Regulation of SIRT 1 mediated NAD dependent deacetylation: a novel role for the multifunctional enzyme CD38. *Biochem Biophys Res Commun* 349: 353-9

Aksoy P, White TA, Thompson M, Chini EN (2006) Regulation of intracellular levels of NAD: a novel role for CD38. *Biochem Biophys Res Commun* 345: 1386-92

Alizadeh A, Dyck SM, Karimi-Abdolrezaee S (2015) Myelin damage and repair in pathologic CNS: challenges and prospects. *Front Mol Neurosci* 8: 35

Alizadeh A, Karimi-Abdolrezaee S (2016) Microenvironmental regulation of oligodendrocyte replacement and remyelination in spinal cord injury. *J Physiol* 594: 3539-52

Amici SA, Young NA, Narvaez-Miranda J, Jablonski KA, Arcos J, Rosas L, Papenfuss TL, Torrelles JB, Jarjour WN, Guerau-de-Arellano M (2018) CD38 Is Robustly Induced in Human Macrophages and Monocytes in Inflammatory Conditions. *Front Immunol* 9: 1593

Barbosa MT, Soares SM, Novak CM, Sinclair D, Levine JA, Aksoy P, Chini EN (2007) The enzyme CD38 (a NAD glycohydrolase, EC 3.2.2.5) is necessary for the development of diet-induced obesity. *FASEB J* 21: 3629-39

Birgbauer E, Rao TS, Webb M (2004) Lysolecithin induces demyelination in vitro in a cerebellar slice culture system. *J Neurosci Res* 78: 157-66

Blacher E, Dadali T, Bespalko A, Haupenthal VJ, Grimm MO, Hartmann T, Lund FE, Stein R, Levy A (2015) Alzheimer's disease pathology is attenuated in a CD38-deficient mouse model. *Ann Neurol* 78: 88-103

bioRxiv preprint doi: https://doi.org/10.1101/2020.06.10.143941; this version posted June 12, 2020. The copyright holder for this preprint (which was not certified by peer review) is the author/funder, who has granted bioRxiv a license to display the preprint in perpetuity. It is made available under aCC-BY 4.0 International license.

683 Boslett J, Helal M, Chini E, Zweier JL (2018) Genetic deletion of CD38 confers post-ischemic
684 myocardial protection through preserved pyridine nucleotides. *J Mol Cell Cardiol* 118: 81-
685 94

686 Boven LA, Montagne L, Nottet HS, De Groot CJ (2000) Macrophage inflammatory protein-1alpha
687 (MIP-1alpha), MIP-1beta, and RANTES mRNA semiquantification and protein expression
688 in active demyelinating multiple sclerosis (MS) lesions. *Clin Exp Immunol* 122: 257-63

689 Bruck W, Popescu B, Lucchinetti CF, Markovic-Plese S, Gold R, Thal DR, Metz I (2012)
690 Neuromyelitis optica lesions may inform multiple sclerosis heterogeneity debate. *Ann*
691 *Neurol* 72: 385-94

692 Bruzzone S, Verderio C, Schenk U, Fedele E, Zocchi E, Matteoli M, De Flora A (2004) Glutamate-
693 mediated overexpression of CD38 in astrocytes cultured with neurones. *J Neurochem* 89:
694 264-72

695 Buckman LB, Thompson MM, Lippert RN, Blackwell TS, Yull FE, Ellacott KL (2015) Evidence
696 for a novel functional role of astrocytes in the acute homeostatic response to high-fat diet
697 intake in mice. *Mol Metab* 4: 58-63

698 Buckman LB, Thompson MM, Moreno HN, Ellacott KL (2013) Regional astrogliosis in the mouse
699 hypothalamus in response to obesity. *J Comp Neurol* 521: 1322-33

700 Camacho-Pereira J, Tarrago MG, Chini CCS, Nin V, Escande C, Warner GM, Puranik AS, Schoon
701 RA, Reid JM, Galina A, Chini EN (2016) CD38 Dictates Age-Related NAD Decline and
702 Mitochondrial Dysfunction through an SIRT3-Dependent Mechanism. *Cell Metab* 23:
703 1127-1139

bioRxiv preprint doi: https://doi.org/10.1101/2020.06.10.143941; this version posted June 12, 2020. The copyright holder for this preprint (which was not certified by peer review) is the author/funder, who has granted bioRxiv a license to display the preprint in perpetuity. It is made available under aCC-BY 4.0 International license.

704 Camargo N, Goudriaan A, van Deijk AF, Otte WM, Brouwers JF, Lodder H, Gutmann DH, Nave
705 KA, Dijkhuizen RM, Mansvelder HD, Chrast R, Smit AB, Verheijen MHG (2017)
706 Oligodendroglial myelination requires astrocyte-derived lipids. *PLoS Biol* 15: e1002605
707 Canto C, Menzies KJ, Auwerx J (2015) NAD(+) Metabolism and the Control of Energy
708 Homeostasis: A Balancing Act between Mitochondria and the Nucleus. *Cell Metab* 22: 31-
709 53
710 Chiang SH, Harrington WW, Luo G, Milliken NO, Ulrich JC, Chen J, Rajpal DK, Qian Y,
711 Carpenter T, Murray R, Geske RS, Stimpson SA, Kramer HF, Haffner CD, Becherer JD,
712 Preugschat F, Billin AN (2015) Genetic Ablation of CD38 Protects against Western Diet-
713 Induced Exercise Intolerance and Metabolic Inflexibility. *PLoS One* 10: e0134927
714 Chini C, Hogan KA, Warner GM, Tarrago MG, Peclat TR, Tchkonia T, Kirkland JL, Chini E
715 (2019) The NADase CD38 is induced by factors secreted from senescent cells providing a
716 potential link between senescence and age-related cellular NAD(+) decline. *Biochem*
717 *Biophys Res Commun* 513: 486-493
718 Chini EN, Chini CCS, Espindola Netto JM, de Oliveira GC, van Schooten W (2018) The
719 Pharmacology of CD38/NADase: An Emerging Target in Cancer and Diseases of Aging.
720 *Trends Pharmacol Sci* 39: 424-436
721 Choi JW, Gardell SE, Herr DR, Rivera R, Lee CW, Noguchi K, Teo ST, Yung YC, Lu M,
722 Kennedy G, Chun J (2011) FTY720 (fingolimod) efficacy in an animal model of multiple
723 sclerosis requires astrocyte sphingosine 1-phosphate receptor 1 (S1P1) modulation. *Proc*
724 *Natl Acad Sci U S A* 108: 751-6
725 Clarke LE, Liddelow SA, Chakraborty C, Munch AE, Heiman M, Barres BA (2018) Normal aging
726 induces A1-like astrocyte reactivity. *Proc Natl Acad Sci U S A* 115: E1896-E1905

bioRxiv preprint doi: https://doi.org/10.1101/2020.06.10.143941; this version posted June 12, 2020. The copyright holder for this preprint (which was not certified by peer review) is the author/funder, who has granted bioRxiv a license to display the preprint in perpetuity. It is made available under aCC-BY 4.0 International license.

727 Clarner T, Janssen K, Nellessen L, Stangel M, Skripuletz T, Krauspe B, Hess FM, Denecke B,
728 Beutner C, Linnartz-Gerlach B, Neumann H, Vallieres L, Amor S, Ohl K, Tenbrock K,
729 Beyer C, Kipp M (2015) CXCL10 triggers early microglial activation in the cuprizone
730 model. *J Immunol* 194: 3400-13
731 Deckert J, Wetzel MC, Bartle LM, Skaletskaya A, Goldmacher VS, Vallee F, Zhou-Liu Q, Ferrari
732 P, Pouzieux S, Lahoute C, Dumontet C, Plesa A, Chiron M, Lejeune P, Chittenden T, Park
733 PU, Blanc V (2014) SAR650984, a novel humanized CD38-targeting antibody,
734 demonstrates potent antitumor activity in models of multiple myeloma and other CD38+
735 hematologic malignancies. *Clin Cancer Res* 20: 4574-83
736 Denver P, Gault VA, McClean PL (2018) Sustained high-fat diet modulates inflammation, insulin
737 signalling and cognition in mice and a modified xenin peptide ameliorates neuropathology
738 in a chronic high-fat model. *Diabetes Obes Metab* 20: 1166-1175
739 Dimas P, Montani L, Pereira JA, Moreno D, Trotzmuller M, Gerber J, Semenkovich CF, Kofeler
740 HC, Suter U (2019) CNS myelination and remyelination depend on fatty acid synthesis by
741 oligodendrocytes. *Elife* 8
742 Domingues HS, Portugal CC, Socodato R, Relvas JB (2016) Oligodendrocyte, Astrocyte, and
743 Microglia Crosstalk in Myelin Development, Damage, and Repair. *Front Cell Dev Biol* 4:
744 71
745 Escande C, Chini CC, Nin V, Dykhouse KM, Novak CM, Levine J, van Deursen J, Gores GJ, Chen
746 J, Lou Z, Chini EN (2010) Deleted in breast cancer-1 regulates SIRT1 activity and
747 contributes to high-fat diet-induced liver steatosis in mice. *J Clin Invest* 120: 545-58
748 Escande C, Nin V, Price NL, Capellini V, Gomes AP, Barbosa MT, O'Neil L, White TA, Sinclair
749 DA, Chini EN (2013) Flavonoid apigenin is an inhibitor of the NAD+ ase CD38:

bioRxiv preprint doi: https://doi.org/10.1101/2020.06.10.143941; this version posted June 12, 2020. The copyright holder for this preprint (which was not certified by peer review) is the author/funder, who has granted bioRxiv a license to display the preprint in perpetuity. It is made available under aCC-BY 4.0 International license.

implications for cellular NAD+ metabolism, protein acetylation, and treatment of metabolic syndrome. *Diabetes* 62: 1084-93

Foolad F, Khodagholi F, Javan M (2019) Sirtuins in Multiple Sclerosis: The crossroad of neurodegeneration, autoimmunity and metabolism. *Mult Scler Relat Disord* 34: 47-58

Freeman LR, Haley-Zitlin V, Rosenberger DS, Granholm AC (2014) Damaging effects of a high-fat diet to the brain and cognition: a review of proposed mechanisms. *Nutr Neurosci* 17: 241-51

Gianfrancesco MA, Acuna B, Shen L, Briggs FB, Quach H, Bellesis KH, Bernstein A, Hedstrom AK, Kockum I, Alfredsson L, Olsson T, Schaefer C, Barcellos LF (2014) Obesity during childhood and adolescence increases susceptibility to multiple sclerosis after accounting for established genetic and environmental risk factors. *Obes Res Clin Pract* 8: e435-47

Ginwala R, McTish E, Raman C, Singh N, Nagarkatti M, Nagarkatti P, Sagar D, Jain P, Khan ZK (2016) Apigenin, a Natural Flavonoid, Attenuates EAE Severity Through the Modulation of Dendritic Cell and Other Immune Cell Functions. *J Neuroimmune Pharmacol* 11: 36-47

Graham LC, Grabowska WA, Chun Y, Risacher SL, Philip VM, Saykin AJ, Alzheimer's Disease Neuroimaging I, Sukoff Rizzo SJ, Howell GR (2019) Exercise prevents obesity-induced cognitive decline and white matter damage in mice. *Neurobiol Aging* 80: 154-172

Haffner CD, Becherer JD, Boros EE, Cadilla R, Carpenter T, Cowan D, Deaton DN, Guo Y, Harrington W, Henke BR, Jeune MR, Kaldor I, Milliken N, Petrov KG, Preugschat F, Schulte C, Shearer BG, Shearer T, Smalley TL, Jr., Stewart EL et al. (2015) Discovery, Synthesis, and Biological Evaluation of Thiazoloquin(az)olin(on)es as Potent CD38 Inhibitors. *J Med Chem* 58: 3548-71

bioRxiv preprint doi: https://doi.org/10.1101/2020.06.10.143941; this version posted June 12, 2020. The copyright holder for this preprint (which was not certified by peer review) is the author/funder, who has granted bioRxiv a license to display the preprint in perpetuity. It is made available under aCC-BY 4.0 International license.

772 Haider L, Fischer MT, Frischer JM, Bauer J, Hoftberger R, Botond G, Esterbauer H, Binder CJ,
773 Witztum JL, Lassmann H (2011) Oxidative damage in multiple sclerosis lesions. *Brain* 134:
774 1914-24
775 Harlan BA, Pehar M, Sharma DR, Beeson G, Beeson CC, Vargas MR (2016) Enhancing NAD+
776 Salvage Pathway Reverts the Toxicity of Primary Astrocytes Expressing Amyotrophic
777 Lateral Sclerosis-linked Mutant Superoxide Dismutase 1 (SOD1). *J Biol Chem* 291: 10836-
778 46
779 Hasan M, Seo JE, Rahaman KA, Min H, Kim KH, Park JH, Sung C, Son J, Kang MJ, Jung BH,
780 Park WS, Kwon OS (2017) Novel genes in brain tissues of EAE-induced normal and obese
781 mice: Upregulation of metal ion-binding protein genes in obese-EAE mice. *Neuroscience*
782 343: 322-336
783 Hathorn T, Snyder-Keller A, Messer A (2011) Nicotinamide improves motor deficits and
784 upregulates PGC-1alpha and BDNF gene expression in a mouse model of Huntington's
785 disease. *Neurobiol Dis* 41: 43-50
786 Hattori T, Kaji M, Ishii H, Jureepon R, Takarada-Iemata M, Minh Ta H, Manh Le T, Konno A,
787 Hirai H, Shiraishi Y, Ozaki N, Yamamoto Y, Okamoto H, Yokoyama S, Higashida H,
788 Kitao Y, Hori O (2017) CD38 positively regulates postnatal development of astrocytes cell-
789 autonomously and oligodendrocytes non-cell-autonomously. *Glia* 65: 974-989
790 Herrmann MM, Barth S, Greve B, Schumann KM, Bartels A, Weissert R (2016) Identification of
791 gene expression patterns crucially involved in experimental autoimmune encephalomyelitis
792 and multiple sclerosis. *Dis Model Mech* 9: 1211-1220
793 Hill RA, Medved J, Patel KD, Nishiyama A (2014) Organotypic slice cultures to study
794 oligodendrocyte dynamics and myelination. *J Vis Exp*: e51835

bioRxiv preprint doi: https://doi.org/10.1101/2020.06.10.143941; this version posted June 12, 2020. The copyright holder for this preprint (which was not certified by peer review) is the author/funder, who has granted bioRxiv a license to display the preprint in perpetuity. It is made available under aCC-BY 4.0 International license.

795 Hoffmann FS, Hofereiter J, Rubsamen H, Melms J, Schwarz S, Faber H, Weber P, Putz B, Loleit
796 V, Weber F, Hohlfeld R, Meinl E, Krumbholz M (2015) Fingolimod induces
797 neuroprotective factors in human astrocytes. *J Neuroinflammation* 12: 184
798 Iqbal J, Zaidi M (2007) CD38 is required for priming by TNF-alpha: a mechanism for extracellular
799 coordination of cell fate. *Am J Physiol Renal Physiol* 292: F1283-90
800 Jablonska B, Gierdalski M, Chew LJ, Hawley T, Catron M, Lichauco A, Cabrera-Luque J, Yuen T,
801 Rowitch D, Gallo V (2016) Sirt1 regulates glial progenitor proliferation and regeneration in
802 white matter after neonatal brain injury. *Nat Commun* 7: 13866
803 Janssen K, Rickert M, Clarner T, Beyer C, Kipp M (2016) Absence of CCL2 and CCL3
804 Ameliorates Central Nervous System Grey Matter But Not White Matter Demyelination in
805 the Presence of an Intact Blood-Brain Barrier. *Mol Neurobiol* 53: 1551-1564
806 Ji S, Doucette JR, Nazarali AJ (2011) Sirt2 is a novel in vivo downstream target of Nkx2.2 and
807 enhances oligodendroglial cell differentiation. *J Mol Cell Biol* 3: 351-9
808 Ji Z, Wu S, Xu Y, Qi J, Su X, Shen L (2019) Obesity Promotes EAE Through IL-6 and CCL-2-
809 Mediated T Cells Infiltration. *Front Immunol* 10: 1881
810 Karim H, Kim SH, Lapato AS, Yasui N, Katzenellenbogen JA, Tiwari-Woodruff SK (2018)
811 Increase in chemokine CXCL1 by ERbeta ligand treatment is a key mediator in promoting
812 axon myelination. *Proc Natl Acad Sci U S A* 115: 6291-6296
813 Kiray H, Lindsay SL, Hosseinzadeh S, Barnett SC (2016) The multifaceted role of astrocytes in
814 regulating myelination. *Exp Neurol* 283: 541-9
815 Kou W, Banerjee S, Eudy J, Smith LM, Persidsky R, Borgmann K, Wu L, Sakhuja N, Deshpande
816 MS, Walseth TF, Ghorpade A (2009) CD38 regulation in activated astrocytes: implications
817 for neuroinflammation and HIV-1 brain infection. *J Neurosci Res* 87: 2326-39

bioRxiv preprint doi: https://doi.org/10.1101/2020.06.10.143941; this version posted June 12, 2020. The copyright holder for this preprint (which was not certified by peer review) is the author/funder, who has granted bioRxiv a license to display the preprint in perpetuity. It is made available under aCC-BY 4.0 International license.

818 Langley M, Ghosh A, Charli A, Sarkar S, Ay M, Luo J, Zielonka J, Brenza T, Bennett B, Jin H,
819 Ghaisas S, Schlichtmann B, Kim D, Anantharam V, Kanthasamy A, Narasimhan B,
820 Kalyanaraman B, Kanthasamy AG (2017) Mito-Apocynin Prevents Mitochondrial
821 Dysfunction, Microglial Activation, Oxidative Damage, and Progressive
822 Neurodegeneration in MitoPark Transgenic Mice. *Antioxid Redox Signal* 27: 1048-1066
823 Langley MR, Yoon H, Kim HN, Choi CI, Simon W, Kleppe L, Lanza IR, LeBrasseur NK,
824 Matveyenko A, Scarisbrick IA (2019) High fat diet consumption results in mitochondrial
825 dysfunction, oxidative stress, and oligodendrocyte loss in the central nervous system.
826 *Biochim Biophys Acta Mol Basis Dis*: 165630
827 Lassmann H, van Horssen J (2016) Oxidative stress and its impact on neurons and glia in multiple
828 sclerosis lesions. *Biochim Biophys Acta* 1862: 506-10
829 Li J, Dou X, Li S, Zhang X, Zeng Y, Song Z (2015) Nicotinamide ameliorates palmitate-induced
830 ER stress in hepatocytes via cAMP/PKA/CREB pathway-dependent Sirt1 upregulation.
831 *Biochim Biophys Acta* 1853: 2929-36
832 Liao PC, Lai MH, Hsu KP, Kuo YH, Chen J, Tsai MC, Li CX, Yin XJ, Jeyashoke N, Chao LK
833 (2018) Identification of beta-Sitosterol as in Vitro Anti-Inflammatory Constituent in
834 Moringa oleifera. *J Agric Food Chem* 66: 10748-10759
835 Liddelow SA, Guttenplan KA, Clarke LE, Bennett FC, Bohlen CJ, Schirmer L, Bennett ML,
836 Munch AE, Chung WS, Peterson TC, Wilton DK, Frouin A, Napier BA, Panicker N,
837 Kumar M, Buckwalter MS, Rowitch DH, Dawson VL, Dawson TM, Stevens B et al. (2017)
838 Neurotoxic reactive astrocytes are induced by activated microglia. *Nature* 541: 481-487
839 Lokhorst HM, Plesner T, Laubach JP, Nahi H, Gimsing P, Hansson M, Minnema MC, Lassen U,
840 Krejcik J, Palumbo A, van de Donk NW, Ahmadi T, Khan I, Uhlar CM, Wang J, Sasser

bioRxiv preprint doi: https://doi.org/10.1101/2020.06.10.143941; this version posted June 12, 2020. The copyright holder for this preprint (which was not certified by peer review) is the author/funder, who has granted bioRxiv a license to display the preprint in perpetuity. It is made available under aCC-BY 4.0 International license.

AK, Losic N, Lisby S, Basse L, Brun N et al. (2015) Targeting CD38 with Daratumumab Monotherapy in Multiple Myeloma. *N Engl J Med* 373: 1207-19

Long A, Klimova N, Kristian T (2017) Mitochondrial NUDIX hydrolases: A metabolic link between NAD catabolism, GTP and mitochondrial dynamics. *Neurochem Int* 109: 193-201

Machado-Santos J, Saji E, Troscher AR, Paunovic M, Liblau R, Gabriely G, Bien CG, Bauer J, Lassmann H (2018) The compartmentalized inflammatory response in the multiple sclerosis brain is composed of tissue-resident CD8+ T lymphocytes and B cells. *Brain* 141: 2066-2082

Mamik MK, Banerjee S, Walseth TF, Hirte R, Tang L, Borgmann K, Ghorpade A (2011) HIV-1 and IL-1beta regulate astrocytic CD38 through mitogen-activated protein kinases and nuclear factor-kappaB signaling mechanisms. *J Neuroinflammation* 8: 145

Manouchehrinia A, Hedstrom AK, Alfredsson L, Olsson T, Hillert J, Ramanujam R (2018) Association of Pre-Disease Body Mass Index With Multiple Sclerosis Prognosis. *Front Neurol* 9: 232

Marrie RA, Rudick R, Horwitz R, Cutter G, Tyry T, Campagnolo D, Vollmer T (2010) Vascular comorbidity is associated with more rapid disability progression in multiple sclerosis. *Neurology* 74: 1041-7

Martin T, Baz R, Benson DM, Lendvai N, Wolf J, Munster P, Lesokhin AM, Wack C, Charpentier E, Campana F, Vij R (2017) A phase 1b study of isatuximab plus lenalidomide and dexamethasone for relapsed/refractory multiple myeloma. *Blood* 129: 3294-3303

Matalonga J, Glaria E, Bresque M, Escande C, Carbo JM, Kiefer K, Vicente R, Leon TE, Beceiro S, Pascual-Garcia M, Serret J, Sanjurjo L, Moron-Ros S, Riera A, Paytubi S, Juarez A, Sotillo F, Lindbom L, Caelles C, Sarrias MR et al. (2017) The Nuclear Receptor LXR

bioRxiv preprint doi: https://doi.org/10.1101/2020.06.10.143941; this version posted June 12, 2020. The copyright holder for this preprint (which was not certified by peer review) is the author/funder, who has granted bioRxiv a license to display the preprint in perpetuity. It is made available under aCC-BY 4.0 International license.

Limits Bacterial Infection of Host Macrophages through a Mechanism that Impacts Cellular NAD Metabolism. *Cell Rep* 18: 1241-1255

Miller ED, Dziedzic A, Saluk-Bijak J, Bijak M (2019) A Review of Various Antioxidant Compounds and their Potential Utility as Complementary Therapy in Multiple Sclerosis. *Nutrients* 11

Mizunoya W, Ohnuki K, Baba K, Miyahara H, Shimizu N, Tabata K, Kino T, Sato Y, Tatsumi R, Ikeuchi Y (2013) Effect of dietary fat type on anxiety-like and depression-like behavior in mice. *Springerplus* 2: 165

Mokry LE, Ross S, Timpson NJ, Sawcer S, Davey Smith G, Richards JB (2016) Obesity and Multiple Sclerosis: A Mendelian Randomization Study. *PLoS Med* 13: e1002053

Mori F, Nistico R, Nicoletti CG, Zagaglia S, Mandolesi G, Piccinin S, Martino G, Finardi A, Rossini PM, Marfia GA, Furlan R, Centonze D (2016) RANTES correlates with inflammatory activity and synaptic excitability in multiple sclerosis. *Mult Scler* 22: 1405-1412

Moyon S, Dubessy AL, Aigrot MS, Trotter M, Huang JK, Dauphinot L, Potier MC, Kerninon C, Melik Parsadaniantz S, Franklin RJ, Lubetzki C (2015) Demyelination causes adult CNS progenitors to revert to an immature state and express immune cues that support their migration. *J Neurosci* 35: 4-20

Negrotto L, Farez MF, Correale J (2016) Immunologic Effects of Metformin and Pioglitazone Treatment on Metabolic Syndrome and Multiple Sclerosis. *JAMA Neurol* 73: 520-8

Ogrodnik M, Zhu Y, Langhi LGP, Tchkonia T, Kruger P, Fielder E, Victorelli S, Ruswhandi RA, Giorgadze N, Pirtskhalava T, Podgorni O, Enikolopov G, Johnson KO, Xu M, Inman C,

bioRxiv preprint doi: https://doi.org/10.1101/2020.06.10.143941; this version posted June 12, 2020. The copyright holder for this preprint (which was not certified by peer review) is the author/funder, who has granted bioRxiv a license to display the preprint in perpetuity. It is made available under aCC-BY 4.0 International license.

886 Palmer AK, Schafer M, Weigl M, Ikeno Y, Burns TC et al. (2019) Obesity-Induced
887 Cellular Senescence Drives Anxiety and Impairs Neurogenesis. *Cell Metab*
888 Ohtomo R, Iwata A, Arai K (2018) Molecular Mechanisms of Oligodendrocyte Regeneration in
889 White Matter-Related Diseases. *Int J Mol Sci* 19
890 Olsson T, Barcellos LF, Alfredsson L (2017) Interactions between genetic, lifestyle and
891 environmental risk factors for multiple sclerosis. *Nat Rev Neurol* 13: 25-36
892 Partida-Sanchez S, Cockayne DA, Monard S, Jacobson EL, Oppenheimer N, Garvy B, Kusser K,
893 Goodrich S, Howard M, Harmsen A, Randall TD, Lund FE (2001) Cyclic ADP-ribose
894 production by CD38 regulates intracellular calcium release, extracellular calcium influx and
895 chemotaxis in neutrophils and is required for bacterial clearance in vivo. *Nat Med* 7: 1209-
896 16
897 Pavelek Z, Vysata O, Sobisek L, Klimova B, Andrys C, Vokurkova D, Mazurova R, Stourac P,
898 Valis M (2018) Lymphocyte populations and their change during five-year glatiramer
899 acetate treatment. *Neurol Neurochir Pol* 52: 587-592
900 Penberthy WT, Tsunoda I (2009) The importance of NAD in multiple sclerosis. *Curr Pharm Des*
901 15: 64-99
902 Peng QY, Wang YM, Chen CX, Zou Y, Zhang LN, Deng SY, Ai YH (2018) Inhibiting the
903 CD38/cADPR pathway protected rats against sepsis associated brain injury. *Brain Res*
904 1678: 56-63
905 Penke M, Schuster S, Gorski T, Gebhardt R, Kiess W, Garten A (2017) Oleate ameliorates
906 palmitate-induced reduction of NAMPT activity and NAD levels in primary human
907 hepatocytes and hepatocarcinoma cells. *Lipids Health Dis* 16: 191

bioRxiv preprint doi: https://doi.org/10.1101/2020.06.10.143941; this version posted June 12, 2020. The copyright holder for this preprint (which was not certified by peer review) is the author/funder, who has granted bioRxiv a license to display the preprint in perpetuity. It is made available under aCC-BY 4.0 International license.

908 Ponath G, Park C, Pitt D (2018) The Role of Astrocytes in Multiple Sclerosis. *Front Immunol* 9:
909 217
910 Ponath G, Ramanan S, Mubarak M, Housley W, Lee S, Sahinkaya FR, Vortmeyer A, Raine CS,
911 Pitt D (2017) Myelin phagocytosis by astrocytes after myelin damage promotes lesion
912 pathology. *Brain* 140: 399-413
913 Prola A, Pires Da Silva J, Guilbert A, Lecru L, Piquereau J, Ribeiro M, Mateo P, Gressette M,
914 Fortin D, Boursier C, Gallerne C, Caillard A, Samuel JL, Francois H, Sinclair DA, Eid P,
915 Ventura-Clapier R, Garnier A, Lemaire C (2017) SIRT1 protects the heart from ER stress-
916 induced cell death through eIF2alpha deacetylation. *Cell Death Differ* 24: 343-356
917 Roboon J, Hattori T, Ishii H, Takarada-Iemata M, Le TM, Shiraishi Y, Ozaki N, Yamamoto Y,
918 Sugawara A, Okamoto H, Higashida H, Kitao Y, Hori O (2019) Deletion of CD38
919 Suppresses Glial Activation and Neuroinflammation in a Mouse Model of Demyelination.
920 *Front Cell Neurosci* 13: 258
921 Sadeghi A, Seyyed Ebrahimi SS, Golestani A, Meshkani R (2017) Resveratrol Ameliorates
922 Palmitate-Induced Inflammation in Skeletal Muscle Cells by Attenuating Oxidative Stress
923 and JNK/NF-kappaB Pathway in a SIRT1-Independent Mechanism. *J Cell Biochem* 118:
924 2654-2663
925 Sarkar S, Malovic E, Harishchandra DS, Ghaisas S, Panicker N, Charli A, Palanisamy BN, Rokad
926 D, Jin H, Anantharam V, Kanthasamy A, Kanthasamy AG (2017) Mitochondrial
927 impairment in microglia amplifies NLRP3 inflammasome proinflammatory signaling in cell
928 culture and animal models of Parkinson's disease. *NPJ Parkinsons Dis* 3: 30
929 Stein LR, Imai S (2014) Specific ablation of Nampt in adult neural stem cells recapitulates their
930 functional defects during aging. *EMBO J* 33: 1321-40

bioRxiv preprint doi: https://doi.org/10.1101/2020.06.10.143941; this version posted June 12, 2020. The copyright holder for this preprint (which was not certified by peer review) is the author/funder, who has granted bioRxiv a license to display the preprint in perpetuity. It is made available under aCC-BY 4.0 International license.

931 Tarrago MG, Chini CCS, Kanamori KS, Warner GM, Caride A, de Oliveira GC, Rud M, Samani
932 A, Hein KZ, Huang R, Jurk D, Cho DS, Boslett JJ, Miller JD, Zweier JL, Passos JF, Doles
933 JD, Becherer DJ, Chini EN (2018) A Potent and Specific CD38 Inhibitor Ameliorates Age-
934 Related Metabolic Dysfunction by Reversing Tissue NAD(+) Decline. *Cell Metab* 27:
935 1081-1095 e10
936 Tejera-Alhambra M, Casrouge A, de Andres C, Seyfferth A, Ramos-Medina R, Alonso B, Vega J,
937 Fernandez-Paredes L, Albert ML, Sanchez-Ramon S (2015) Plasma biomarkers
938 discriminate clinical forms of multiple sclerosis. *PLoS One* 10: e0128952
939 Tettey P, Simpson S, Jr., Taylor B, Blizzard L, Ponsonby AL, Dwyer T, Kostner K, van der Mei I
940 (2014) An adverse lipid profile is associated with disability and progression in disability, in
941 people with MS. *Mult Scler* 20: 1737-44
942 Thaler JP, Yi CX, Schur EA, Guyenet SJ, Hwang BH, Dietrich MO, Zhao X, Sarruf DA, Izgur V,
943 Maravilla KR, Nguyen HT, Fischer JD, Matsen ME, Wisse BE, Morton GJ, Horvath TL,
944 Baskin DG, Tschop MH, Schwartz MW (2012) Obesity is associated with hypothalamic
945 injury in rodents and humans. *J Clin Invest* 122: 153-62
946 Timmermans S, Bogie JF, Vanmierlo T, Lutjohann D, Stinissen P, Hellings N, Hendriks JJ (2014)
947 High fat diet exacerbates neuroinflammation in an animal model of multiple sclerosis by
948 activation of the Renin Angiotensin system. *J Neuroimmune Pharmacol* 9: 209-17
949 Valentin-Torres A, Savarin C, Hinton DR, Phares TW, Bergmann CC, Stohlman SA (2016)
950 Sustained TNF production by central nervous system infiltrating macrophages promotes
951 progressive autoimmune encephalomyelitis. *J Neuroinflammation* 13: 46
952 van de Donk N, Richardson PG, Malavasi F (2018) CD38 antibodies in multiple myeloma: back to
953 the future. *Blood* 131: 13-29

bioRxiv preprint doi: https://doi.org/10.1101/2020.06.10.143941; this version posted June 12, 2020. The copyright holder for this preprint (which was not certified by peer review) is the author/funder, who has granted bioRxiv a license to display the preprint in perpetuity. It is made available under aCC-BY 4.0 International license.

954 Wang C, Zhang Y, Ding J, Zhao Z, Qian C, Luan Y, Teng GJ (2017) Nicotinamide Administration
955 Improves Remyelination after Stroke. *Neural Plast* 2017: 7019803
956 Wang J, Zhao C, Kong P, Sun H, Sun Z, Bian G, Sun Y, Guo L (2016) Treatment with NAD(+)
957 inhibited experimental autoimmune encephalomyelitis by activating AMPK/SIRT1
958 signaling pathway and modulating Th1/Th17 immune responses in mice. *Int*
959 *Immunopharmacol* 39: 287-94
960 Wang YM, Liu ZY, Ai YH, Zhang LN, Zou Y, Peng QY (2017) Blocking the CD38/cADPR
961 pathway plays a double-edged role in LPS stimulated microglia. *Neuroscience* 361: 34-42
962 Wanrooy BJ, Kumar KP, Wen SW, Qin CX, Ritchie RH, Wong CHY (2018) Distinct contributions
963 of hyperglycemia and high-fat feeding in metabolic syndrome-induced neuroinflammation.
964 *J Neuroinflammation* 15: 293
965 Wilhelm F, Hirrlinger J (2012) Multifunctional roles of NAD(+) and NADH in astrocytes.
966 *Neurochem Res* 37: 2317-25
967 Wilms H, Sievers J, Rickert U, Rostami-Yazdi M, Mrowietz U, Lucius R (2010) Dimethylfumarate
968 inhibits microglial and astrocytic inflammation by suppressing the synthesis of nitric oxide,
969 IL-1beta, TNF-alpha and IL-6 in an in-vitro model of brain inflammation. *J*
970 *Neuroinflammation* 7: 30
971 Yoon H, Choi CI, Triplet EM, Langley MR, Kleppe LS, Kim HN, Simon WL, Scarisbrick IA
972 (2020) Blocking the Thrombin Receptor Promotes Repair of Demyelinated Lesions in the
973 Adult Brain. *J Neurosci* 40: 1483-1500
974 Yoon H, Kleven A, Paulsen A, Kleppe L, Wu J, Ying Z, Gomez-Pinilla F, Scarisbrick IA (2016)
975 Interplay between exercise and dietary fat modulates myelinogenesis in the central nervous
976 system. *Biochim Biophys Acta* 1862: 545-55

bioRxiv preprint doi: https://doi.org/10.1101/2020.06.10.143941; this version posted June 12, 2020. The copyright holder for this preprint (which was not certified by peer review) is the author/funder, who has granted bioRxiv a license to display the preprint in perpetuity. It is made available under aCC-BY 4.0 International license.

977 Zhang H, Jarjour AA, Boyd A, Williams A (2011) Central nervous system remyelination in
978 culture--a tool for multiple sclerosis research. *Exp Neurol* 230: 138-48
979 Zhang Y, Chen K, Sloan SA, Bennett ML, Scholze AR, O'Keeffe S, Phatnani HP, Guarnieri P,
980 Caneda C, Ruderisch N, Deng S, Liddelow SA, Zhang C, Daneman R, Maniatis T, Barres
981 BA, Wu JQ (2014) An RNA-sequencing transcriptome and splicing database of glia,
982 neurons, and vascular cells of the cerebral cortex. *J Neurosci* 34: 11929-47
983 Zhang Y, Sloan SA, Clarke LE, Caneda C, Plaza CA, Blumenthal PD, Vogel H, Steinberg GK,
984 Edwards MS, Li G, Duncan JA, 3rd, Cheshier SH, Shuer LM, Chang EF, Grant GA,
985 Gephart MG, Barres BA (2016) Purification and Characterization of Progenitor and Mature
986 Human Astrocytes Reveals Transcriptional and Functional Differences with Mouse. *Neuron*
987 89: 37-53
988 Zou Y, He X, Peng QY, Guo QL (2017) Inhibition of CD38/Cyclic ADP-ribose Pathway Protects
989 Rats against Ropivacaine-induced Convulsion. *Chin Med J (Engl)* 130: 2354-2360

990

991

bioRxiv preprint doi: https://doi.org/10.1101/2020.06.10.143941; this version posted June 12, 2020. The copyright holder for this preprint (which was not certified by peer review) is the author/funder, who has granted bioRxiv a license to display the preprint in perpetuity. It is made available under aCC-BY 4.0 International license.

992 **Figures and Figure Legends**

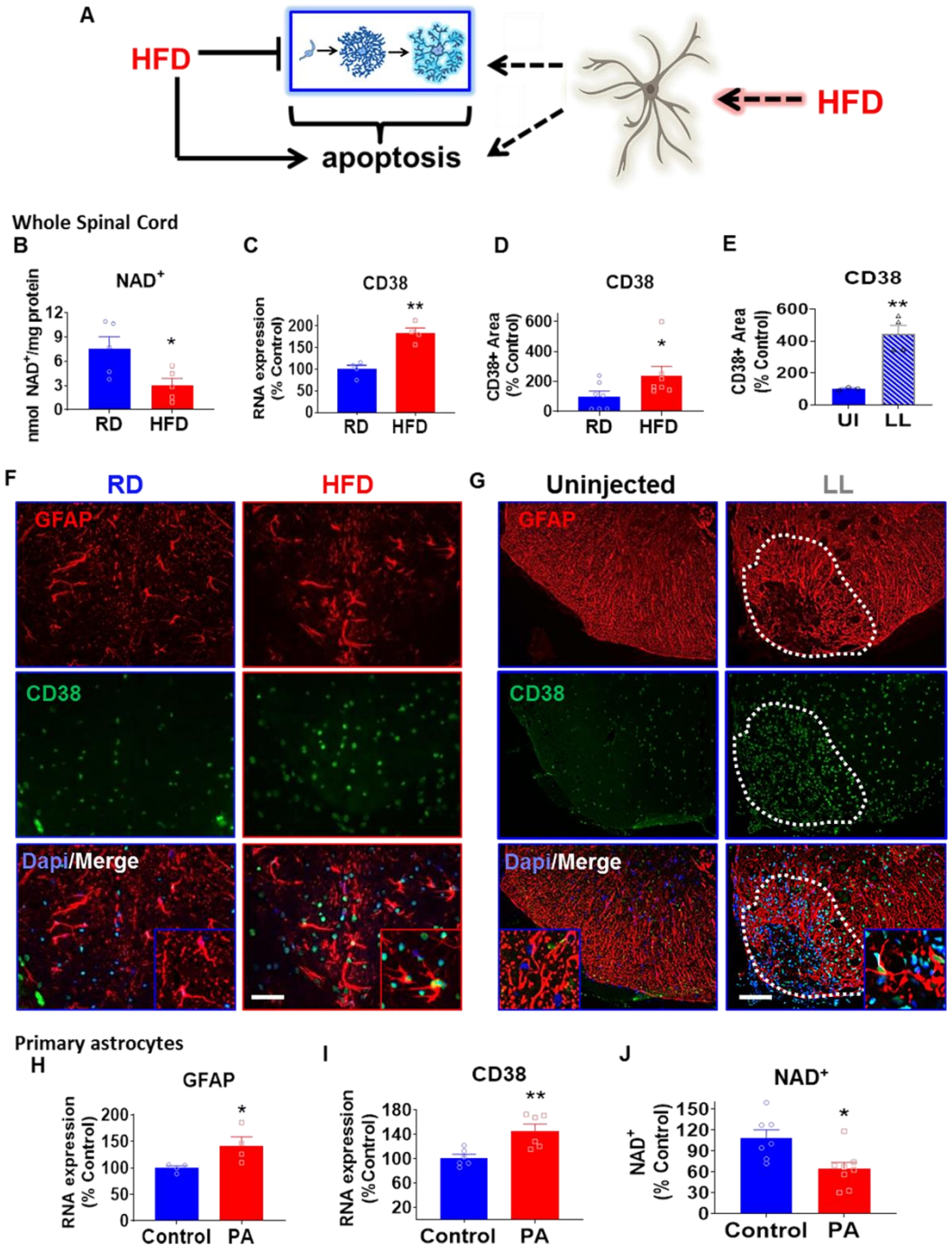

993

994 **<u>Figure 1.</u> CD38 expression in astrocytes of chronic HFD-fed mice and in a model of**

995 **demyelination.**

bioRxiv preprint doi: https://doi.org/10.1101/2020.06.10.143941; this version posted June 12, 2020. The copyright holder for this preprint (which was not certified by peer review) is the author/funder, who has granted bioRxiv a license to display the preprint in perpetuity. It is made available under aCC-BY 4.0 International license.

A Schematic representation of previously shown direct effects of high fat diet (HFD) on oligodendrocyte lineage cells including apoptosis and impaired differentiation with potential astrocyte-mediated indirect effects, represented by dotted lines, that comprise the hypothesis to be tested.

B Spinal cord tissue of regular diet (RD) and high fat diet (HFD) mice showing a depletion of NAD^+ after 12 wk (n=5 mice/group) as determined by cycling assay.

C Increased RNA expression of CD38 (n=4), assessed by qPCR, in spinal cord tissue of HFD-fed mice when compared to RD-fed mice.

D- G Immunofluorescence staining with double-labeling (***F, G***) and corresponding quantification (***D, E)*** indicates increased CD38 (green) immunoreactivity in astrocytes (GFAP, red) within the spinal cords of HFD-fed mice (***D***, ***F,*** n=7) or in the lysolecithin (LL) model of experimental demyelination (***E***, ***G,*** n=4)versus the uninjected (UI) side. Broken white line (***G***) designates lesion boundary. Scale bar = 50 µm (***F***) and 100µm (***G***).

H-J High fat consumption was modeled in primary murine astrocyte cultures by including saturated fat palmitate in the media (PA, 100 µM, 24 h). Increases in RNA expression of GFAP (***H,*** n=4) and CD38 (**I,** n=6) were observed in PA-containing astrocyte cultures. ***J***, Depleted NAD^+ levels were found in PA-treated astrocytes when assessed using an NAD^+ cycling assay, n=7-8. Bar graphs represent the mean +/- SEM. Asterisks indicate levels of statistical significance as determined by Student's t-test, where *, $p<0.05$; **, $p<0.01$; ***, $p<0.001$.

The following figure supplement is available for figure1:

Figure 1- Figure Supplement 1. CD38 RNA expression in mouse spinal cord tissue.

Figure 1- Source Data 1.

bioRxiv preprint doi: https://doi.org/10.1101/2020.06.10.143941; this version posted June 12, 2020. The copyright holder for this preprint (which was not certified by peer review) is the author/funder, who has granted bioRxiv a license to display the preprint in perpetuity. It is made available under aCC-BY 4.0 International license.

1019

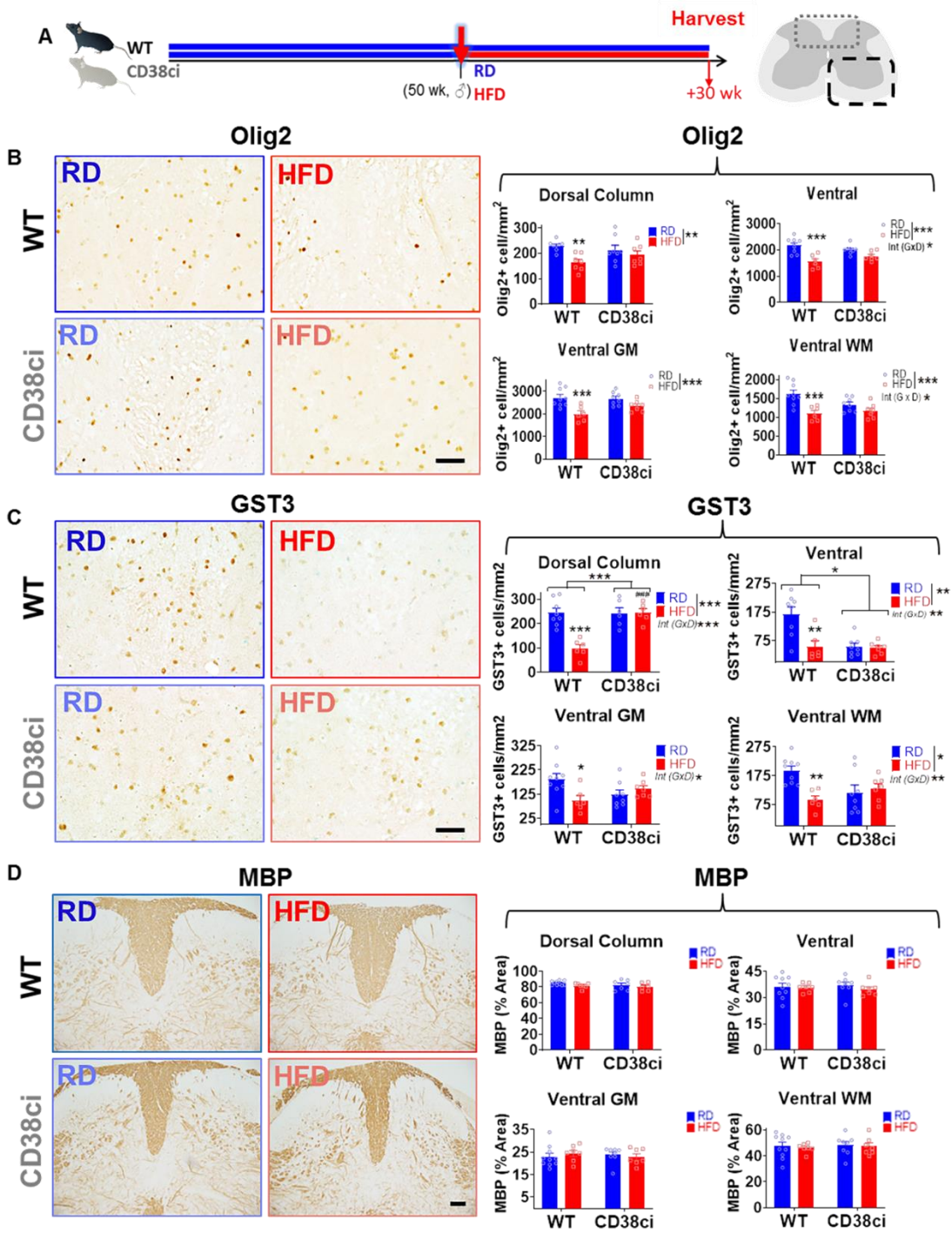

1020

1021 **Figure 2. CD38-catalytically inactive (CD38ci) mice are resistant to HFD-induced**

1022 **oligodendrocyte loss.**

bioRxiv preprint doi: https://doi.org/10.1101/2020.06.10.143941; this version posted June 12, 2020. The copyright holder for this preprint (which was not certified by peer review) is the author/funder, who has granted bioRxiv a license to display the preprint in perpetuity. It is made available under aCC-BY 4.0 International license.

Histological analysis from wildtype (WT) and CD38-catalytically inactive mice (CD38ci) fed a regular diet (RD) or high fat diet (HFD) for 30 wk beginning at 50 wk of age. Red and blue outlined regions depict regions imaged and quantified, including dorsal column and ventral white matter (broken gray line) and ventral grey matter (broken black line).

A Schematic depicting experimental design for diets administration.

B-C Olig2+ oligodendrocyte lineage cells (***B***) and GST3+ mature oligodendrocytes (***C***) were significantly depleted in HFD-fed WT mice, yet CD38ci mice fed a HFD had no reduction in oligodendrocyte numbers. When compared to WT-HFD mice, CD38ci-HFD mice had significantly more oligodendrocytes remaining in the dorsal column (representative images pictured; ###, $p<0.001$). Scale bar = 50 μm.

D Representative images of immunohistochemical staining of the dorsal column and quantification of the dorsal column and ventral grey matter and white matter of the spinal cords confirming no significant changes in MBP immunoreactivity across genotype or diet groups. Scale bar= 100 μm.

Bar graphs represent mean +/- SEM. Two-way ANOVA followed by Bonferroni post-hoc test (n=7-10 mice/group). Asterisks indicate levels of statistical significance when compared to control, where *, $p<0.05$; **, $p<0.01$; ***, $p<0.001$.

The following figure supplement is available for figure 2:

Figure 2- Figure Supplement 1. Effect of direct CD38 inhibition on oligodendrocyte progenitors.

Figure 2- Source Data 1.

bioRxiv preprint doi: https://doi.org/10.1101/2020.06.10.143941; this version posted June 12, 2020. The copyright holder for this preprint (which was not certified by peer review) is the author/funder, who has granted bioRxiv a license to display the preprint in perpetuity. It is made available under aCC-BY 4.0 International license.

1046

1047

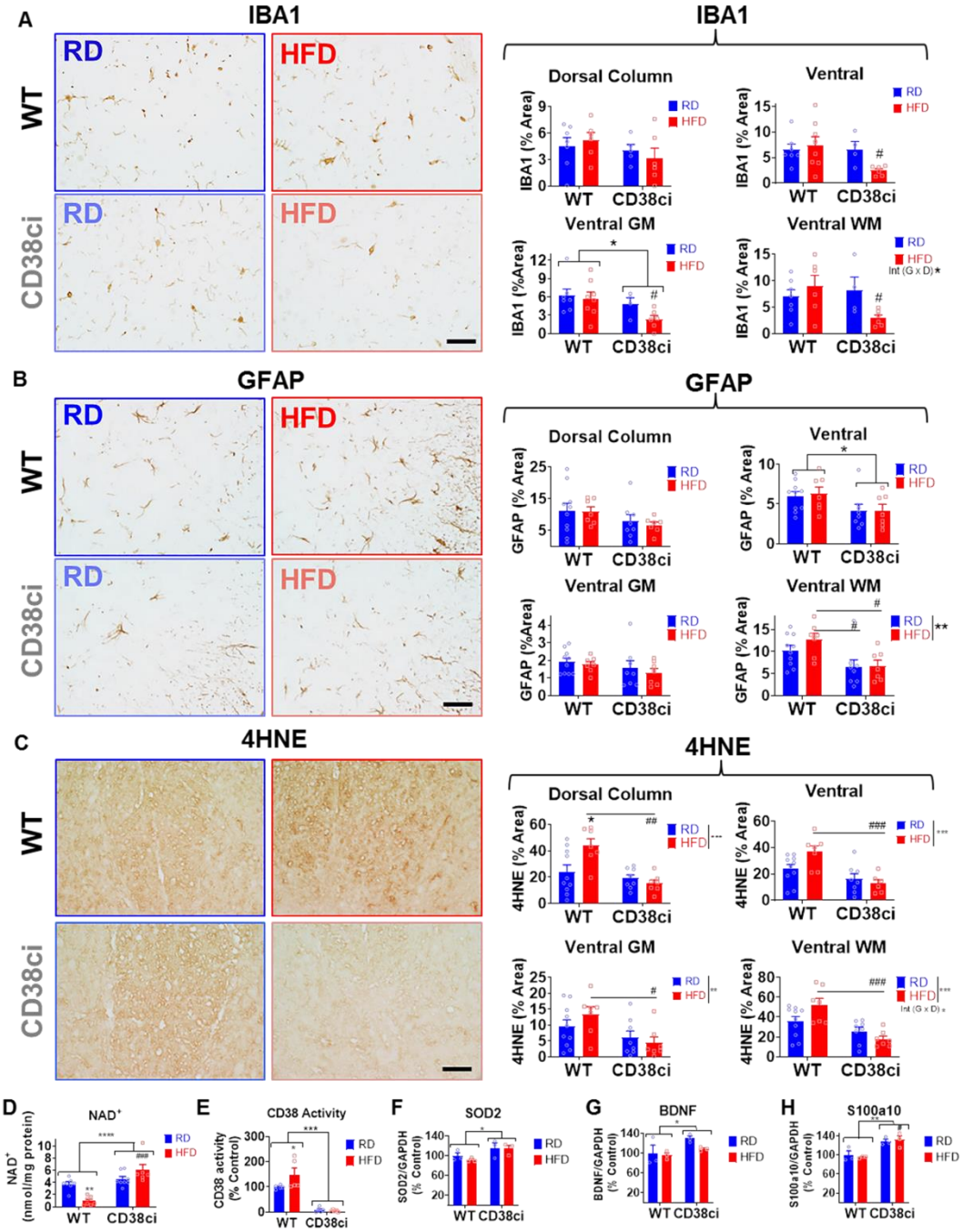

1048

1049 **<u>Figure 3.</u> Diminished neuroinflammatory responses in CD38 catalytically inactive (CD38ci)**

1050 **mice following chronic HFD.**

bioRxiv preprint doi: https://doi.org/10.1101/2020.06.10.143941; this version posted June 12, 2020. The copyright holder for this preprint (which was not certified by peer review) is the author/funder, who has granted bioRxiv a license to display the preprint in perpetuity. It is made available under aCC-BY 4.0 International license.

Histological analysis from wildtype (WT) and CD38-catalytically inactive mice (CD38ci) fed a regular diet (RD) or high fat diet (HFD) for 30 wk beginning at 50 wk of age. Scale bar= 50 µm. and n=7-10 mice/group.

A Representative images of the ventral white matter and immunohistochemical analysis of spinal cord regions demonstrates decreased microgliosis (IBA1) in CD38ci mice. When compared to WT-HFD mice, CD38ci-HFD mice had significantly less IBA1+ immunoreactivity in the spinal cord ventral gray and white matter.

B Representative images of the ventral white matter and corresponding quantification confirm reduced astrogliosis (GFAP) in the spinal cords of CD38 catalytically inactive (CD38ci) mice overall when compared to wildtype (WT) mice. Decreased GFAP+ immunoreactivity in the ventral white matter when compared to HFD mice.

C Representative images of the dorsal column and quantification of the spinal cords confirming significant changes in 4HNE immunoreactivity, an oxidative stress marker, between genotypes for HFD mice.

D NAD^+ levels as determined by cycling assay indicate reductions in WT-HFD mice compared to WT-RD and increased NAD^+ levels in the CD38ci mice versus WT.

E CD38 activity levels based on etheno-NAD^+ assay show impaired activity in CD38ci mice versus WTs and higher activity in WT-HFD mice than WT-RD (n=5/group).

F-H qRT-PCRs data indicting differences in antioxidant (F) and pro-repair astrocyte marker genes (G-H, BDNF and S100a10, respectively) in the CD38ci mice versus controls.

Bar graphs represent mean +/- SEM. Two-way ANOVA with Bonferroni post-test. Asterisks indicate levels of statistical significance, where *, $p<0.05$ and **, $p<0.01$. When compared to WT-HFD mice, #, $p<0.05$.

bioRxiv preprint doi: https://doi.org/10.1101/2020.06.10.143941; this version posted June 12, 2020. The copyright holder for this preprint (which was not certified by peer review) is the author/funder, who has granted bioRxiv a license to display the preprint in perpetuity. It is made available under aCC-BY 4.0 International license.

1074 The following figure supplement is available for figure 3:

1075 **Figure 3- Source Data 1.**

1076

bioRxiv preprint doi: https://doi.org/10.1101/2020.06.10.143941; this version posted June 12, 2020. The copyright holder for this preprint (which was not certified by peer review) is the author/funder, who has granted bioRxiv a license to display the preprint in perpetuity. It is made available under aCC-BY 4.0 International license.

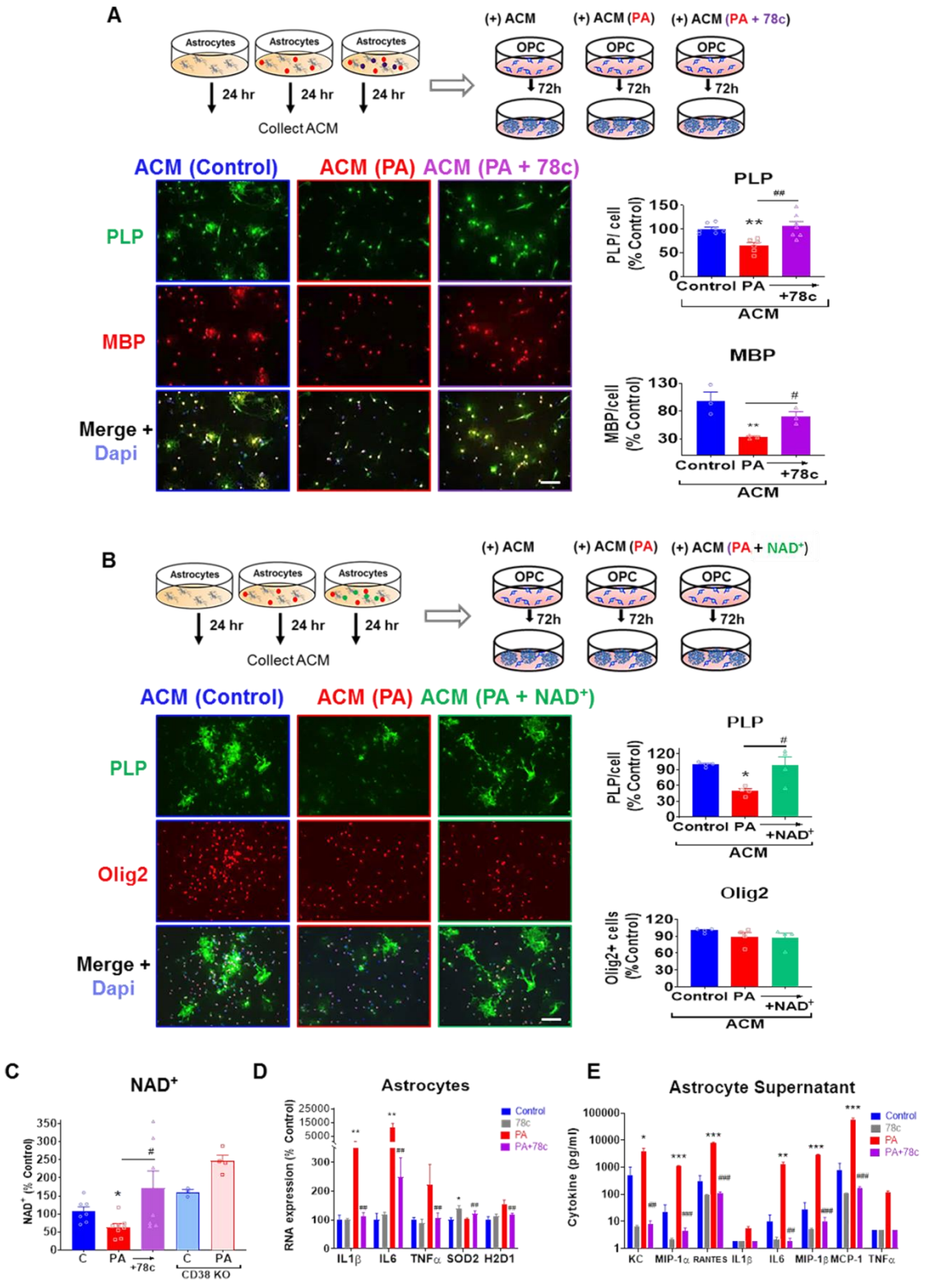

Figure 4. Astrocytes cultured in high saturated fat conditions increase CD38 and pro-inflammatory cytokine expression and inhibit oligodendrocyte differentiation.

bioRxiv preprint doi: https://doi.org/10.1101/2020.06.10.143941; this version posted June 12, 2020. The copyright holder for this preprint (which was not certified by peer review) is the author/funder, who has granted bioRxiv a license to display the preprint in perpetuity. It is made available under aCC-BY 4.0 International license.

A-D Schematic depicting how astrocyte conditioned media (ACM) treatments on primary murine oligodendrocytes were performed (***A***). Conditioned media obtained from PA-treated murine astrocytes (ACM (PA)) reduced protein expression of mature oligodendrocyte markers PLP (***B, C***) and MBP (***B, D***), while PA-78c-ACM-treated OLCs have enhanced PLP and MBP expression.

E-H Representational diagram (**E**) of astrocyte treatments with PA and NAD^+ to collect ACM for OPC treatments. The addition of NAD^+ restored PLP levels (***F, G***) when compared to ACM-PA, but had no effect on Olig2 (***F, H***). Scale bar = 100µm.

I-K High fat consumption was modeled in primary murine astrocyte cultures by including saturated fat palmitate in the media (PA, 100 µM, 24 h). ***I***, Addition of a small molecule CD38 inhibitor (78c, 3µM) was effective to restore NAD^+ levels in PA-treated astrocytes when assessed using an NAD^+ cycling assay. Astrocytes derived from CD38 knockout mice did not show depleted NAD^+ levels in response to PA. RNA levels by qPCR (***J***) of proinflammatory cytokines, antioxidant enzyme, and an astrocyte activation marker in PA and 78c treated astrocytes and cytokine levels (***K***) detected in astrocyte conditioned media (ACM) by Bioplex assay.

Bar graphs represent the mean +/- SEM. Asterisks indicate levels of statistical significance when compared to control as determined by Student's t-test (***A***, ***B***) or one-way ANOVA with Bonferroni post-test (***C-L***), where *, $p<0.05$; **, $p<0.01$; ***, $p<0.001$. # indicates $p<0.05$ when compared to ACM-PA group by one-way ANOVA with Bonferroni post-test.

The following figure supplement is available for figure 4:

Figure 4- Source Data 1.

bioRxiv preprint doi: https://doi.org/10.1101/2020.06.10.143941; this version posted June 12, 2020. The copyright holder for this preprint (which was not certified by peer review) is the author/funder, who has granted bioRxiv a license to display the preprint in perpetuity. It is made available under aCC-BY 4.0 International license.

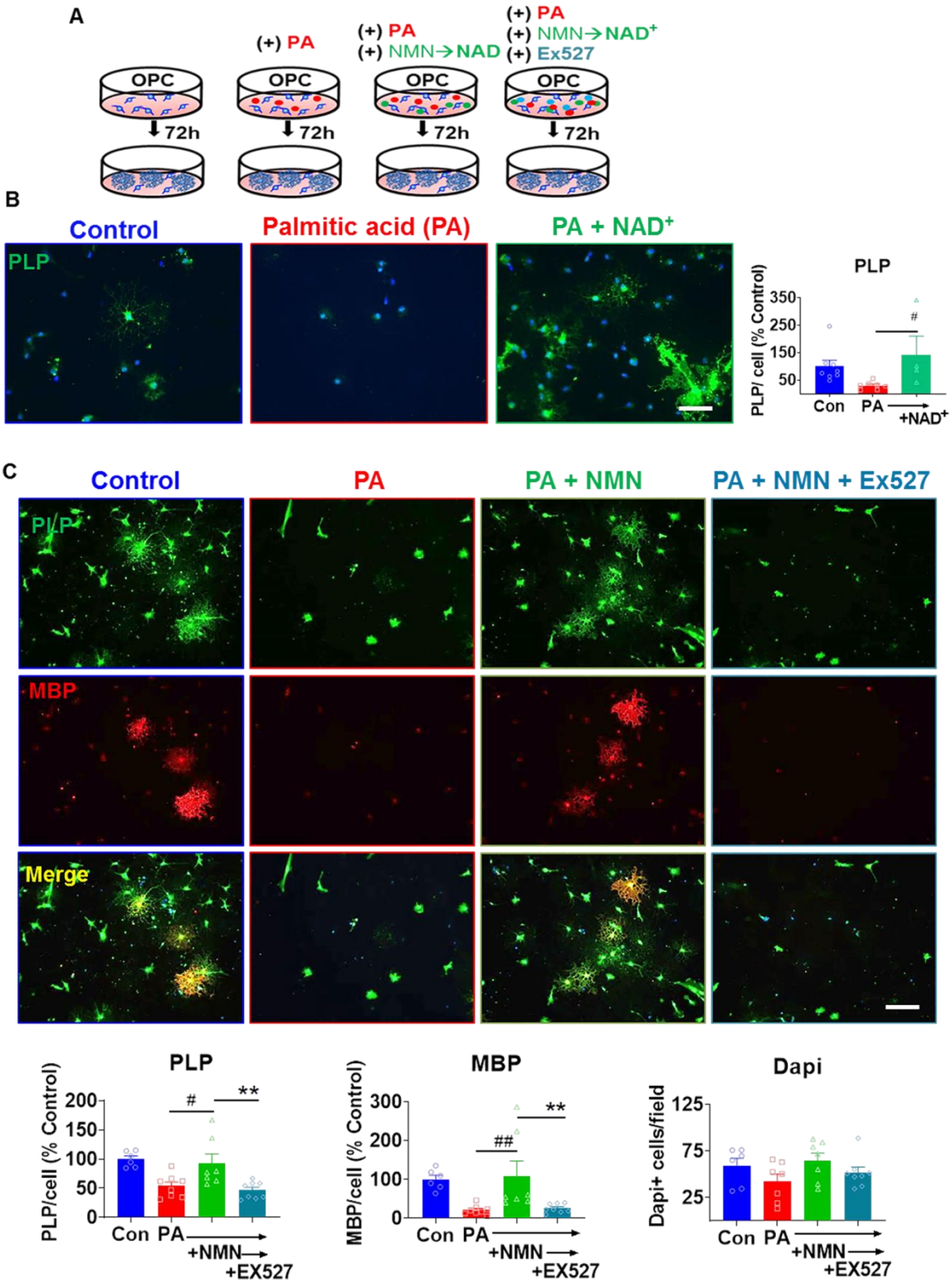

Figure 5. NAD$^+$ replenishment attenuates PA-induced deficits in oligodendrocyte differentiation in a SIRT1-dependent manner.

bioRxiv preprint doi: https://doi.org/10.1101/2020.06.10.143941; this version posted June 12, 2020. The copyright holder for this preprint (which was not certified by peer review) is the author/funder, who has granted bioRxiv a license to display the preprint in perpetuity. It is made available under aCC-BY 4.0 International license.

A-C Representational diagram (***A***) of experimental treatments in primary murine oligodendrocyte lineage cells (OLCs). Adding exogenous NAD^+ (50 μM) to oligodendrocyte cultures significantly restores PLP protein expression (***B, C***) in PA-exposed OLCs.

D-G Treatment with NAD^+ precursor nicotinamide mononucleotide (NMN,100 μM) also enhances expression of mature oligodendrocyte markers in PA-treated cultures, although not when SIRT1 inhibitor Ex-527 (5 μM) is also included in the media, as determined by immunostaining quantification for PLP (***D, E***) and MBP (***D, F)*** per DAPI+ cell (***G***). Scale bar= 100 μm.

Graphical results represented as the mean ± SEM (n=4-8/group). Asterisks indicate levels of statistical significance when compared to designated group as determined by one-way ANOVA with Bonferroni post-test, where *, $p<0.05$; **, $p<0.01$; ***, $p<0.001$. # indicates $p<0.05$ and ## represents $p<0.001$when compared to the ACM-PA group.

The following figure supplement is available for figure 5:

Figure 5- Source Data 1.

bioRxiv preprint doi: https://doi.org/10.1101/2020.06.10.143941; this version posted June 12, 2020. The copyright holder for this preprint (which was not certified by peer review) is the author/funder, who has granted bioRxiv a license to display the preprint in perpetuity. It is made available under aCC-BY 4.0 International license.

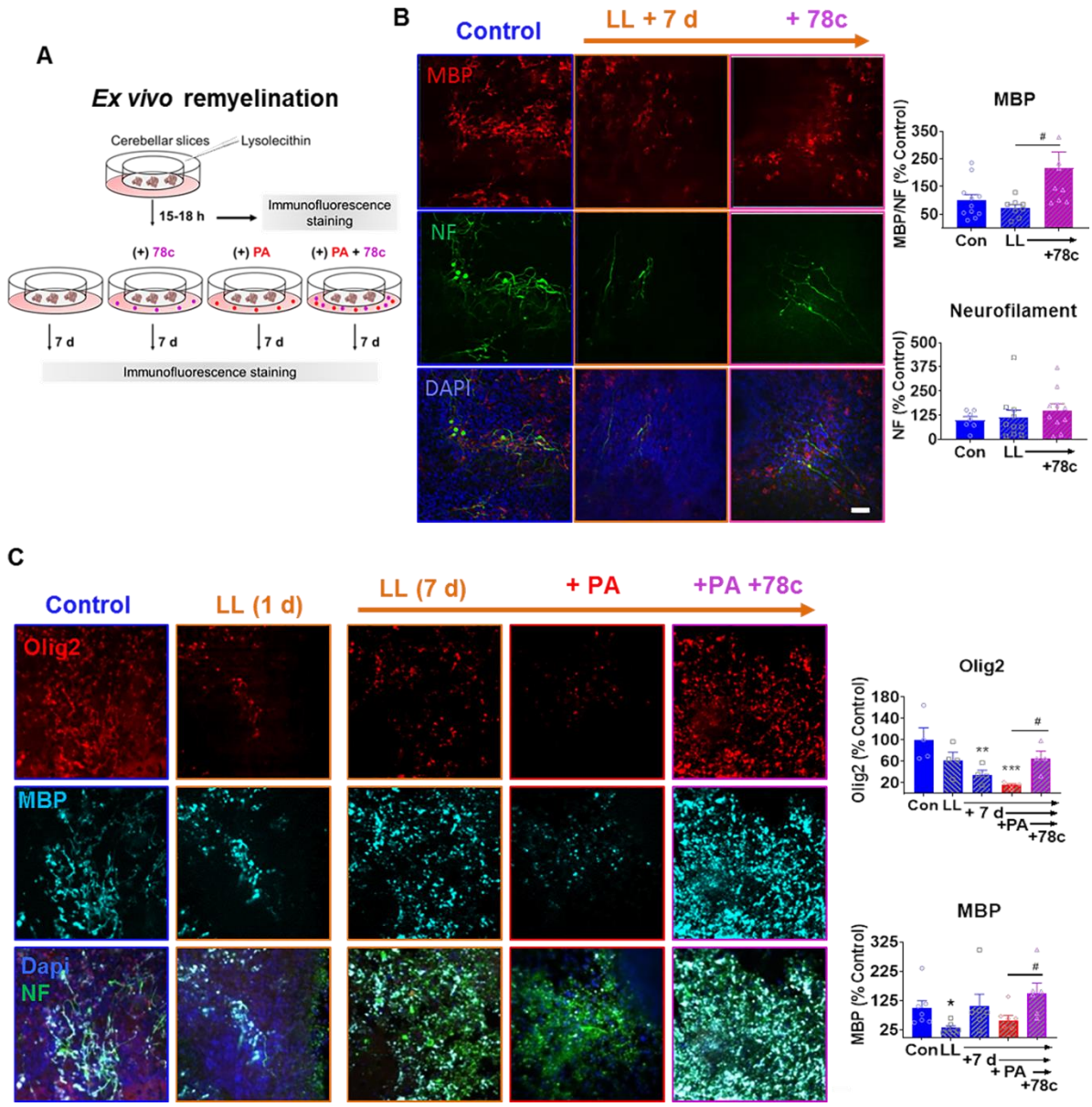

Figure 6. CD38 inhibition protects from saturated fat and lysolecithin-induced demyelination in cerebellar slices

A-C Representational diagram (**A**) of *ex vivo* remyelination experiments where murine organotypic cerebellar slices were demyelinated with lysolecithin (LL, 0.5 mg/ml, overnight) followed by subsequent culture in control media for 1 wk. Confocal microscopic imaging of slices indicate reduced MBP (red, ***B***) expression when normalized to neurofilament (NF, green).

bioRxiv preprint doi: https://doi.org/10.1101/2020.06.10.143941; this version posted June 12, 2020. The copyright holder for this preprint (which was not certified by peer review) is the author/funder, who has granted bioRxiv a license to display the preprint in perpetuity. It is made available under aCC-BY 4.0 International license.

LL-demyelinated slices cultured with 78c had significantly increased MBP expression when normalized to NF staining and expressed as a percentage of the control group (***C***).

D-F Slices cultured in media containing both LL-palmitic acid (PA, 100 μM) and 78c, a CD38 inhibitor, 3 μM) had significant improvements in Olig2 (***D,E***) and MBP (***D, F***) expression compared to the LL-PA alone group (#, $p<0.05$).

Bar graphs represent the mean ± SEM (n=4-8/group); *, $p<0.05$, **, $p<0.01$, and ***, $p<0.001$ when compared to control by one-way ANOVA with Bonferroni post-test.

The following figure supplement is available for Figure 6:

Figure Supplement 1. Cerebellar slice culture treatment controls.

Figure 6- Source Data 1.

bioRxiv preprint doi: https://doi.org/10.1101/2020.06.10.143941; this version posted June 12, 2020. The copyright holder for this preprint (which was not certified by peer review) is the author/funder, who has granted bioRxiv a license to display the preprint in perpetuity. It is made available under aCC-BY 4.0 International license.

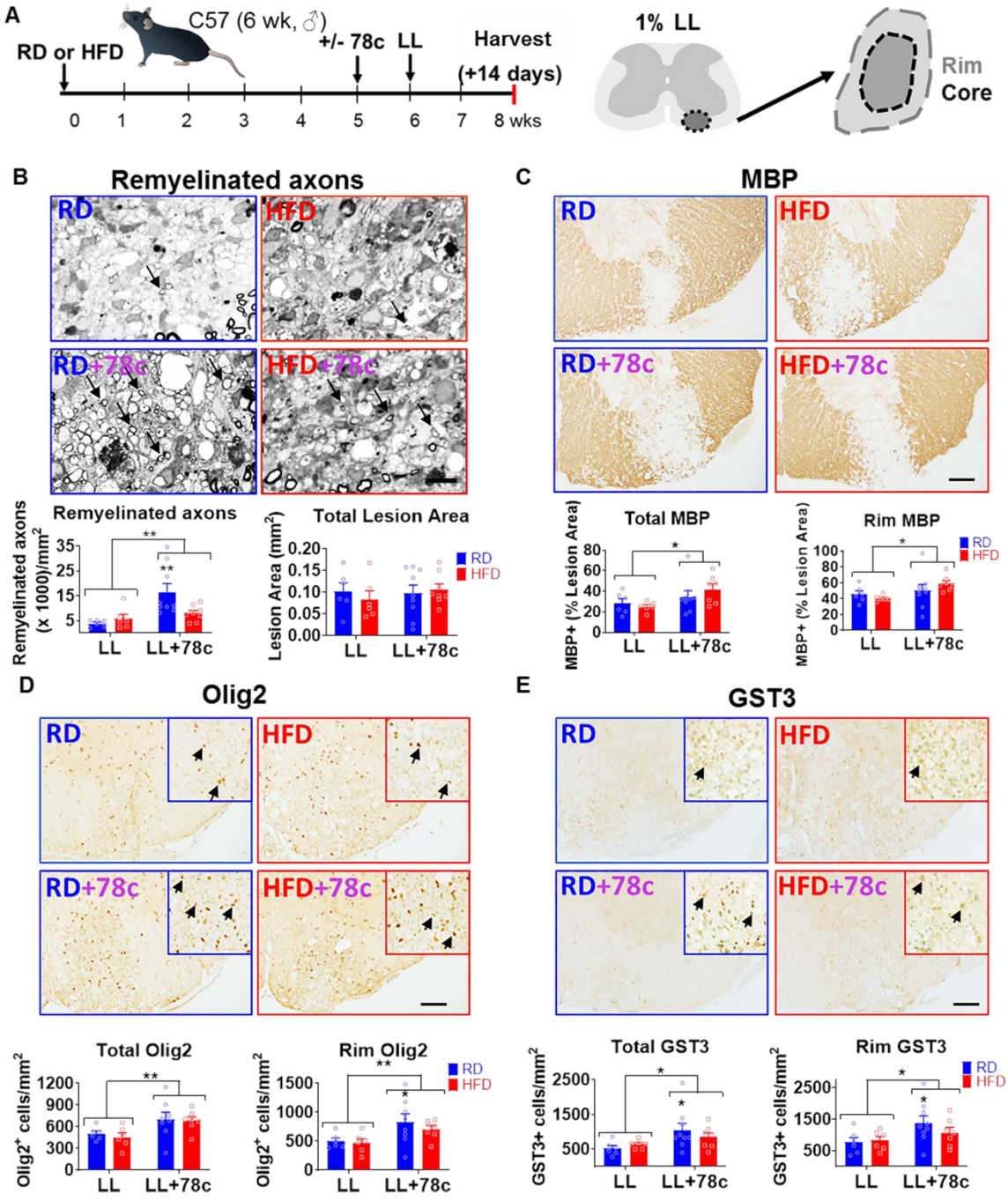

Figure 7. CD38 inhibition with 78c improves myelin repair following lysolecithin-induced focal demyelination to the ventral spinal cord.

Eight week old male C57Bl6 mice were fed a regular diet (RD) or high fat diet (HFD) for 5 wks, then split into two additional groups: one receiving the same diet and the other half receiving the

bioRxiv preprint doi: https://doi.org/10.1101/2020.06.10.143941; this version posted June 12, 2020. The copyright holder for this preprint (which was not certified by peer review) is the author/funder, who has granted bioRxiv a license to display the preprint in perpetuity. It is made available under aCC-BY 4.0 International license.

respective diet with 78c added (600 ppm). One week later, a focal demyelinating lesion to the ventral spinal cord was induced by lysolecithin (LL, 1% with Evans Blue dye) and mice were allowed to recover for two weeks. Lesion boundary regions were determined by limiting to the area of continuous myelin loss (core) or by including the entire inflammatory lesion (rim) based on immunohistochemical analyses.

A Schematic depicting experimental design and lesion boundaries.

B Representative images and corresponding analysis illustrating the mean number of remyelinated axons after focal lysolecithin-mediated demyelination of the ventral spinal cord was increased in 78c-treated mice at 14 days post injury when compared to LL only mice (**, $p<0.01$, two-way ANOVA with Bonferroni post-test) as assessed by paraphenylenediamine (PPD)-stained semi-thin sections of araldite-embedded spinal cord tissue. Scale bar= 20 µm.

C Immunohistochemical staining of the total lesion and lesion rim identified significant changes in MBP immunoreactivity in 78c treated animals.

D-E Olig2+ oligodendrocyte lineage cells (OLCs, ***D***) and GST3+ mature oligodendrocytes (***E***) were significantly higher in 78c-RD mice when compared to RD controls.

Bar graphs represent mean +/- SEM. Two-way ANOVA (n=7-10 mice/group). Asterisks indicate levels of statistical significance, where *, $p<0.05$ and **, $p<0.01$.

The following figure supplements are available for Figure 7:

Figure 7- Figure supplement 1. Lysolecithin-induced demyelination model characterization.

Figure 7- Figure supplement 2. 78c attenuates HFD-induced oligodendrocyte loss.

Figure 7- Source Data 1.

bioRxiv preprint doi: https://doi.org/10.1101/2020.06.10.143941; this version posted June 12, 2020. The copyright holder for this preprint (which was not certified by peer review) is the author/funder, who has granted bioRxiv a license to display the preprint in perpetuity. It is made available under aCC-BY 4.0 International license.

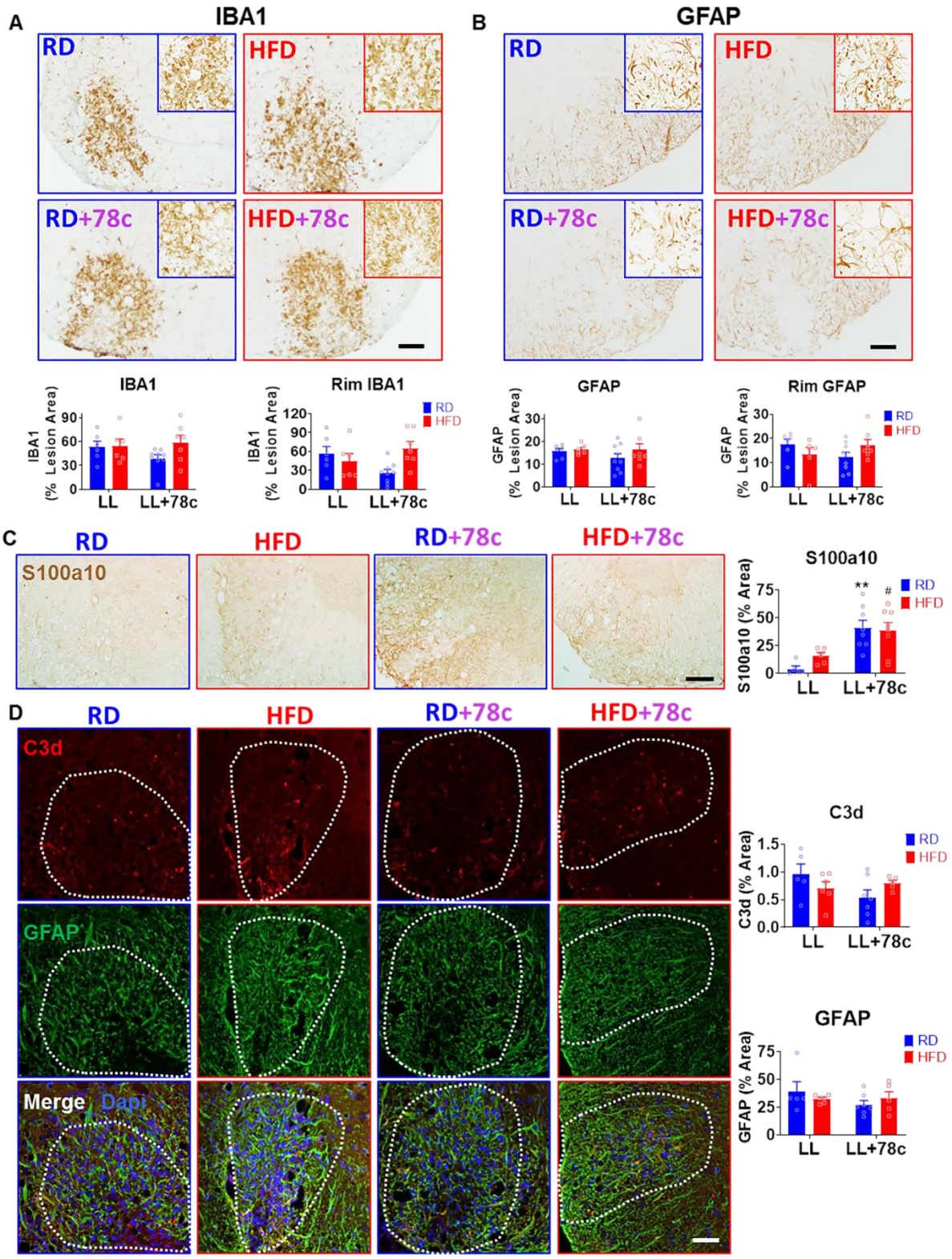

Figure 8. 78c promotes pro-repair astrocytes after lysolecithin-induced demyelination.

bioRxiv preprint doi: https://doi.org/10.1101/2020.06.10.143941; this version posted June 12, 2020. The copyright holder for this preprint (which was not certified by peer review) is the author/funder, who has granted bioRxiv a license to display the preprint in perpetuity. It is made available under aCC-BY 4.0 International license.

Histological analysis of markers of neuroinflammation in animals fed a regular diet (RD) or high fat diet (HFD) with or without 78c (CD38 inhibitor, 600 ppm) and injected with lysolecithin (LL) followed by a 2-week recovery period.

A, B IBA1 (**A**, microgliosis) and GFAP (**B**, astrogliosis) were not significantly affected by either diet or 78c alone, although a significant interaction for drug and diet was detected for IBA1 immunoreactivity in the lesion rim. Scale bar= 100 microns.

C-D, Changes in and pro-repair (S100a10, brown) pro-inflammatory (C3d, red) astrocyte (GFAP, green) markers in adjacent sections within the LL lesion area indicates a shift toward pro-repair in the 78c-treated mice. Scale bar = 100 μm.

Bar graphs represent mean +/- SEM. Two-way ANOVA (n=5-8 mice/group). Asterisks indicate levels of statistical significance, where **, $p<0.01$ when compared to LL-RD and #, $p<0.05$ when compared to LL-HFD group by Bonferroni post-test.

The following figure supplement is available for figure 8:

Figure 8- Source Data 1.

bioRxiv preprint doi: https://doi.org/10.1101/2020.06.10.143941; this version posted June 12, 2020. The copyright holder for this preprint (which was not certified by peer review) is the author/funder, who has granted bioRxiv a license to display the preprint in perpetuity. It is made available under aCC-BY 4.0 International license.

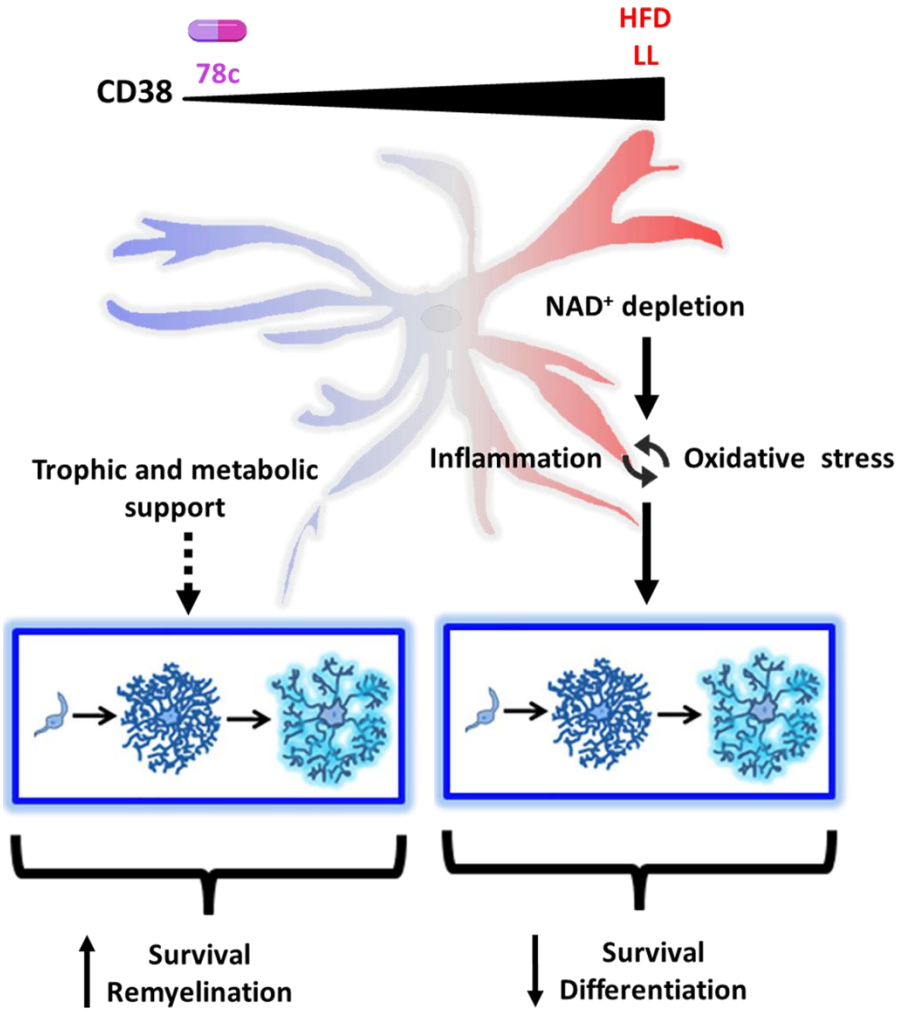

Figure 9. Schematic representation of proposed hypothesis.

Resting astrocytes typically help to provide a supportive environment for oligodendrocyte differentiation and repair, when necessary. High fat diet (HFD) and lysolecithin (LL) increase CD38 expression in reactive astrocytes, thereby depleting NAD^+ levels. Reductions in NAD^+ result in oxidative stress and inflammation which triggers impaired differentiation and survival in oligodendrocyte lineage cells. 78c inhibits CD38 to attenuate the described detrimental effects of astrocytes on oligodendrocytes.

bioRxiv preprint doi: https://doi.org/10.1101/2020.06.10.143941; this version posted June 12, 2020. The copyright holder for this preprint (which was not certified by peer review) is the author/funder, who has granted bioRxiv a license to display the preprint in perpetuity. It is made available under aCC-BY 4.0 International license.

Supplemental Figures and Figure Legends

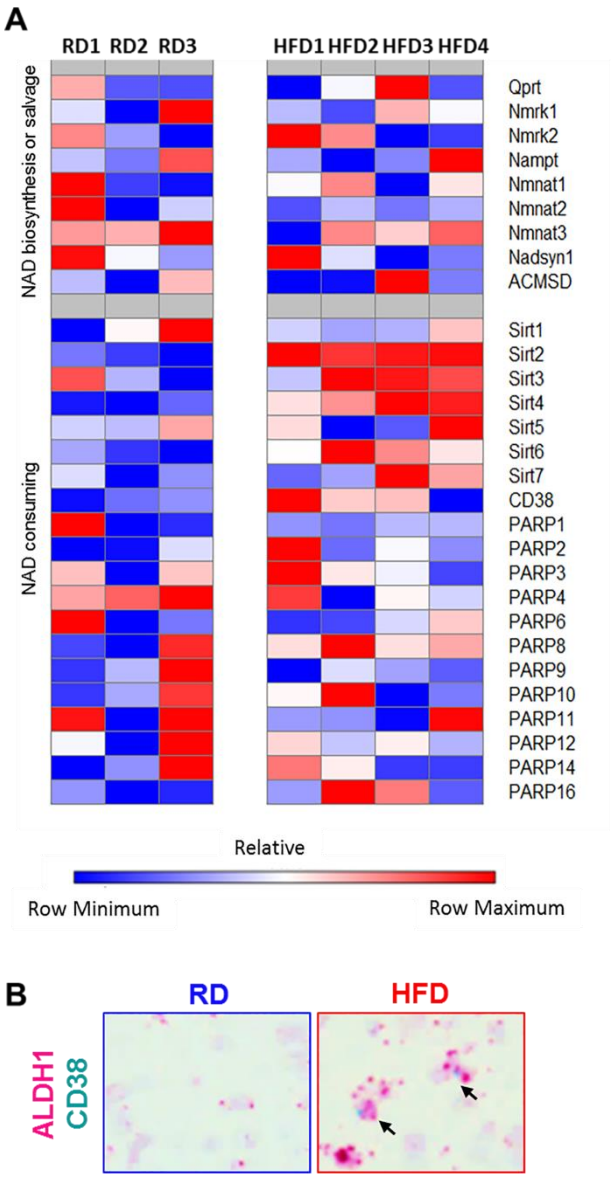

Figure 1- Figure Supplement 1. CD38 RNA expression in mouse spinal cord tissue.

A Heat map of HFD-induced changes in RNA expression of NAD^+-related genes acquired from previously published dataset (Langley et al, 2019).

B RNA scope *in situ* hybridization identified more CD38+ puncta in ALDH1+ (astrocyte marker) cells following HFD versus RD.

bioRxiv preprint doi: https://doi.org/10.1101/2020.06.10.143941; this version posted June 12, 2020. The copyright holder for this preprint (which was not certified by peer review) is the author/funder, who has granted bioRxiv a license to display the preprint in perpetuity. It is made available under aCC-BY 4.0 International license.

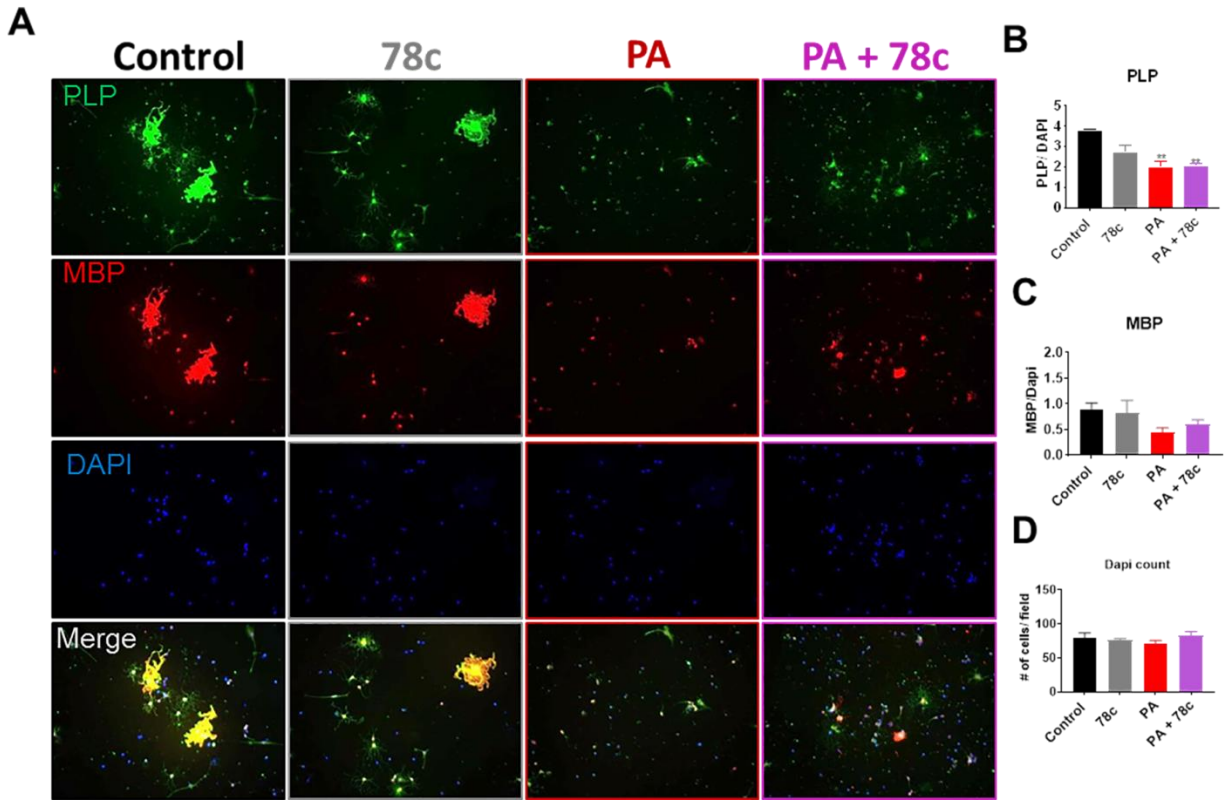

Figure 2- Figure Supplement 1. Effect of direct CD38 inhibition on oligodendrocyte progenitors.

A-D Immunofluorescent staining of primary murine oligodendrocyte progenitors cultured in differentiation media indicates reduced PLP (B) and MBP (C) expression per cell (D) in the presence of palmitate (PA, 100 µm) that was not attenuated by direct 78c (3 µM) treatment. Graphical results represented as the mean ± SEM (n=3/group). Asterisks indicate levels of statistical significance when compared to designated group as determined by one-way ANOVA with Bonferroni post-test, where *, $p<0.05$; **, $p<0.01$.

bioRxiv preprint doi: https://doi.org/10.1101/2020.06.10.143941; this version posted June 12, 2020. The copyright holder for this preprint (which was not certified by peer review) is the author/funder, who has granted bioRxiv a license to display the preprint in perpetuity. It is made available under aCC-BY 4.0 International license.

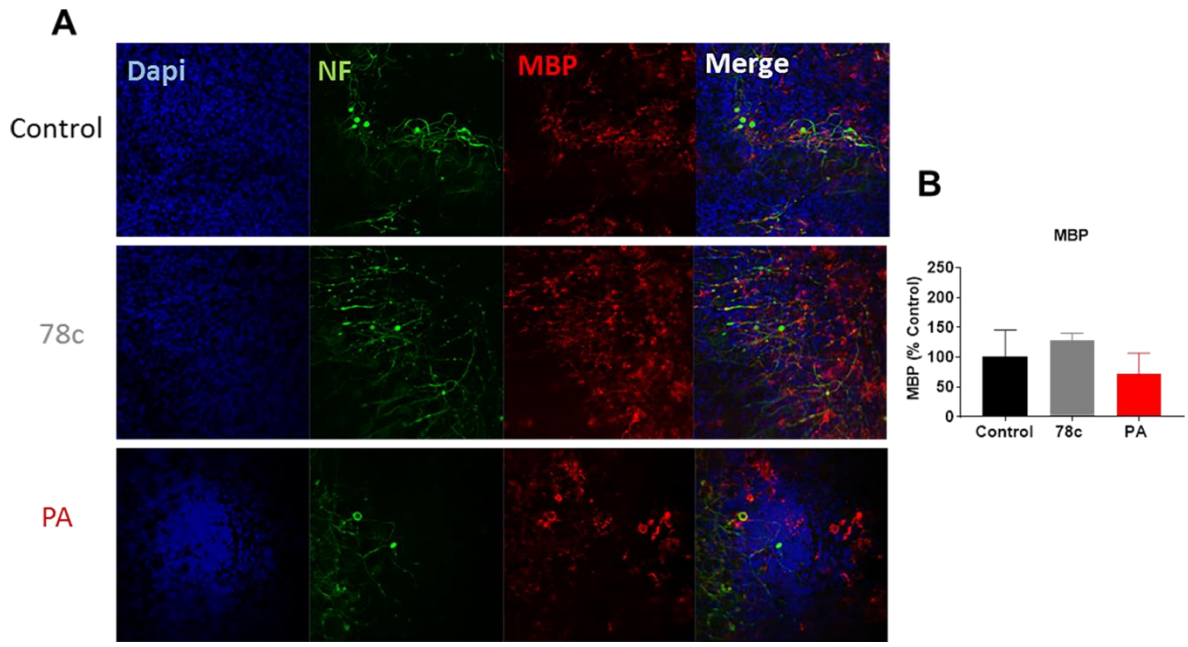

Figure 6- Figure Supplement 1. Cerebellar slice culture treatment controls.

A-B Confocal imaging of cerebellar murine slice cultures after two weeks shows no changes in MBP expression with 78c (3 µm) or palmitate (PA, 100 µm) treatments.

Bar graphs represent the mean ± SEM (n=3-4/group); Data were analyzed by one-way ANOVA with Bonferroni post-test.

bioRxiv preprint doi: https://doi.org/10.1101/2020.06.10.143941; this version posted June 12, 2020. The copyright holder for this preprint (which was not certified by peer review) is the author/funder, who has granted bioRxiv a license to display the preprint in perpetuity. It is made available under aCC-BY 4.0 International license.

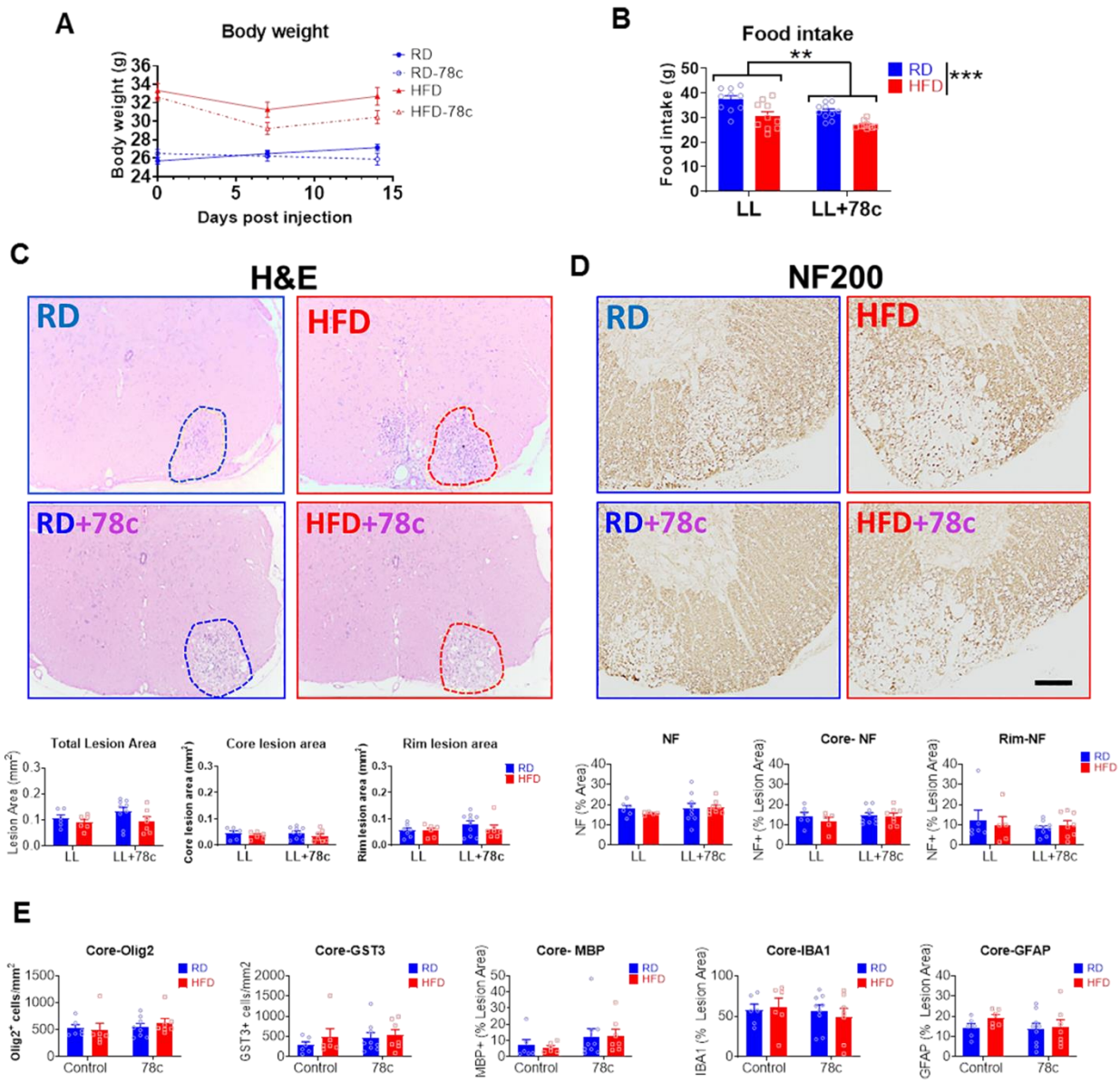

Figure 7- Figure Supplement 1. Lysolecithin-induced demyelination model characterization.

Eight week old male C57Bl6 mice were fed a regular diet (RD) or high fat diet (HFD) for 5 wks, and then split into two additional groups: one receiving the same diet and the other half receiving the respective diet with 78c added (600 ppm). One week later, a focal demyelinating lesion to the ventral spinal cord was induced by lysolecithin (LL, 1% with Evans Blue dye) and mice were allowed to recover for two weeks. Lesion boundary regions were determined by limiting to the

bioRxiv preprint doi: https://doi.org/10.1101/2020.06.10.143941; this version posted June 12, 2020. The copyright holder for this preprint (which was not certified by peer review) is the author/funder, who has granted bioRxiv a license to display the preprint in perpetuity. It is made available under aCC-BY 4.0 International license.

area of continuous myelin loss (core) or by including the entire inflammatory lesion (rim) based on immunohistochemical analyses.

A Body weights were not significantly affected by 78c, but were by high fat diet (HFD) consumption when compared to regular diet (RD).

B Food intake was significantly altered by HFD or 78c consumption.

C H&E staining shows the lesion area (C, entire boundary outlined by dotted line and determined by consideration of all stains performed). No significant differences between RD and HFD groups were noted.

D Neurofilament, (a marker of axon integrity) as determined by immunohistochemical quantification, was unchanged by either drug or diet.

E Quantification of the core only region from histological analyses indicates no significant changes.

Bar graphs represent mean +/- SEM. Two-way ANOVA (n=7-10 mice/group). Asterisks indicate levels of statistical significance, where *, $p<0.05$ and **, $p<0.01$.

bioRxiv preprint doi: https://doi.org/10.1101/2020.06.10.143941; this version posted June 12, 2020. The copyright holder for this preprint (which was not certified by peer review) is the author/funder, who has granted bioRxiv a license to display the preprint in perpetuity. It is made available under aCC-BY 4.0 International license.

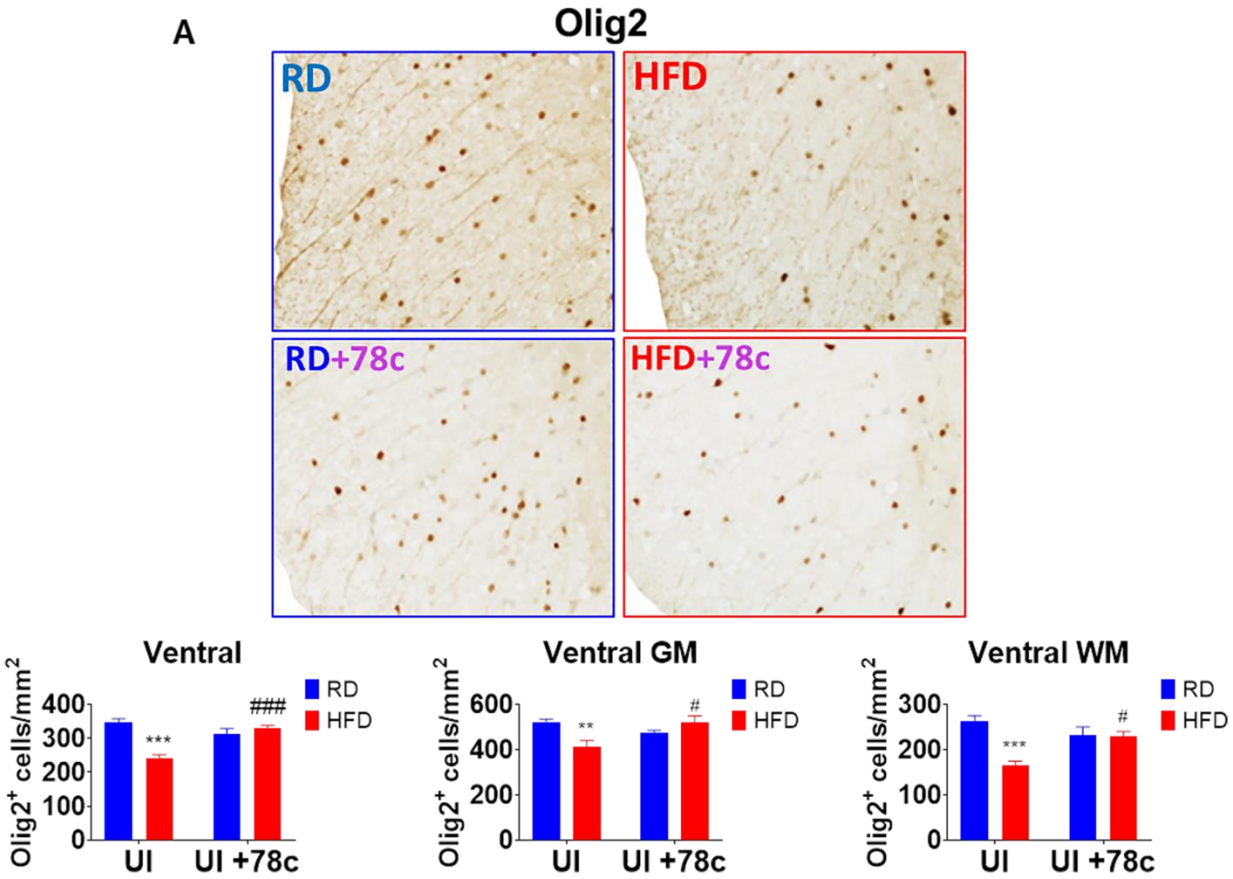

Figure 7- Figure Supplement 2. 78c attenuates HFD-induced oligodendrocyte loss.

A Histological analysis of the uninjected (UI) ventral side of the spinal cord from mice fed a regular diet (RD) or high fat diet (HFD) for 5 wks, and then split into two additional groups: one receiving the same diet and the other half receiving the respective diet with 78c added (600 ppm). Olig2+ oligodendrocyte lineage cells are depleted in HFD-fed mice compared to RD, yet mice fed HFD with 78c added had significantly more oligodendrocytes than HFD alone mice (#, $p<0.05$).

Bar graphs represent mean +/- SEM. Two-way ANOVA followed by Bonferroni post-hoc test (n=6-9 mice/group). Asterisks indicate levels of statistical significance when compared to control, where **, $p<0.01$; ***, $p<0.001$.

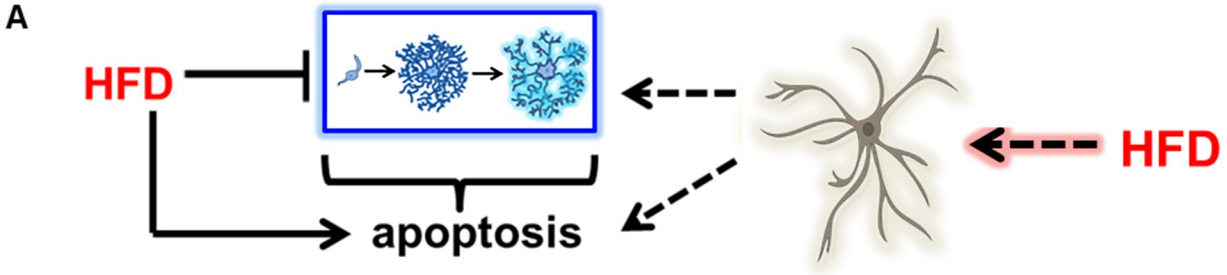

Whole Spinal Cord

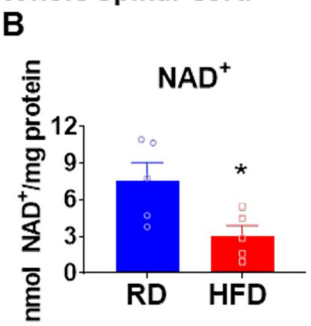

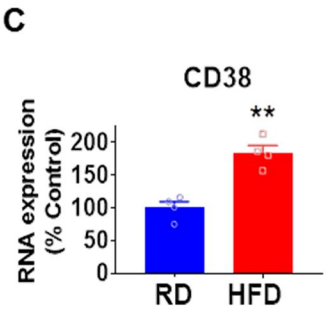

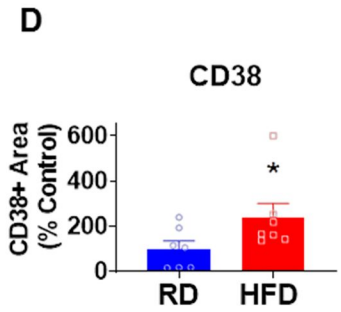

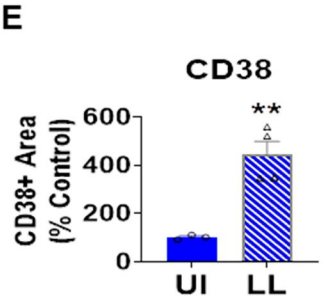

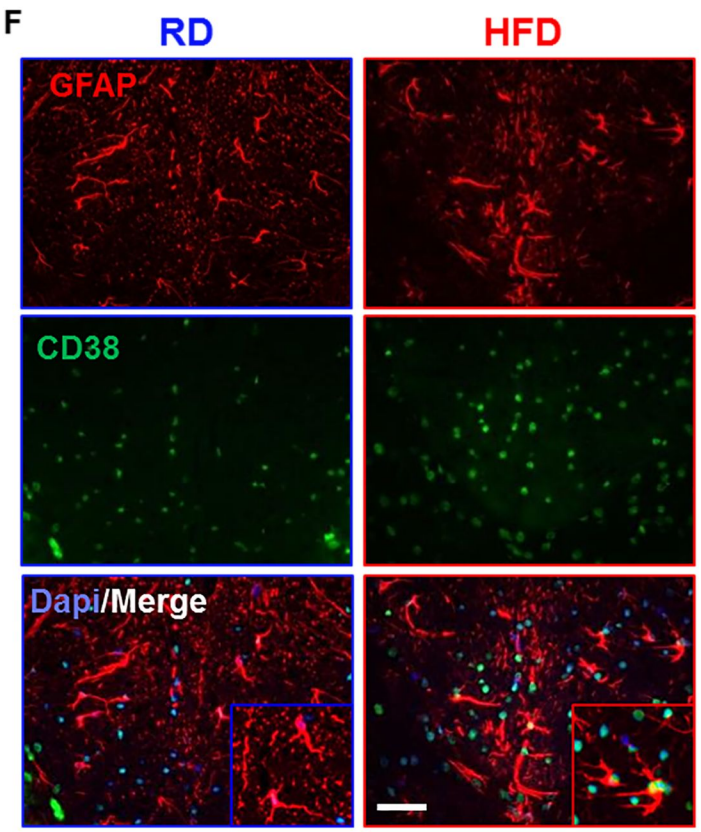

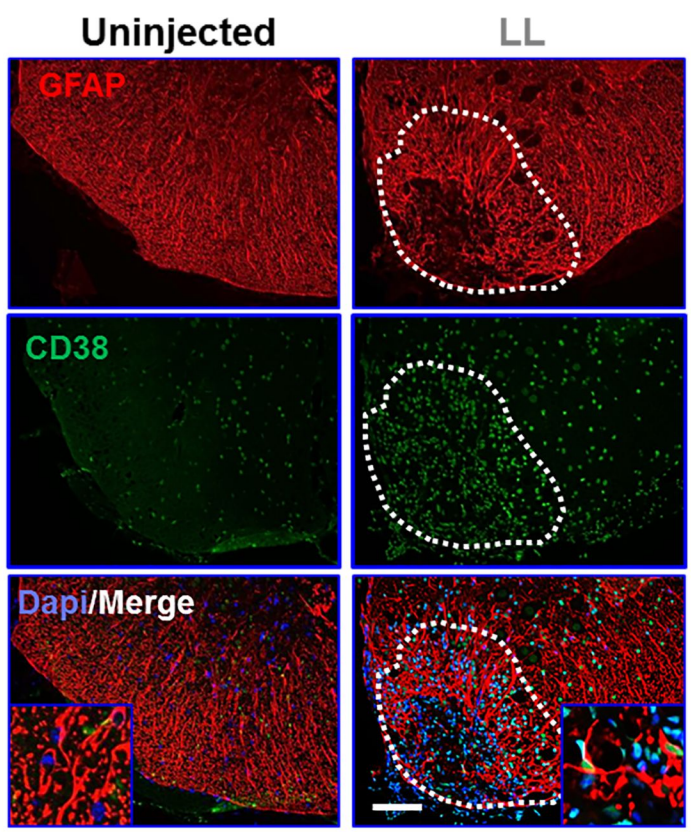

Primary astrocytes

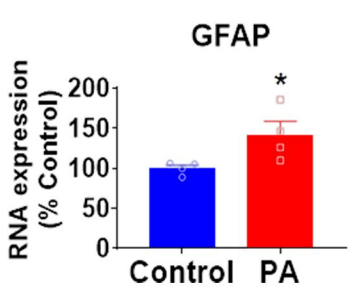

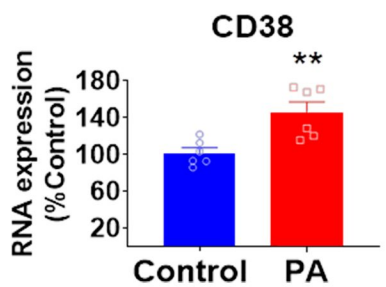

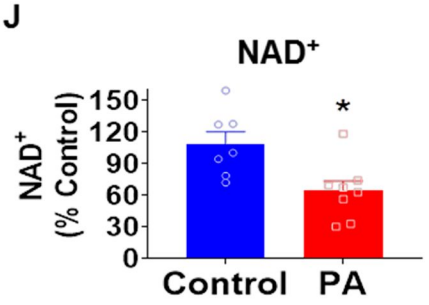

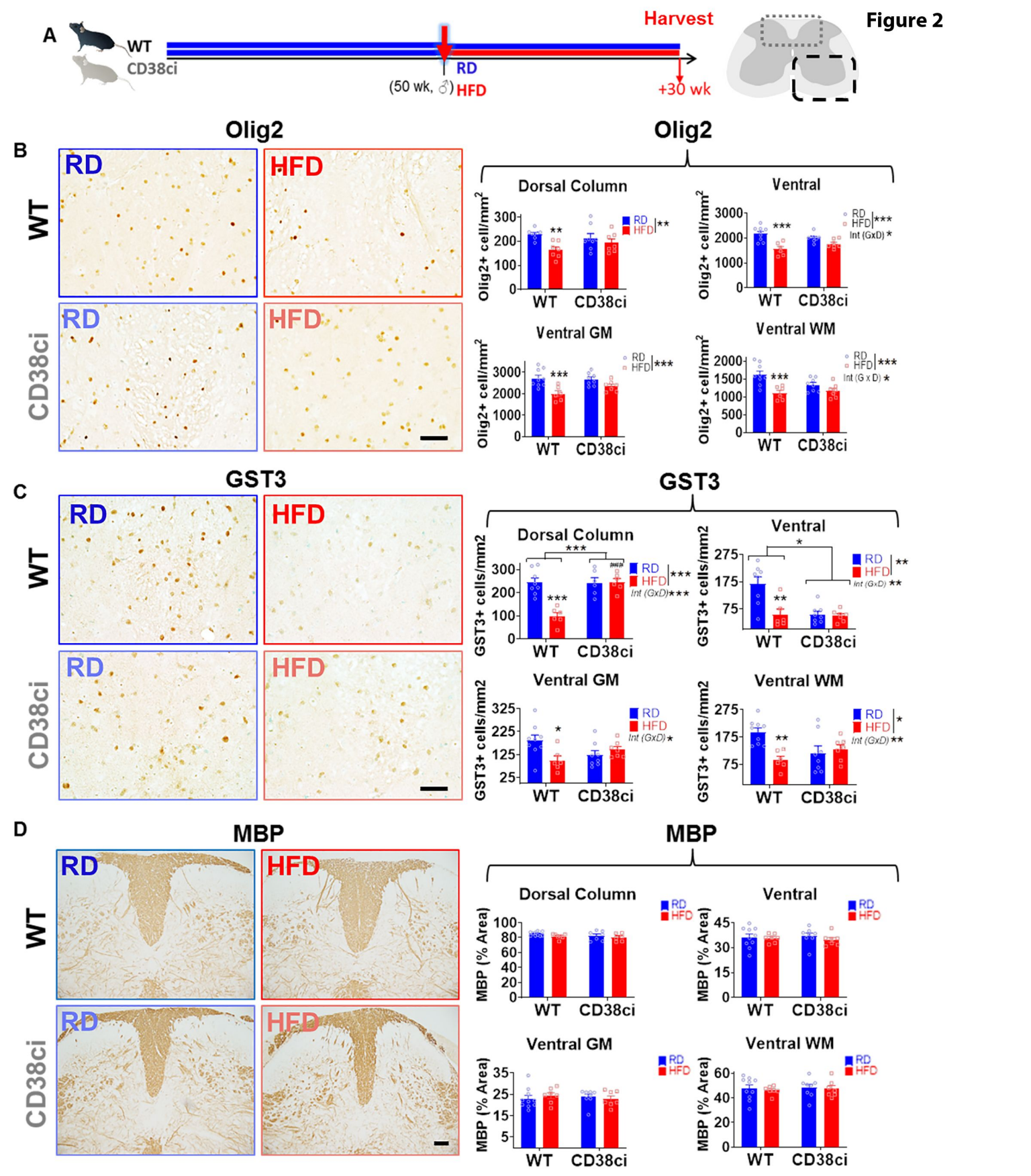
A
WT
CD38ci
RD
(50 wk, ♂) HFD
Harvest
+30 wk
Figure 2
B
Olig2
RD
HFD
WT
CD38ci
Olig2
Dorsal Column
Olig2+ cell/mm2
RD
HFD
**
WT
CD38ci
Ventral
***
Int (GxD) *
Ventral GM
Ventral WM
Int (G x D) *
C
GST3
GST3+ cells/mm2
Int (GxD)***
Int (GxD) **
Int (GxD)*
D
MBP
MBP (% Area)

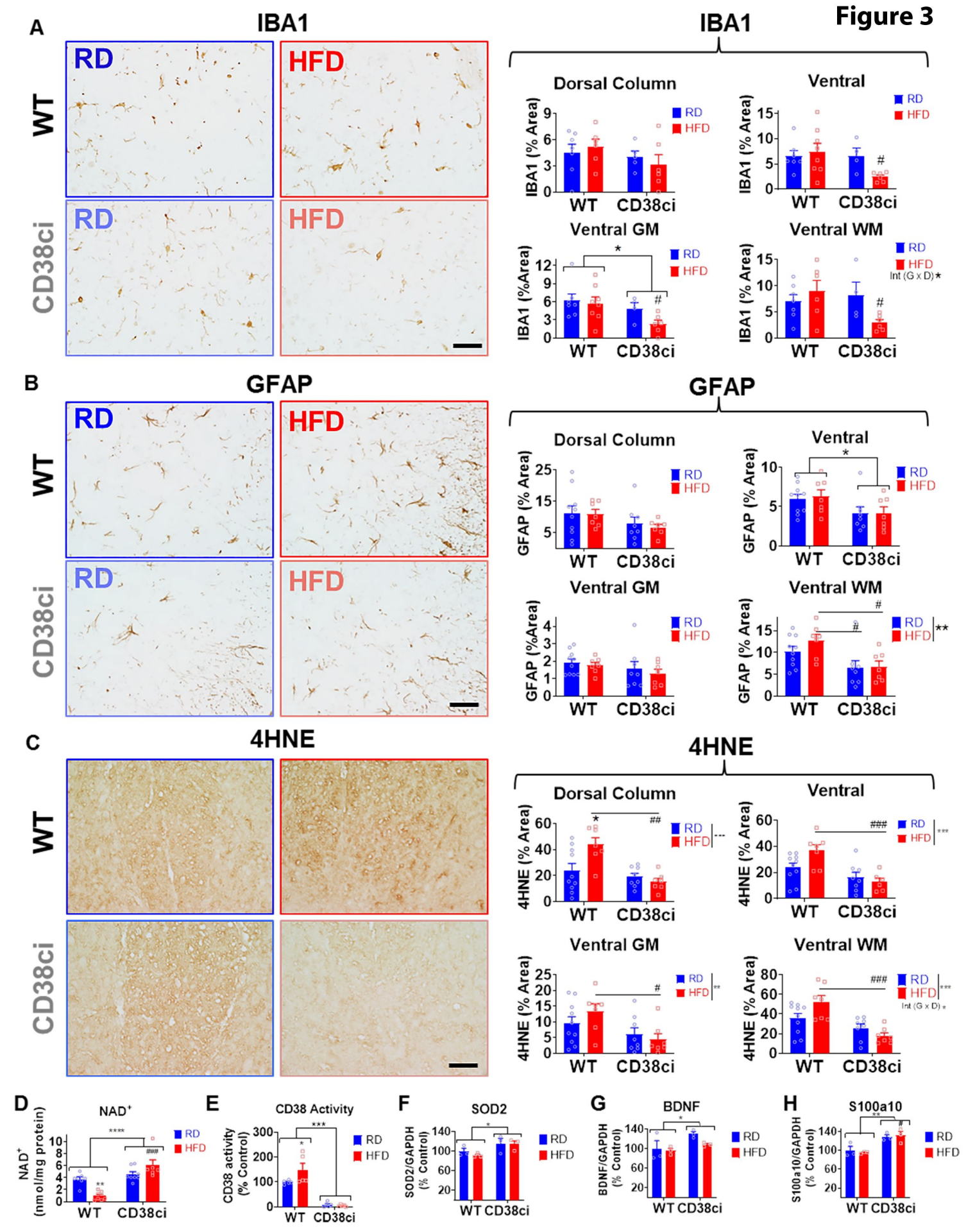
A
IBA1
RD
HFD
WT
CD38ci
IBA1
Dorsal Column
Ventral
Ventral GM
Ventral WM
IBA1 (% Area)
IBA1 (%Area)
RD
HFD
WT
CD38ci
Int (G x D) *
B
GFAP
GFAP (% Area)
GFAP (%Area)
C
4HNE
4HNE (% Area)
D
NAD+
NAD+ (nmol/mg protein)
E
CD38 Activity
CD38 activity (% Control)
F
SOD2
SOD2/GAPDH (% Control)
G
BDNF
BDNF/GAPDH (% Control)
H
S100a10
S100a10/GAPDH (% Control)

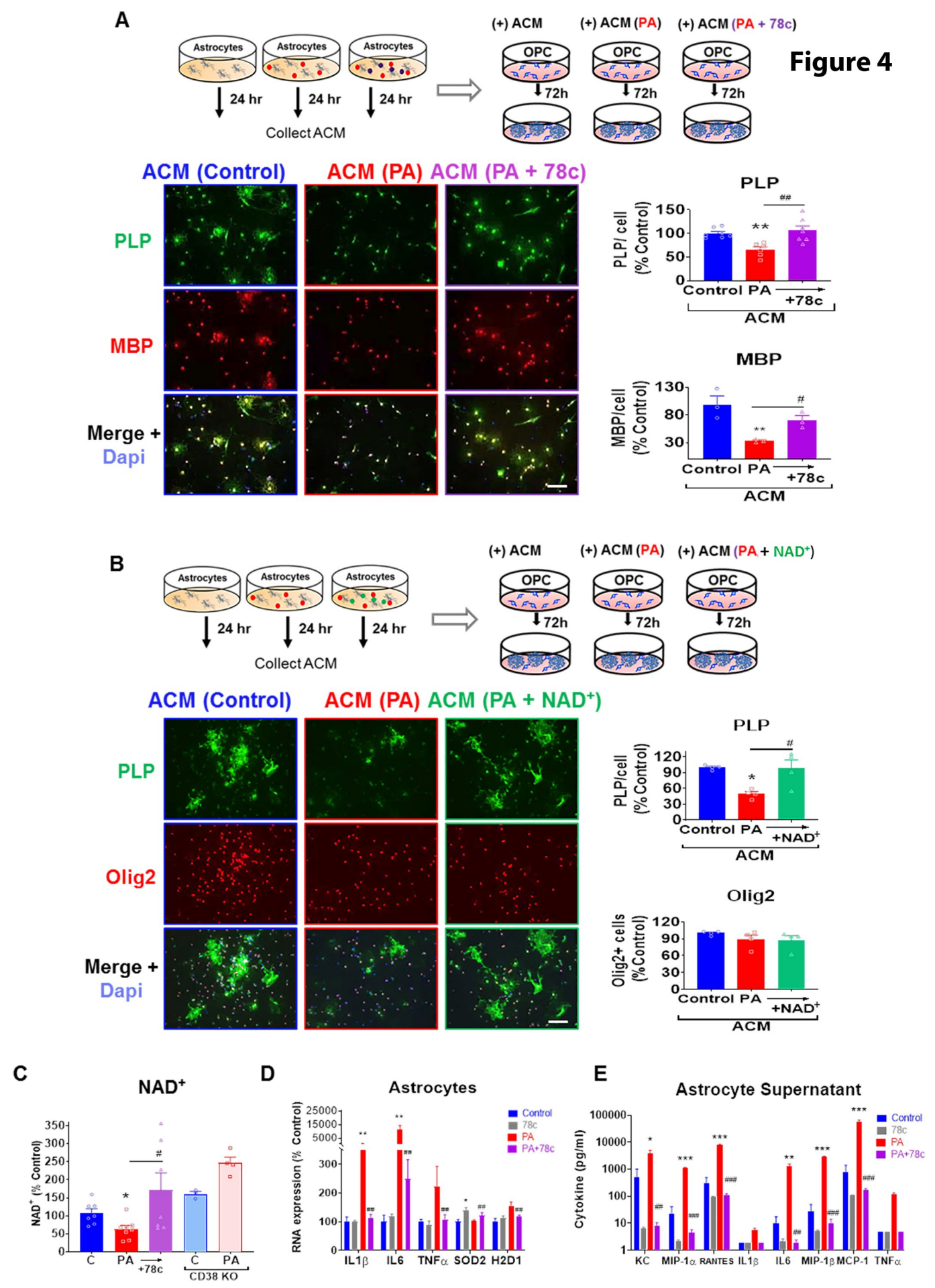
A
Astrocytes
24 hr
Collect ACM
(+) ACM
(+) ACM (PA)
(+) ACM (PA + 78c)
OPC
72h
ACM (Control)
ACM (PA)
ACM (PA + 78c)
PLP
MBP
Merge + Dapi
PLP/ cell (% Control)
Control
PA
+78c
ACM
MBP/cell (% Control)
B
(+) ACM (PA + NAD+)
ACM (PA + NAD+)
Olig2
PLP/cell (% Control)
+NAD+
Olig2+ cells (%Control)
C
NAD+
NAD+ (% Control)
CD38 KO
D
Astrocytes
RNA expression (% Control)
Control
78c
PA
PA+78c
IL1β
IL6
TNFα
SOD2
H2D1
E
Astrocyte Supernatant
Cytokine (pg/ml)
KC
MIP-1α
RANTES
MCP-1

Figure 4

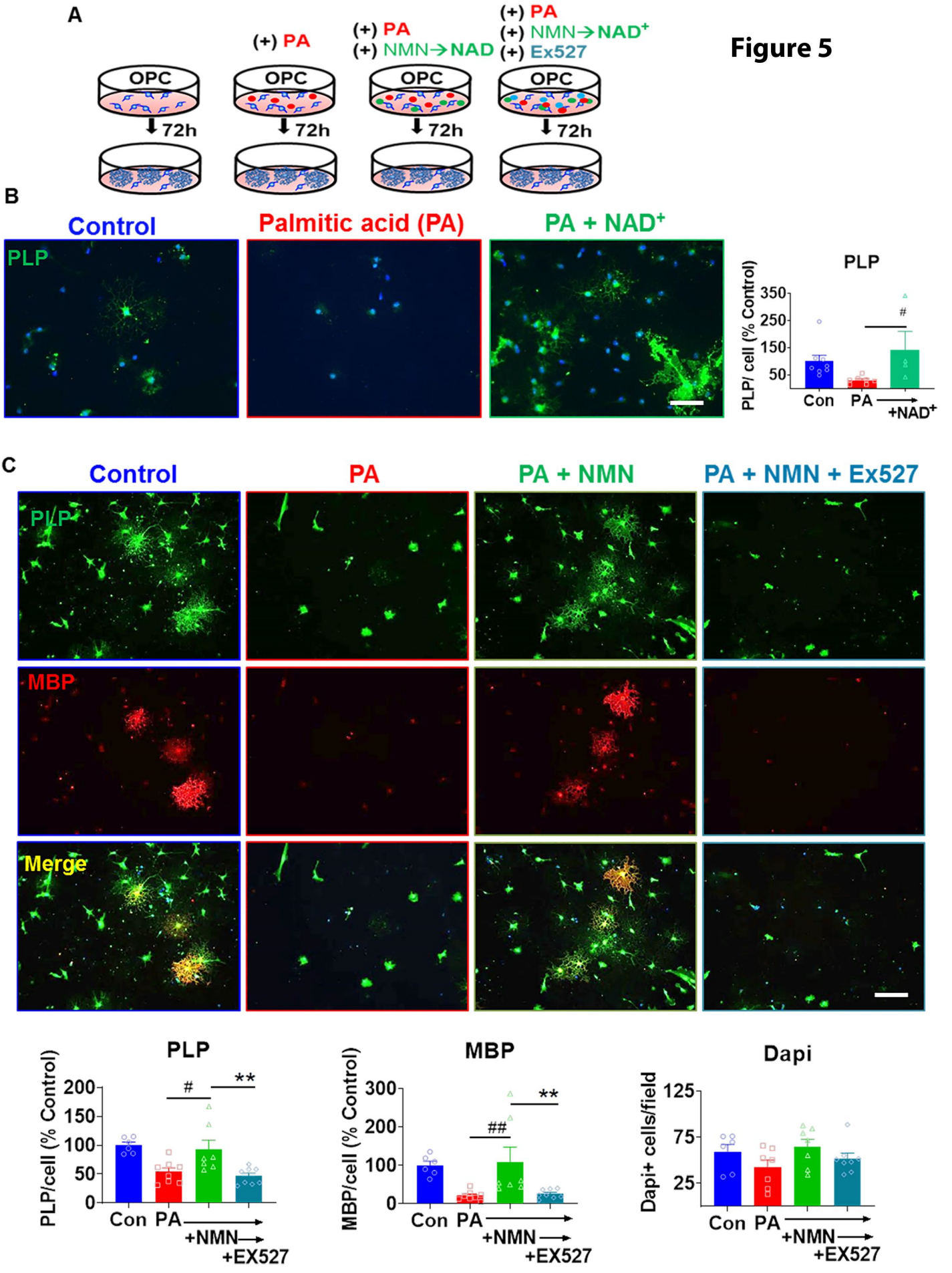
A
(+) PA
(+) PA
(+) NMN→NAD
(+) PA
(+) NMN→NAD+
(+) Ex527
OPC
72h
B
Control
Palmitic acid (PA)
PA + NAD+
PLP
PLP
PLP/ cell (% Control)
350
250
150
50
#
Con
PA
+NAD+
C
Control
PA
PA + NMN
PA + NMN + Ex527
PLP
MBP
Merge
PLP
PLP/cell (% Control)
200
150
100
50
0
#
**
Con
PA
+NMN
+EX527
MBP
MBP/cell (% Control)
300
200
100
0
##
**
Con
PA
+NMN
+EX527
Dapi
Dapi+ cells/field
125
75
25
Con
PA
+NMN
+EX527

Figure 5

Figure 6

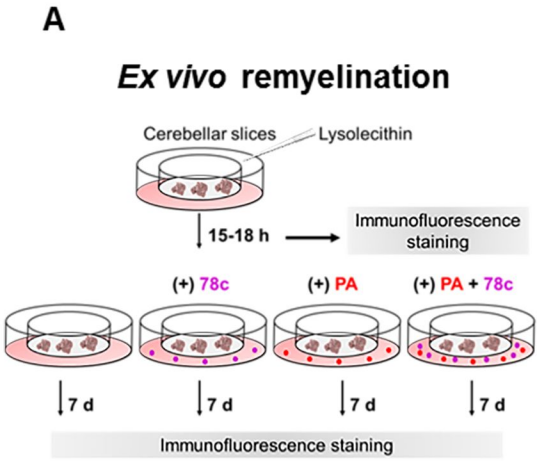
A
Ex vivo remyelination
Cerebellar slices
Lysolecithin
15-18 h
Immunofluorescence staining
(+) 78c
(+) PA
(+) PA + 78c
7 d
7 d
7 d
7 d
Immunofluorescence staining

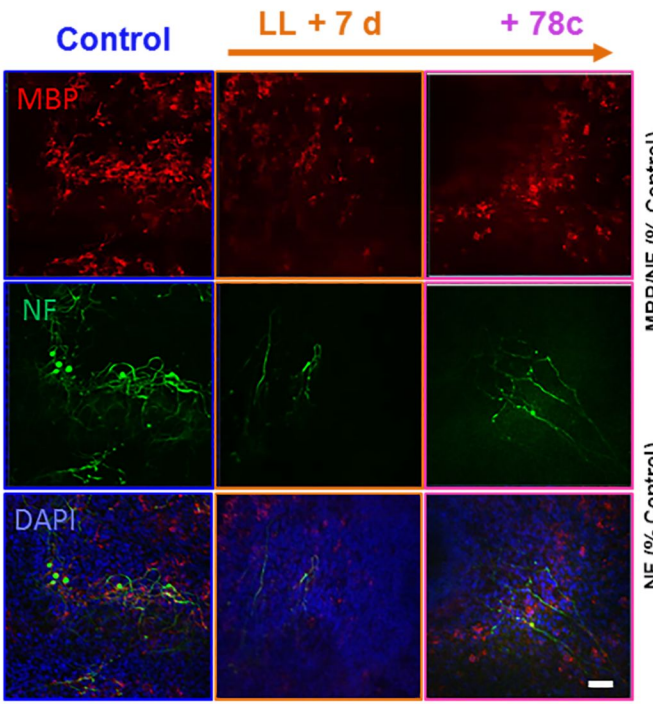
B
Control
LL + 7 d
+ 78c
MBP
NF
DAPI

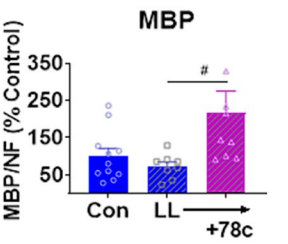
MBP
MBP/NF (% Control)
350
250
150
50
#
Con
LL
+78c

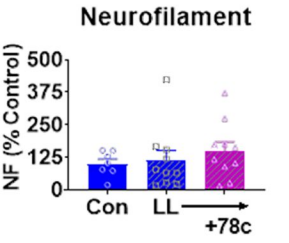
Neurofilament
NF (% Control)
500
375
250
125
0
Con
LL
+78c

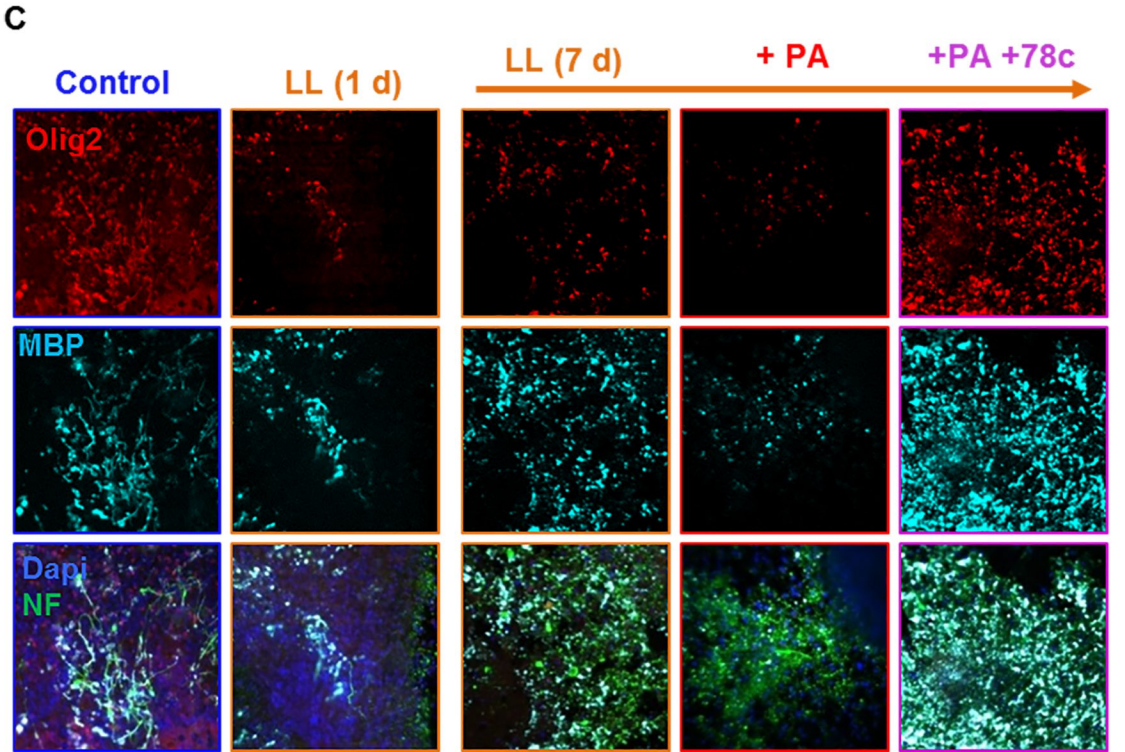
C
Control
LL (1 d)
LL (7 d)
+ PA
+PA +78c
Olig2
MBP
Dapi
NF

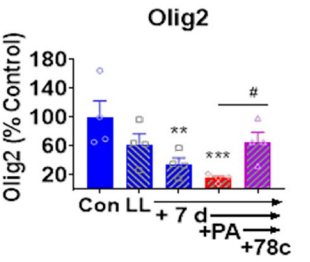
Olig2
Olig2 (% Control)
180
140
100
60
20
**
***
#
Con
LL
+ 7 d
+PA
+78c

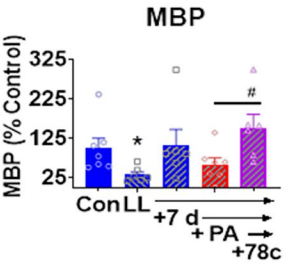
MBP
MBP (% Control)
325
225
125
25
*
#
Con
LL
+7 d
+ PA
+78c

Figure 7
A
C57 (6 wk, ♂)
RD or HFD
+/- 78c
LL
Harvest
(+14 days)
0 1 2 3 4 5 6 7 8 wks
1% LL
Rim
Core
B
Remyelinated axons
RD
HFD
RD+78c
HFD+78c
Remyelinated axons
Remyelinated axons (x 1000)/mm2
LL
LL+78c
Total Lesion Area
Lesion Area (mm2)
RD
HFD
C
MBP
Total MBP
MBP+ (% Lesion Area)
Rim MBP
D
Olig2
Total Olig2
Olig2+ cells/mm2
Rim Olig2
E
GST3
Total GST3
GST3+ cells/mm2
Rim GST3

Figure 8

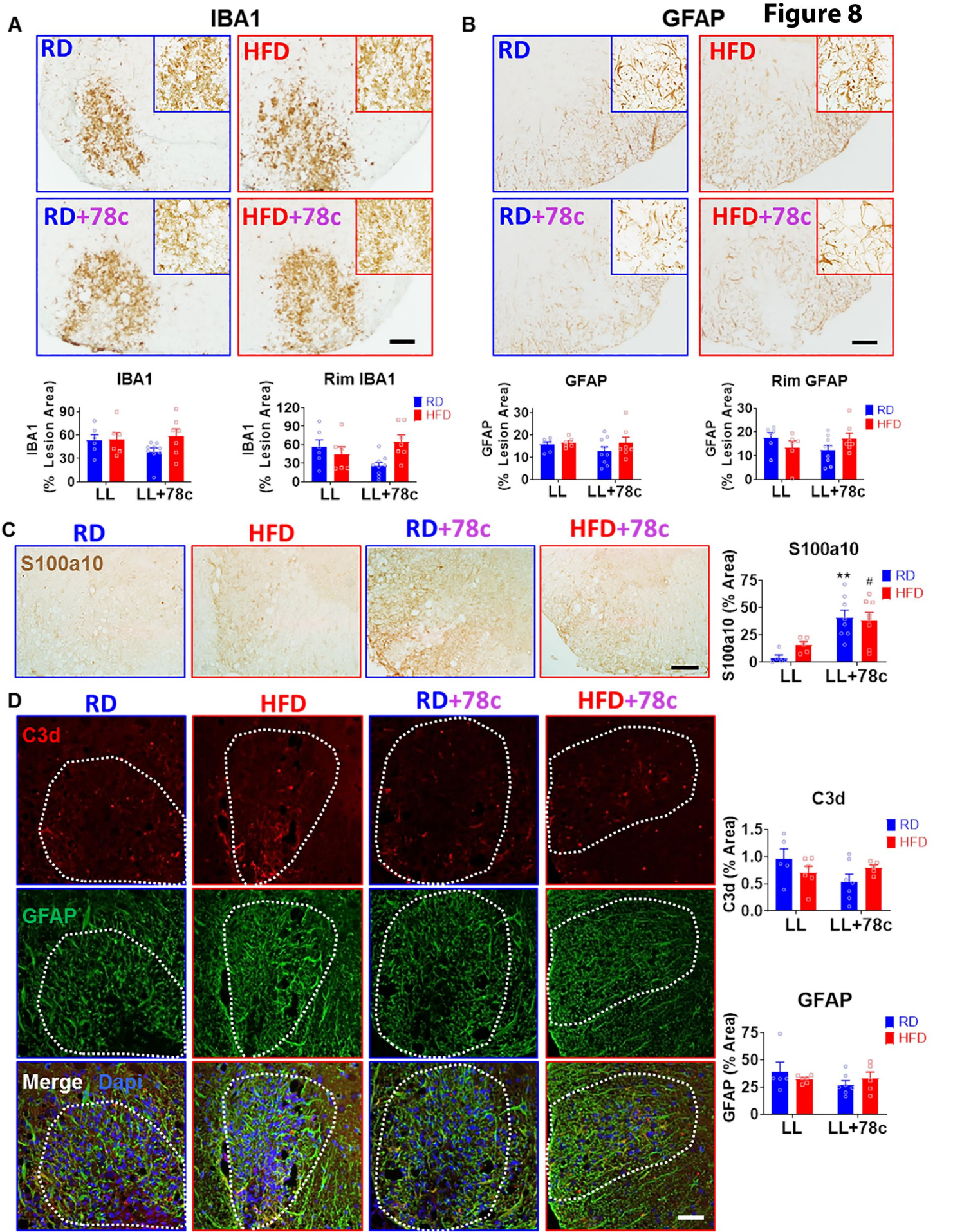
A
IBA1
RD
HFD
RD+78c
HFD+78c
B
GFAP
RD
HFD
RD+78c
HFD+78c
IBA1
IBA1 (% Lesion Area)
LL
LL+78c
Rim IBA1
IBA1 (% Lesion Area)
RD
HFD
LL
LL+78c
GFAP
GFAP (% Lesion Area)
LL
LL+78c
Rim GFAP
GFAP (% Lesion Area)
RD
HFD
LL
LL+78c
C
RD
HFD
RD+78c
HFD+78c
S100a10
S100a10
S100a10 (% Area)
**
#
RD
HFD
LL
LL+78c
D
RD
HFD
RD+78c
HFD+78c
C3d
GFAP
Merge
Dapi
C3d
C3d (% Area)
RD
HFD
LL
LL+78c
GFAP
GFAP (% Area)
RD
HFD
LL
LL+78c

Figure 9

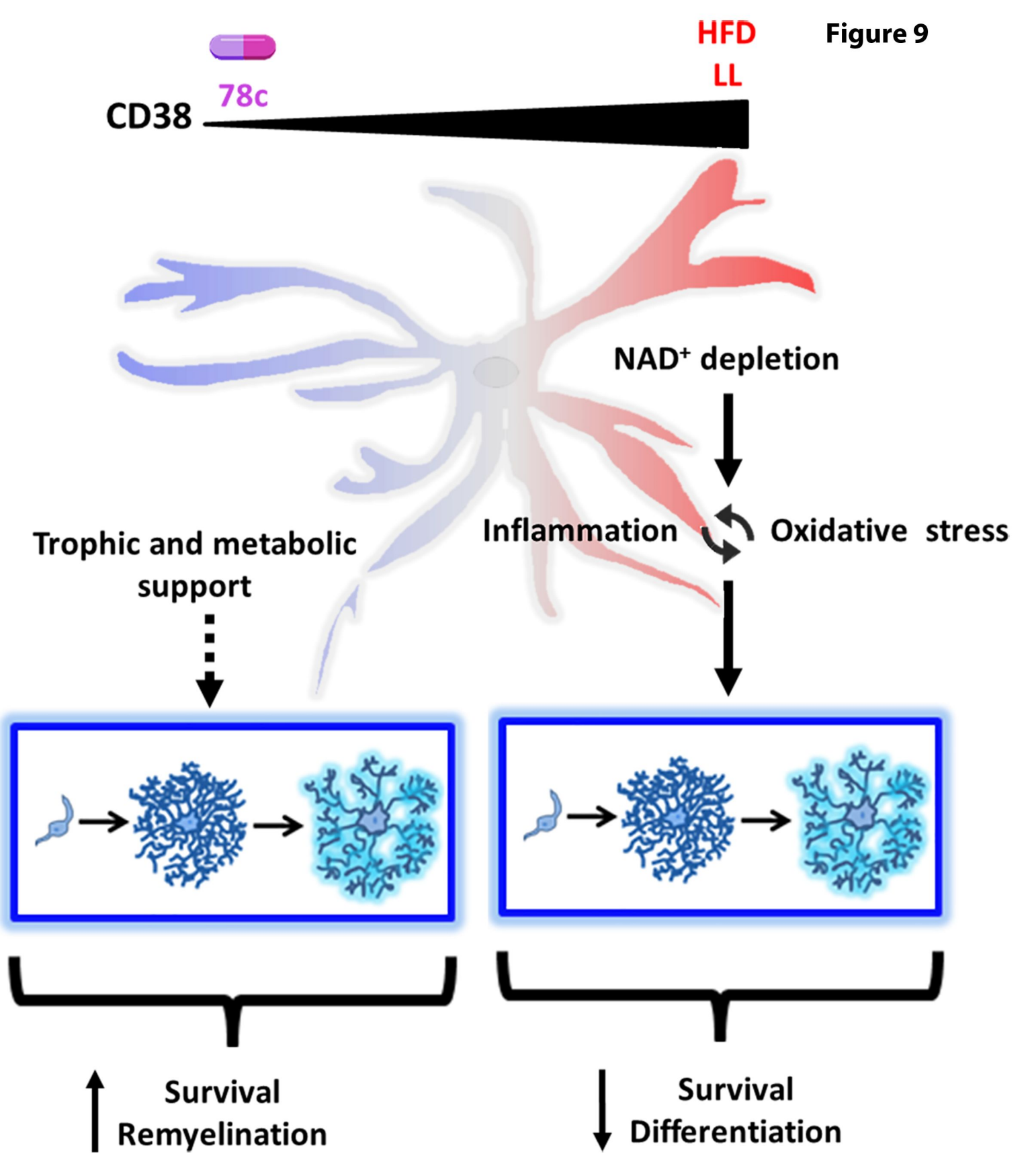
HFD
LL
78c
CD38
NAD+ depletion
Inflammation
Oxidative stress
Trophic and metabolic support
Survival
Remyelination
Survival
Differentiation

Figure 1- supplement 1

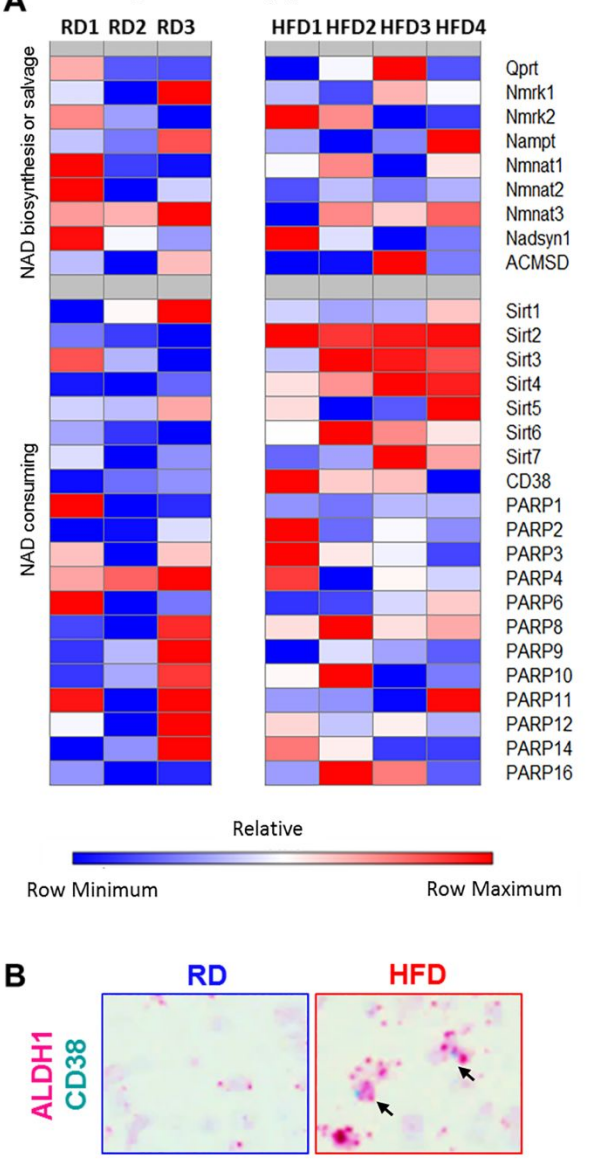

Figure 2- supplement 1

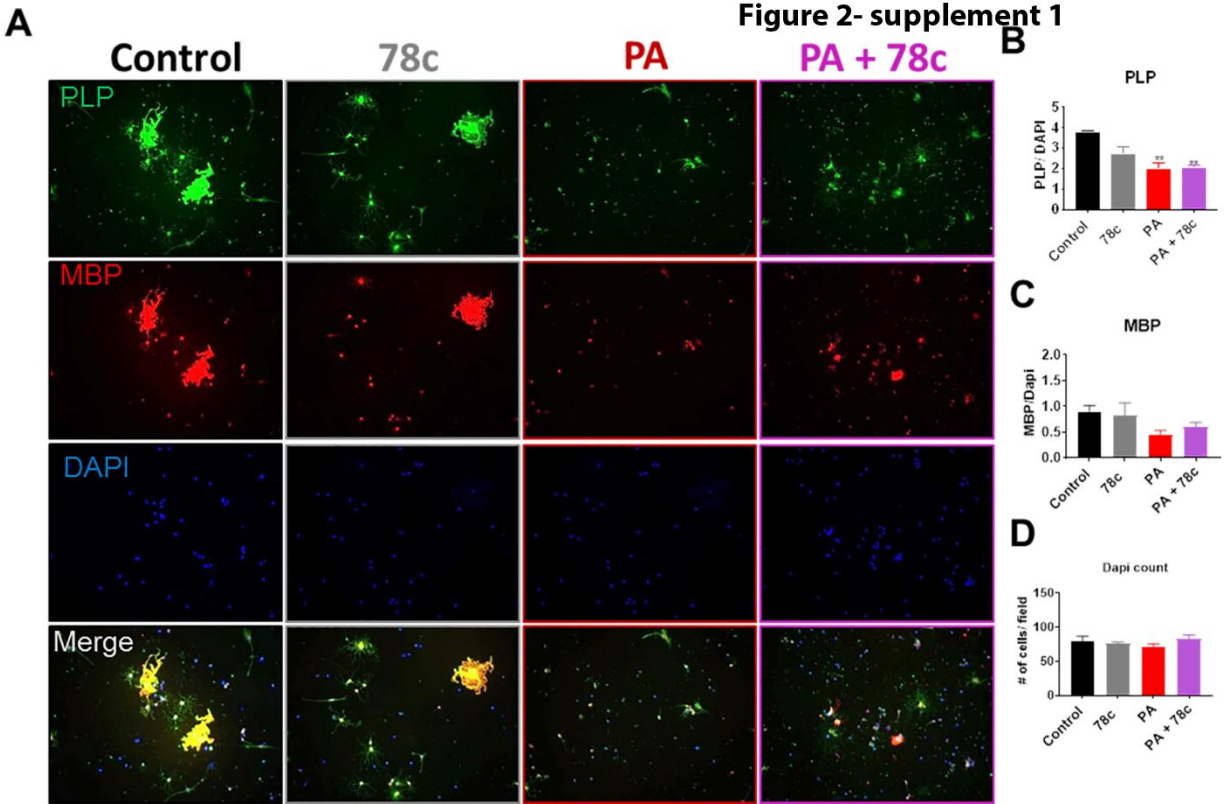

Figure 6- supplement 1

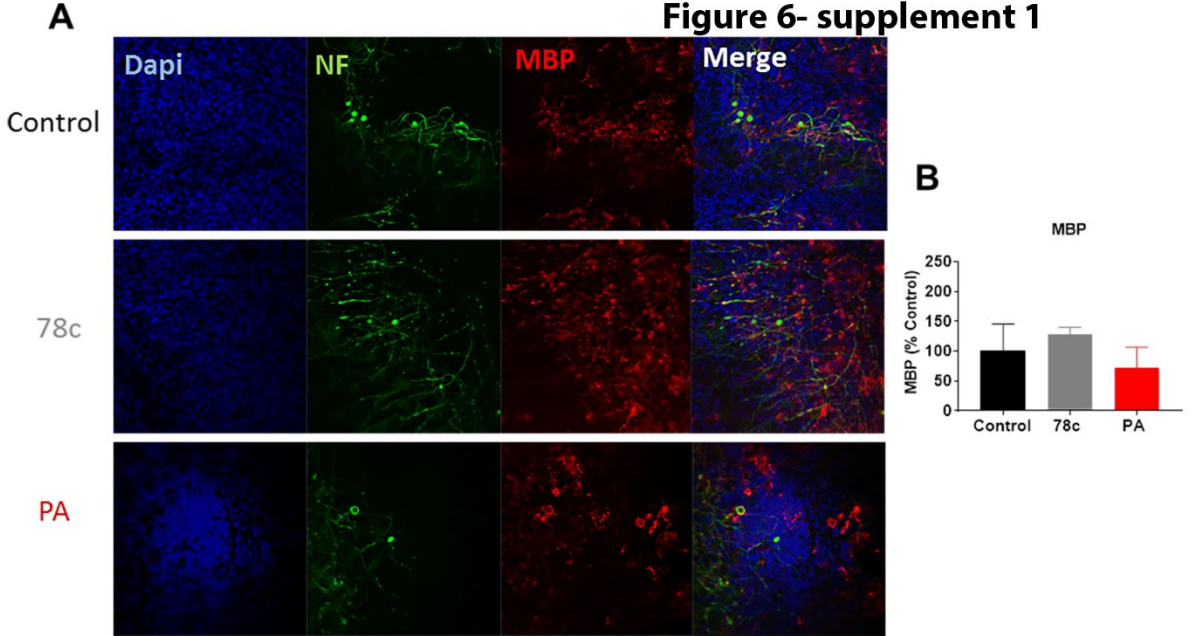

Figure 7- supplement 1

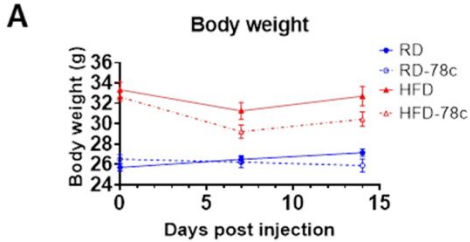

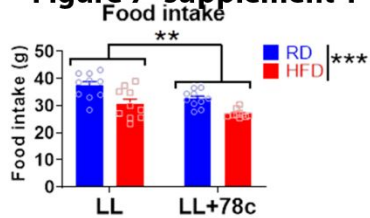

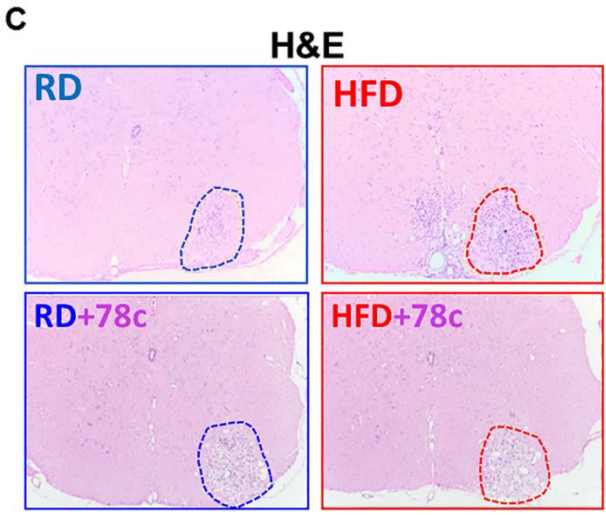

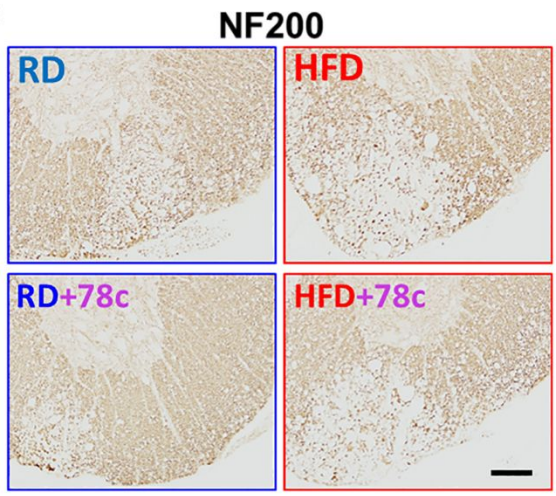

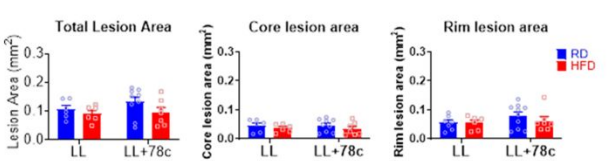

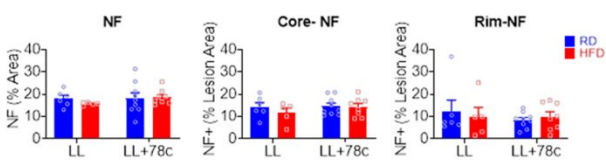

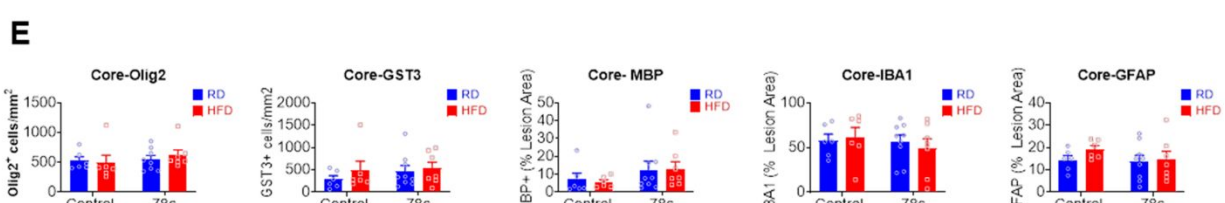
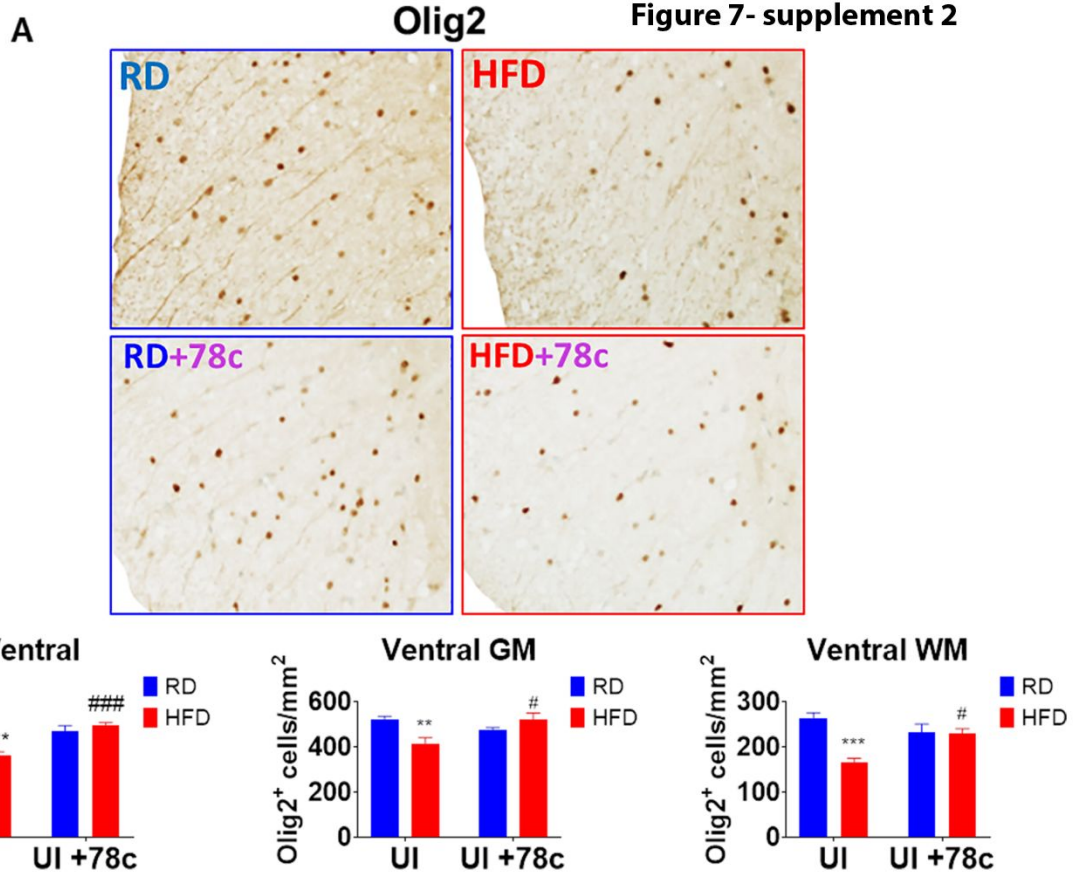
Figure 7- supplement 2